



HTSC SUPERCONDUCTING EDGE-TRANSITION  
INFRARED DETECTORS; PRINCIPLES,  
FABRICATION, AND CHARACTERIZATION

A THESIS

SUBMITTED TO THE DEPARTMENT OF ELECTRICAL AND  
ELECTRONICS ENGINEERING

AND THE INSTITUTE OF ENGINEERING AND SCIENCES  
OF BILKENT UNIVERSITY

IN PARTIAL FULFILLMENT OF THE REQUIREMENTS  
FOR THE DEGREE OF  
MASTER OF SCIENCE

By

Rizwan Akram

January 2000


QC  
612  
.38  
A37  
2000

B 051145

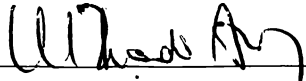
I certify that I have read this thesis and that in my opinion it is fully adequate,  
in scope and in quality, as a thesis for the degree of Master of Science.

  
Assist. Prof. Dr. Mehdi Fardmanesh(Supervisor)


I certify that I have read this thesis and that in my opinion it is fully adequate,  
in scope and in quality, as a thesis for the degree of Master of Science.

  
Assoc. Prof. Dr. Orhan Arıkan

I certify that I have read this thesis and that in my opinion it is fully adequate,  
in scope and in quality, as a thesis for the degree of Master of Science.

  
Prof. Dr. İrşadi Aksun

Approved for the Institute of Engineering and Sciences:

  
Prof. Dr. Mehmet Baray  
Director of Institute of Engineering and Sciences

## ABSTRACT

# HTSC SUPERCONDUCTING EDGE-TRANSITION INFRARED DETECTORS; PRINCIPLES, FABRICATION, AND CHARACTERIZATION

Rizwan Akram

M.S. in Electrical and Electronics Engineering

Supervisor: Assist. Prof. Dr. Mehdi Fardmanesh

January 2000

Since the discovery of High temperature superconductors, superconductivity became one of the fast emerging technologies being used in numerous applications ranging from large-scale to small-scale applications such as IR-detectors. High temperature superconductors such as  $YBa_2Cu_3O_7$  due to their properties are the prime candidates for the fabrication of detectors. Their responsivity and detectivity can be improved by changing the design and SC characteristics. In this thesis, one-dimensional thermal model has been considered to improve the characteristic parameters of the SC. Based on the model, the annealing profile and manufacturing process is modified to further enhance the responsivity and detectivity of the detectors. A characterization setup is established to perform dc & ac measurements at low temperatures. In order to improve the cryogenic setup, a thermal equivalent model for the system is also proposed.

*Keywords:* Superconductor, bolometers. cryogenic system, squids.

## ÖZET

### HTSC SÜPERİLETEN AYRIT GEÇİŞLİ KIZILÖTESİ SEZİCİLER: İLKELER, ÜRETİM VE KARAKTERİZASYON

Rizwan Akram

Elektrik ve Elektronik Mühendisliği Bölümü Yüksek Lisans

Tez Yöneticisi: Yrd. Doç. Dr. Mehdi Fardmanesh

Ocak 2000

Yüksek sıcaklık süperiletkenlerinin keşfinden beri, süperiletkenlik, kızılötesi seziciler gibi küçük ölçek uygulamalardan, büyük ölçekli uygulamalara kadar birçok alanda kullanılan önemli bir teknoloji haline gelmiştir. Uygun özellikleri nedeniyle,  $YBa_2Cu_3O_7$  gibi yüksek sıcaklık süperiletkenleri, sezici üretiminde kullanılan malzemeler arasında birinci sıradadır. Uygun tasarımlarla ve süperiletken özelliklerinin ayarlanmasıyla sezicilerin tepkisi ve sezicilik seviyesi geliştirilebilir.

Bu tezde, süperiletken parametrelerinin iyileştirilmesi amacıyla, tek boyutlu ısı model ele alınmıştır. Bu modelle, sezici tepkisinin ve seziciliğinin artırılması için, ısıtma/soğutma profili ve üretim işlemi uygun şekilde değiştirilmiştir. Düşük sıcaklıklarda DC ve AC ölçümlerinin yapılabildiği bir karakterizasyon düzeneği kurulmuştur. Ayrıca kriyogenik düzeneğini iyileştirmek için, sistemin bir ısı-eşlenim modeli önerilmiştir.

*Anahtar Kelimeler:* Süperiletken, bolometre, kriyogenik sistem, SQUID.

## ACKNOWLEDGMENTS

I would like to use this opportunity to express my deepest gratitude to Dr. Mehdi Fardmanesh for his supervision, guidance, suggestions and encouragement throughout the development of this thesis.

I would also like to thank Assoc. Prof. Dr. Orhan Arıkan and Prof. Dr. İrşadi Aksun for reading and commenting on the thesis.

I am intended to Murat Güre and Güngör Sincer from Physics Department for their assistance and also want to express my appreciation to Salim Ersen Başar, Ergün Hırlakoğlu and İsmail Kır for their continuous help in establishing the electrical and the mechanical setup for data collection. I am also thankful to all my friends, inside and out of the department for their continuous support throughout the development of this thesis.

Finally, I am grateful to my family, especially my parents for their prayers. And deeply indebted to Dr. Fakhre Mahmood and his family for their relentless encouragement and moral support during my endeavors.

# Contents

<b>1</b>	<b>INTRODUCTION</b>	<b>1</b>
<b>2</b>	<b>SUPERCONDUCTIVITY: AN OVERVIEW</b>	<b>6</b>
2.1	Review of superconductivity . . . . .	6
2.1.1	Superconductive properties . . . . .	8
2.1.2	Theory of Superconductivity . . . . .	12
2.1.3	Magnetic Properties	30
2.2	HTSC physical and electrical properties, and the YBCO superconducting material . . . . .	33
2.2.1	Overview of HTSC . . . . .	33
2.2.2	Basic Structure . . . . .	36
2.2.3	Resistance	38
2.2.4	Magnetism . . . . .	42



2.3	Applications . . . . .	44
2.3.1	Introduction	44
2.3.2	Large-scale applications . . . . .	45
2.3.3	Small-scale applications . . . . .	48
<b>3</b>	<b>DETECTORS AND DETECTORS PARAMETERS</b>	<b>55</b>
3.1	Infrared Radiation . . . . .	55
3.2	Detector Parameters	58
3.2.1	Responsivity . . . . .	58
3.2.2	Noise . . . . .	58
3.2.3	Signal to Noise Ratio . . . . .	63
3.2.4	Noise Equivalent Power . . . . .	63
3.2.5	Specific Detectivity . . . . .	64
3.2.6	Dynamic Range . . . . .	66
3.2.7	Spatial Considerations . . . . .	66
3.2.8	Cross Talk . . . . .	67
3.3	Detectors type . . . . .	68
3.3.1	Photon Detector	68

3.3.2	Thermal Detector . . . . .	70
3.4	HTSC Bolometers and the Thermal model . . . . .	82
3.5	Conclusion . . . . .	92
<b>4</b>	<b>CRYOGENICS AND INSTRUMENTATION</b>	<b>94</b>
4.1	Introduction . . . . .	94
4.2	Thermal Properties Consideration	95
4.2.1	Thermal Expansion . . . . .	95
4.2.2	Thermal Conductivity . . . . .	97
4.2.3	Specific Heat . . . . .	100
4.2.4	Electrical Analogous . . . . .	102
4.2.5	Liquid Nitrogen . . . . .	102
4.2.6	Temperature Sensors . . . . .	104
4.3	Mechanical Setup and the Cryogenics . . . . .	108
4.3.1	Introduction . . . . .	108
4.3.2	Thermal modeling . . . . .	109
4.3.3	Dewar design . . . . .	113
4.4	Electrical setup . . . . .	120

4.4.1	Resistance Vs. Temperature measurement . . . . .	121
4.4.2	Responsivity measurement . . . . .	130
<b>5</b>	<b>FABRICATION AND CHARACTERISATION</b>	<b>132</b>
5.1	High $T_c$ superconducting YBCO device fabrication and material development . . . . .	132
5.1.1	Overview of various thin-film deposition technologies . . .	133
5.2	Fabrication . . . . .	139
5.2.1	Fabrication of SC Disc, thick film and the Annealing profile	139
5.2.2	Device Fabrication . . . . .	143
5.2.3	Substrate and Selection rules . . . . .	144
5.3	Characterisation . . . . .	153
5.3.1	Magnetic Levitation . . . . .	153
5.3.2	Resistance vs. Temperature . . . . .	154
5.3.3	Mutual Induction . . . . .	156
5.3.4	Comparison between R vs. T and mutual induction measurement . . . . .	159
5.3.5	Responsivity vs. frequency . . . . .	161
<b>6</b>	<b>EXPERIMENTAL RESULTS AND THE ANALYSIS</b>	<b>163</b>

6.1	Resistance vs. temperature measurement . . . . .	163
6.1.1	Superconducting Tape . . . . .	164
6.1.2	Superconducting Disk . . . . .	166
6.1.3	Resistance vs. temperature for thin and thick films . . .	171
6.2	Mutual induction vs. bias temperature . . . . .	177
6.3	Mutual induction vs. bias current . . . . .	179
6.4	Responsivity vs. frequency . . . . .	181
<b>7</b>	<b>SUMMARY AND CONCLUSIONS</b>	<b>184</b>
	<b>APPENDICES</b>	<b>187</b>
<b>A</b>	<b>Computer program for Quasi-dc analysis of thick and thin film superconductors</b>	<b>187</b>
<b>B</b>	<b>Tables</b>	<b>190</b>

# List of Figures

2.1	The critical surface for superconductivity shown as a surface of constant electric field, $E(\vec{B}, T, J)$ . With an appropriate selection of the electric field criterion this surface can be used to define $T_c(\vec{B})$ , $B_{c2}(T)$ and $J_c(\vec{B}, T)$ . . . . .	7
2.2	Resistance vs. temperature characteristics of Superconductors. .	8
2.3	Phase diagram for type-I and type-II superconductors.	10
2.4	Magnetic behavior of perfect conductor (left) and superconductor (right). . . . .	12
2.5	The behaviour of wave function. . . . .	16
2.6	Schematic representation of electron-electron interaction transmitted by a phonon.	21

2.7	(a) normal-state, free electron, quadratic density of states is filled with electrons up to $E_F$ . Then, the superconducting energy gap $2 \Delta(0)$ is shown and the allowed states that were in the gap are pushed into regions just above and below the gap. (b) More detail of the density of states above the Fermi energy (taken as zero).	23
2.8	(a) Conduction band in the normal state, (b) energy gap at the Fermi level in the superconducting state. Electrons in excited states above the gap behave as normal electrons in rf fields: they cause resistance; at dc they are shorted out by the superconducting electrons. The gap $E_g$ is exaggerated in the figure: typically $E_g \sim 10^{-4} \epsilon_F$ .	25
2.9	Reduced values of the observed energy gap as a function of the reduced temperature $T/T_c$ , after Townsend and Sutton. The solid curve is drawn for the BCS theory Type of superconductors with the structure for YBCO (e.g. low $T_c$ metals, alloys, HTSC oxides, C60).	26
2.10	Energy bands of $YBa_2Cu_3O_7$ along some high symmetry directions for $k_z = 0$ of the orthorhombic BZ, from Krakauer and Pickett.	29
2.11	Dependence of penetration depth on the temperature.	31
2.12	Experimental set-up for laser ablation deposition.	37

2.13 (a) The a-, b-, c-direction resistivities. { For detail, see T.A.Friedmann, Phys. Rev.B42, 6217(1990)}. The dashed curve is a schematic result for $\rho_c$ . (b) and (c) $\rho_{ab}$ and $\rho_c$ for 2-Bi (n=1) superconductor with $T_c$ (7K. { For details, see S. Marten, Phys. Rev. B41,846(1990)}. . . . .	40
2.14 A unit cell of $La_2CuO_4$ . The larger black arrows in the Cu atoms denote the spin directions below TN. The smaller arrows attached to the O atoms surrounding the central Cu atom indicate the tilts that cause the tetragonal material to become orthorhombic at low temperatures.	43
2.15 First way used to levitate the train. . . . .	47
2.16 Second possible technique for magnetic laveitation for train.	48
2.17 (a) Schematic diagram of a dc-SQUID, (b) I-V characteristic for $\phi = n\phi_0$ and $\phi = (n + 1/2)$ , (c) $V - \phi$ characteristic for a constant bias current. . . . .	50
2.18 (a) Schematic representation of an rf-SQUID, (b) peak amplitude of $V_{rf}$ versus $I_{rf}$ for $\phi = n\phi_0$ and $\phi = (n + 1/2)\phi_0$ (c) peak amplitude of $V_{rf}$ vs. flux for fixed $I_{rf}$ . . . . .	51
2.19 (a) Superconducting flux transformer for measuring a field Bz; (b) superconducting first order gradiometer for measuring a field gradient $\frac{\partial B_z}{\partial z}$ ; $L_i$ is inductance of the input coil of the transformer and $M_i$ is mutual inductance between the input coil and the SQUID loop.	52

3.1	Infrared radiation spectrum. . . . .	56
3.2	Cross talk. . . . .	68
3.3	Thermal detector. . . . .	71
3.4	Golay cell. . . . .	76
3.5	Schematic circuit of pyroelectric detector. . . . .	77
3.6	Schematic circuit of bolometer. . . . .	79
3.7	Performance of cooled bolometer NEP of carbon, germanium, silicon and thallium selenide semiconducting bolometers and tin, aluminum and titanium superconducting bolometers.. . . .	82
3.8	Configuration of superconducting sample, heater, sample holder and the cryogenic cold head. . . . .	85
3.9	Equivalent thermophysical diagram of the sample in contact to the cryogenics holder, $q$ is the input radiation power, $C_{fs}$ is a lumped heat capacitance of the film, $C_s$ and $R_s$ are the heat capacity and thermal conductivity of the substrate material, and $R_{fs}$ and $R_{sc}$ are the thermal boundary resistance values at the film-substrate and the substrate-holder respectively.. . . .	86
4.1	Definition of thermal conductivity. . . . .	97
4.2	Thermal conductivity for common cryogenic building materials..	98
4.3	Cross section of the Dewar. . . . .	110



4.4	Thermal model for the conduction without including the inner environment. . . . .	111
4.5	Thermal model for the dewar where the heat transfer involves the inner environment. . . . .	112
4.6	Non steady state model for the dewar. . . . .	114
4.7	Cross section of the Dewar. . . . .	115
4.8	Cross section of the Dewar with modification.. . . .	119
4.9	Basic setup for four probe measurement. . . . .	121
4.10	Basic configuration for four probe measurement. . . . .	124
4.11	Van der Pauw and Kelvin resistor structures: (a) sample with an arbitrary shape; (b) an in-process tester design; (c) a Kelvin resistor design for measuring the effective window width.. . . .	125
4.12	A relay configuration used to switch the current. . . . .	126
4.13	Computerized system for dc characterisation of superconducting thin and thick films. . . . .	127
4.14	Schematic diagram for mutual induction measurement. . . . .	128
4.15	A setup for the response measurement for thick and thin film. . .	131
5.1	Experimental set-up for laser ablation deposition. . . . .	144
5.2	A high temperature superconductor in magnetic suspension.. . .	153

5.3	Temperature dependence of resistance for Y-Ba-Cu-O SQUID on MgO substrate. Measuring current is 1mA and critical temperature is about 90K. . . . .	155
5.4	Effect of the bias current on the resistance vs. temperature measurement. . . . .	156
5.5	Temperature dependence of coupling voltage for thin film at LaAlO <sub>3</sub> substrate. . . . .	157
5.6	coupling voltage vs. input current applied to the primary coil at 80K for superconducting thin film. . . . .	158
5.7	Response measurements by using the thermal model discusses in section 3.4, for different substrate materials. . . . .	162
6.1	Typical Resistance vs. temperature curve for superconductors. .	164
6.2	Resistance vs. temperature of the Bi-based Superconducting tape by using non quasi dc measurement. . . . .	165
6.3	Resistance vs. temperature measurement for Bi-Based Superconducting tape . . . . .	166
6.4	Resistance vs. temperature measurement effected due to unstable heating caused by the cooling process. . . . .	167
6.5	Effect of bias current under unstable heating of the disk due to non-equilibrium freezing process. . . . .	168
6.6	Resistance vs. temperature for SC. Disk (ds950ArO). . . . .	170

6.7	Effect of bias current on the resistance vs. temperature characterization for bulk of superconducting materials. . . . .	171
6.8	Effect of bias current on the resistance at fixed temperature (77K). 172	
6.9	Effect of thermal cycle on the room temperature resistance for superconducting bulk resistance. . . . .	173
6.10	Resistance vs. Temperature measurement for SQUID at bias current of 1 mA, with $T_c$ of about 90 K. . . . .	174
6.11	Effect of the bias current on the resistance vs. temperature measurement for SQUID01. . . . .	175
6.12	Effect of thermal cycle on the resistance vs. temperature measurement. . . . .	176
6.13	Mutual induction vs. temperature for thin film Superconductors. 177	
6.14	The effect on the mutual induction by reducing the temperature of the superconducting thin film on SrTiO <sub>3</sub> substrate. . . . .	178
6.15	Effect of the bias current at the primary coil on the coupling vs. temperature curve. . . . .	180
6.16	Measurement for the critical current density at 81K for the thin film SC on SrTiO <sub>3</sub> substrate. . . . .	181
6.17	Effect of applied current to primary coil for thin film SC on SrTiO <sub>3</sub> substrate. . . . .	182
6.18	Frequency response for the SQUID on linear scale. . . . .	183

# List of Tables

2.1	Memorable steps in the history of Superconductor structures. . .	36
4.1	Electrical Analogous. . . . .	102
4.2	Correction factor C.F for the measurement of sheet resistances with the four-point probe. . . . .	122
5.1	The parameters of pules excimer laser. . . . .	143
5.2	Issues in substrate selection for epitaxial films. . . . .	148
5.3	Issues in substrate selection for applications. . . . .	151
B.1	Thermal Conductivity and Integrated Thermal Conductivity for common Cryogenic Building Materials. . . . .	190

B.2	Properties of selected superconductors. $H_c$ at 0K is given for the elemental materials and $H_{c2}$ at 0K for the compounds, which are all type II superconductors. While the units of $H_c$ are mT, those of $H_{c2}$ are $10^4\text{Oe}=1\text{T}$ . $N(E_F)$ is the density of states at the Fermi energy and its units are states/(atom-eV); it is obtained from the linear term in the normal-state specific heat. . . . .	191
B.3	Specific Heat Capacity and Integrated Values for common Cryogenic Building Materials. . . . .	191
B.4	Common Cryogens and Their Characteristics. . . . .	192
B.5	Thermocouple types, structure and application temperature rangess. . . . .	193
B.6	Survey and Classification of Thin-film deposition Technologies. .	194
B.7	Global issues in substrate selection. . . . .	195

To the one WHO is ONE ...

# Chapter 1

## INTRODUCTION

The superconductivity phenomena was discovered in 1908 according to which, a material loses its electrical resistance below some certain temperature called critical temperature,  $T_c$ . Initially it was thought that superconductors could not be used widely because of the very low  $T_c$  of the known superconducting materials at the time. After the discovery of a new class of superconductors in 1986, which have critical temperatures above 32K and usually called as high temperature superconductors, a new area was opened in the field. Since the discovery of superconductivity different theories have been established in order to understand the physical properties associated with phenomena of superconductivity. One of these theories is BCS theory which has predicted most of the properties very efficiently and until today it is considered to be the reliable frame work.

Now after about 100 years following the discovery of superconductivity we are at the point where we have high temperature superconductors with  $T_c$  up to about 140 K. The recent advancements in the fabrication technology of materials make it possible to use superconductors for verity of applications. Large scale applications of superconductors include manufacturing of Transformers, power transmission lines, cables, magnetically levitated trains, etc. Small scale applications includes detection systems, microwave circuits, amplifiers, and many more.

Recent advancements in solid state technology make it possible to have detectors with high performance and efficiency. There are a variety of different detectors used for different purposes. Superconductors due to their physical properties is a prime candidate for the fabrication of thermal detectors specially as bolometers. Bolometers are one type of thermal detectors whose working principal is the change in the resistance due the change of the temperature. Applications of bolometers range from medical to the agriculture and from military to space technologies.

There are many ways to develop and approach the technology advancement of the detectors, which mainly depends on the application. One of the applications is detection in the infrared region where responsivity and detectivity are the most important parameters to be improved for the any used kind of the detectors.



In this thesis efforts have been done in order to improve the above mentioned properties. Thermal equivalent model has been considered to investigate which parameters of the detectors directly influence the responsivity and detectivity. Once the related parameters has been found new method has been purposed to fabricate the detectors.

Once a detector has been fabricated we need to have a characterization setup which should be capable of providing a reliable data. Hence a cryogenic system has also been developed which can work at atmospheric pressure with almost constant temperature at the sample of about and over 77K. It has been found that this system reduces the noise specially the vibrational noise, which is usually found in other pump-based cryogenic systems. Secondly there is no need to have a vacuum for better operation, and it works with self-vacuum system. In order to improve the thermal properties of the system a one-dimensional thermal model for Dewar was also proposed.

The first chapter starts with the common superconductor's properties and some very basic concepts. It also provides good references for those interested in the subject and prevents any extra research in order to understand the topics mentioned in the thesis on his/her part. It also works as a preliminary for the advanced topics used in the fabrication and resulting processes. Furthermore, the first chapter discusses our used  $YBa_2Cu_3O_{7-x}$  material's properties and provides concise yet a thorough account of its applications.

The second chapter discusses detectors and makes a connection between superconductors and detectors. It defines the detector parameters. Various topics such as noise, responsivity, specific detectivity, dynamic range, etc. are discussed in this chapter. Many recently developed types of detectors are also mentioned here termed in major categories like photon detectors, thermal detectors and heterodyne detectors. A thermal equivalent model for detectors, has been discussed in detail.

Chapter 3 is about the experimental setup developed based on the model derived in the previous chapter. The two electrical and mechanical models are discussed here. For the mechanical model, we are to know various thermal properties, which are explained in a compact form. The mechanical model provides an account of the work done recently at Bilkent University during the course of this thesis, the Dewar design. Whereas the electrical setup has computer controlled systems for performing the DC (R vs. T, mutual induction measurements) and AC analysis.

The original course of experimentation requires rigorous comparison of some known standards, which is discussed in Chapter 4. This is indeed the idealistic part of the thesis, which shall be compared with the experimental measurements. This has been the reason for prior explanation of a few existing and successful techniques about fabrication processes which include the fabrication of thick and thin films and also the bulk superconducting discs. Afterwards the chapter defines some standards regarding the superconductivity and infrared

detectors such as, magnetic levitation, resistance vs. temperature, mutual induction and inductances, responsivity vs. frequency, and the temperature and the noise measurements.

## Chapter 2

# SUPERCONDUCTIVITY: AN OVERVIEW

### 2.1 Review of superconductivity

After the discovery of superconductivity many theories, like BCS, Ginzburg-Landau, have been established in order to understand the behavior of superconductors. According to these theories the number of independent parameters needed to describe homogeneous superconductors can be surprisingly few. From BCS theory, four parameters suffice (critical temperature,  $T_c$ , critical magnetic field,  $B_{c2}$ , order parameter,  $\kappa$ , the normal resistivity,  $\rho_n$ ) to describe the superconductor. On the other hand near to  $T_c$ , the Ginzburg - Landau theory uses only two independent parameters. For example  $T_c$  and  $B_{c2}$  and others can be derived.

However from the practical point of view, inhomogeneity, anisotropy and granularity in the SC materials further much complicate the picture.

The typical relation between  $T_c$ ,  $B_{c2}$  and  $J_c$  for a superconducting material is shown in the following figure.

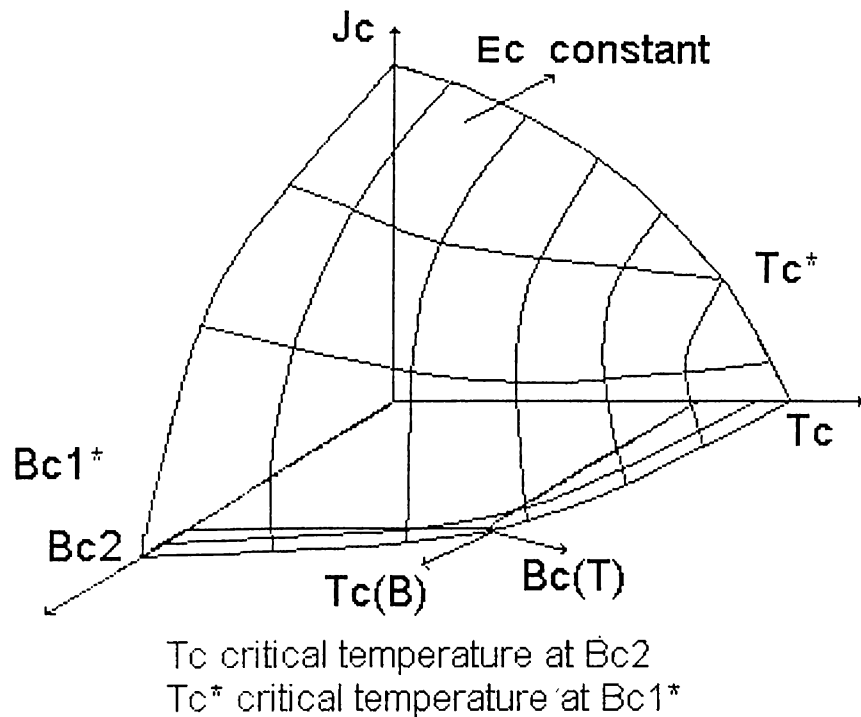


Figure 2.1: The critical surface for superconductivity shown as a surface of constant electric field,  $E(B,T,J)$ . With an appropriate selection of the electric field criterion this surface can be used to define  $T_c(B)$ ,  $B_{c2}(T)$  and  $J_c(B,T)$ .

Near  $T_c$  and  $B_{c2}$ , inhomogeneity in a material leads to the broadening of the transition from the superconductivity to the normal state. Each of the above properties are discussed in the next sub-section.

### 2.1.1 Superconductive properties

#### Critical Temperature:

Critical Temperature,  $T_c$ , is defined as the temperature at which the superconductor loses its resistance. Hence critical temperature drives a specimen with a finite normal electrical resistivity to a superconducting state undergoing a phase transition as depicted in Fig. 2.2.

$T_c$  being a characteristic property differs for metal and alloy superconductors. However,  $T_c$  is not affected much by the impurities, but magnetic impurities tends to lower the transition temperature. Superconductivity is a rare phenomenon not shown by all elements of the periodic table. Though some alloys composed of two or more metals can exhibit superconductivity properties even though the same cannot be said when they are separated, e.g., Bi-Pb.

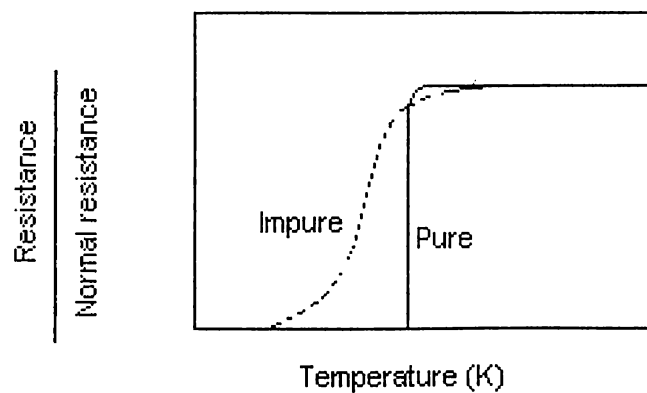


Figure 2.2: Resistance vs. temperature characteristics of Superconductors.

The  $T_c$  transition for physically perfect elements is extremely sharp which can be broadened by adding impurity and disturbing the crystal as shown in Fig. 2.2.

### **Critical Magnetic Field:**

When a superconductor is driven into normal state due to high applied magnetic field, the magnitude of the magnetic field is called the Critical Magnetic Field,  $H_c$ . The basic of above from the physical phenomena is that the net superelectron momentum must not exceed a certain value, which refers to a current density, if the material is to remain superconductor. This critical current density is both represented by the current due to an external source and to the screening current which shield the specimen from an applied magnetic field.

With respect to the magnetization, a dia-magnetism arises in a superconductor when the surface super-currents circulate within the specimen to cancel the flux density inside. The current magnitude can be increased sufficiently by increasing the magnetic field until an upper limit for the current is reached. Then the shielding current will cease to increase with increasing magnetic field, allowing the magnetic field to penetrate.

As shown in the Fig. 2.3, the critical magnetic field is found to be dependent on the temperature. The phase diagram as shown in the Figure 2.3a shows the magnetic field falling from some value  $H_o$  to zero below  $T_c$  and the

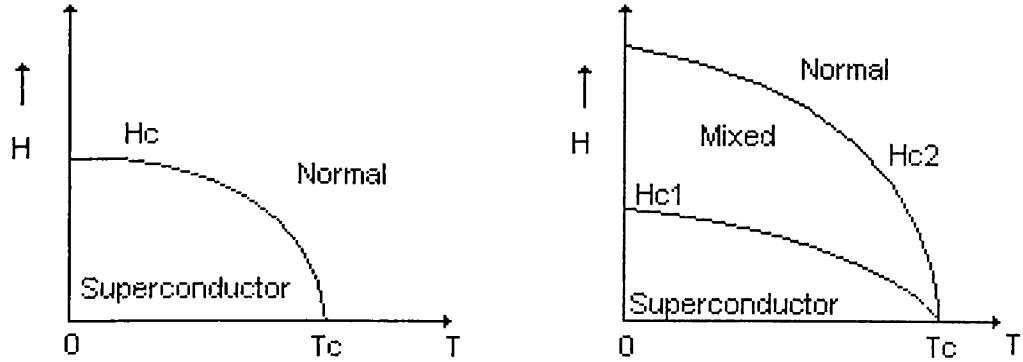


Figure 2.3: Phase diagram for type-I and type-II superconductors.

material will be superconductor for a point lying in the area under this curve. The relationship between  $T_c$  and  $H_c$ , in specific for low  $T_c$  materials can be formulated as follows:

$$H_c = \begin{cases} H_0[1 - (\frac{T}{T_c})^2] & T < T_c \\ 0 & T > T_c \end{cases} \quad (2.1)$$

By virtue of critical magnetic field, we can categorize the superconductors into two types:

**Type I:** superconductors, which are forced into normal state by one critical magnetic field.

**Type II:** superconductors, which are forced into normal state by two critical magnetic fields, as shown in Fig. 2.3b



Below  $H_{c1}$  curve the material is in superconducting state, between  $H_{c1}$  and  $H_{c2}$ , the material is in a mixed state, and above  $H_{c2}$  the material is driven into normal state.

### **Meissner Effect:**

Till the year of 1933, it was believed that the superconductors behave like a perfect conductor as shown in Fig. 2.4 (left). But in the same year experiments led by Meissner and Ochsenfeld on the flux distribution outside tin and lead in superconducting stage showed that the specimen becomes perfectly Demagnetized cancelling all flux inside as in Fig. 2.4(right)c, unlike the expected situation Fig. 2.4 (left)f. The reason behind this phenomenon is the generation of persistent surface currents when a superconductor is cooled in a weak magnetic field at transition. This whole process is called **Meissner Effect**.

Hence it can be stated that the superconductor is independent of the state of magnetism and depends entirely on the actual values of the applied field and temperature while its counterpart perfect conductor takes the state into account as well.

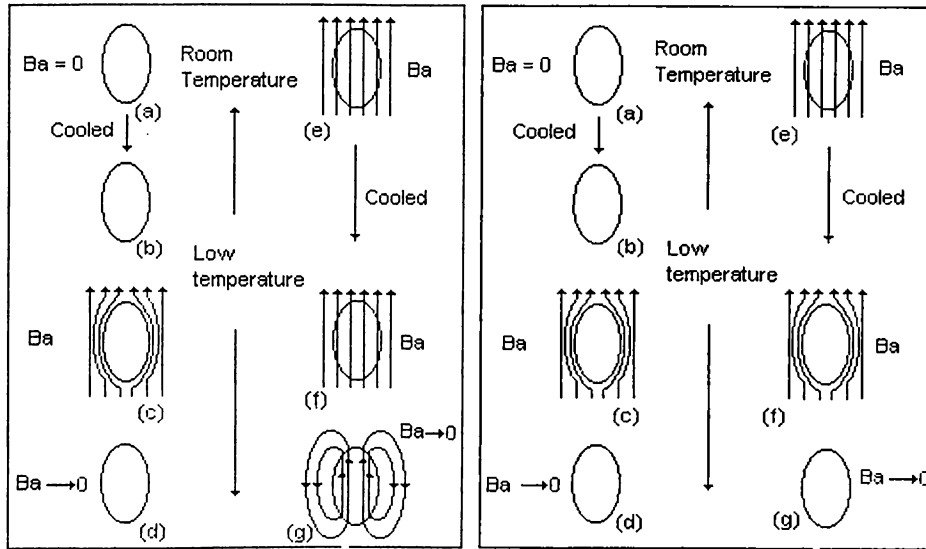


Figure 2.4: Magnetic behavior of perfect conductor (left) and superconductor (right).

### 2.1.2 Theory of Superconductivity

#### Two Fluid Model (London Equation):

Two fluid model is a good starting point in order to understand the superfluid properties of Helium. Helium is assumed to be composed of atoms in two states, one being in condensed Bose-Einstein ground state and the rest in the normal state. This idea was used in practice for superconductivity purposes by Gorter and Casimer (1934) for the first time. They proposed the following system of equations: if  $N$  represents conduction electron then conduction electron density  $n = N/V$  and  $n = n_n + n_s$  where  $n_n$  and  $n_s$  are the densities of normal and superconducting state electrons respectively. Though a drastic assumption of electron separation, the scientists suggested the following free energy equations for the conduction electron of atom:

$f_n = -\gamma T^2/2$  usual free electron energy in normal state

$f_s = -\beta$  constant, condensed state energy.

Minimization of free energy,  $F(x,T)$ , for conduction electron with respect to  $x$  yields:

$$x = \frac{n_s}{n} = \left(\frac{T}{T_c}\right)^4. \quad (2.2)$$

The equation above shows a sharp dependence of fractional electron states below  $T_c$ . This model gives a hard physical basis for understanding superconductivity.

#### London Equation:

Using the above assumptions and knowing the fact from condensed matter physics that the superconducting electron current is given by  $\mathbf{J} = -e\mathbf{V}_s n_s$ , plus the Newton's law  $m(d\mathbf{V}/dt) = -e\mathbf{E}$ , by using the  $\Delta \times \mathbf{E} = -\frac{1}{c} \frac{d\mathbf{B}}{dt}$  we have;

$$\frac{d\mathbf{J}}{dt} = \left(\frac{e^2 n_s}{m}\right) \mathbf{E}, \quad (2.3)$$

where  $\mathbf{E} = \frac{d(\Lambda \mathbf{J})}{dt}$  and  $\Lambda = \frac{m}{e^2 n_s}$ .

Combining the above results with Maxwell's equations we get the following general equation for the metals:

$$\frac{d[c\Delta \times (\Lambda\mathbf{J}) + \mathbf{B}]}{dt} = 0. \quad (2.4)$$

In 1935, London brothers used the above idea of two fluids to understand the Meissner effect. London characterized the behavior of superconductors by restricting the full solution set to the following:

$$-c\Delta \times (\Lambda\mathbf{J}) = \mathbf{B}, \quad (2.5)$$

Which is named as 'London's equation'. Taking the curl of both sides using Maxwell's equation  $\Delta \times \mathbf{B} = \frac{4\pi}{c}\mathbf{J}$  and using the identity  $\Delta \times \Delta \times \mathbf{B} = \Delta(\Delta \cdot \mathbf{B}) - \Delta^2\mathbf{B}$  we obtain  $\Delta^2\mathbf{B} = \frac{\mathbf{B}}{\lambda_l^2}$  and  $-\Delta^2\mathbf{J} = \frac{\mathbf{J}}{\lambda_l^2}$

$$\lambda_l^2 = \frac{m_c^2}{4\pi n_s e^2}, \quad (2.6)$$

where  $\lambda$  is the London penetration depth. The above equation shows that the magnetic field decays from surface to bulk exponentially. London equation simplifies Meissner effect a great deal by declaring that a shielding current is setup that protects the sample interior from external magnetic field. Hence by using the results of the penetration depth concept of the two fluid model and the following consequent equation of it, we see that below  $T_c$ ,  $\lambda_l$  decreases rapidly, leading to the exclusion of flux from the bulk of the sample, the Meissner effect in other words.

$$\lambda_l(t) = \frac{\lambda_l(0)}{[1 - (T/T_c)^4]^{1/2}}. \quad (2.7)$$

Vector approach can also be an intuitive approach towards solving the London equations, which is used in describing Ginzburg-Landau theory in the following section.

### **The Ginzburg-Landau Theory:**

Related with Landau's theory of second order structural phase transition, Ginzburg and Landau proposed a phenomenological theory of superconductivity in 1950. According to the theory, electrons were described to be in order at low temperatures while the free energy in terms of an order parameter was zero at high temperature phase. This entailed certain assumptions, one of them being the superconducting behaviour defined as a complex pseudo wave function  $\Psi$  as the order parameter, which has the significance that  $|\Psi(r)|^2 = n_s = N_s/V$ . The second assumption in this regard is that the free energy of the superconducting state differs from that of normal state by an amount, which can be written as a power series. However, it is sufficient to retain only first two of its terms in this expression. The nonlinear and spatial variation effects of  $n_s$  were then treated by using the GL formalism in magnetic fields. Not only did the theory defined a temperature dependent penetration depth  $\lambda$ , it also introduced a coherence length dependent on temperature. Coherence length  $\zeta$  is the distance over which  $\Psi(r)$  can vary without a substantial energy increase. The important GL parameter is defined as;

$$\kappa = \lambda/\zeta. \tag{2.8}$$

The Fig. 2.5 shows how  $\Psi$  increases in the superconductor to its values at infinity  $\Psi_\infty$  in a distance ( $\zeta$ ) and how the magnetic field penetrates the superconductor (to a depth  $\lambda$ ).

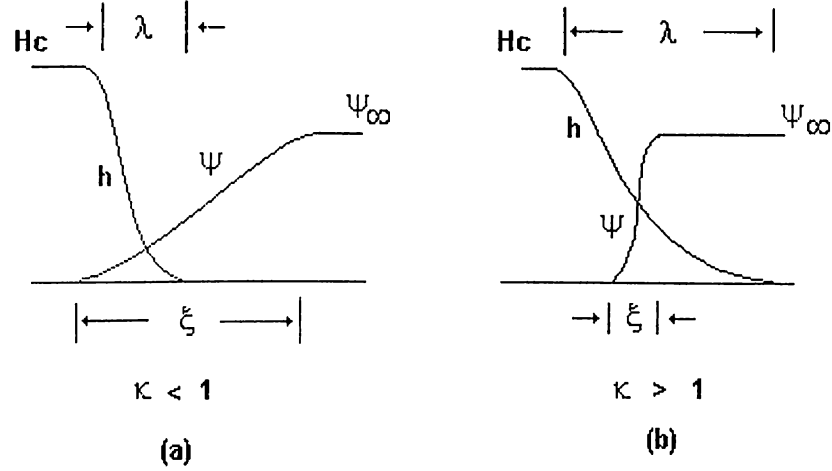


Figure 2.5: The behaviour of wave function.

Considering the GL free energy, in the presence of magnetic field and spatial gradients, the free energy density is taken as;

$$f = f_n + \alpha|\Psi|^4 + \frac{1}{2m^*} \left| \left( \frac{\hbar}{i} \Delta - \frac{e^*}{c} A \right) \Psi \right|^2 + \frac{h^2}{8\pi}, \quad (2.9)$$

where the free energy density in the normal state ( $\Psi = 0$ ) is  $f_n(t) = f_{n0}(0) - \frac{1}{2}\gamma T^2$ ; equation 2.9,  $h^2/8\pi$  is the classic magnetic energy density and the middle terms leads to the linear-temperature specific heat for a metal, where  $h(r)$  is local microscopic field. It is sufficient to keep the leading term  $|grad(\Psi)|$  only if  $n_s$  varies slowly in space.  $|grad(\Psi)|$  is combined with the

vector potential  $A(\mathbf{r})$  in a gauge invariant manner. The total magnetic contribution to the free energy of the superconducting state is therefore given by;

$$\frac{\hbar^2}{2m} \int \Psi^* \left[ i \text{grad} + \frac{eA}{\hbar} \right]^2 \Psi dV, \quad (2.10)$$

the integral being taken over the whole volume  $V$  of the specimen. The functions  $\Psi(r)$  and  $A(r)$  which make the total free energy of the specimen a minimum subject to appropriate boundary conditions is the central problem of the Ginzburg-Landau approach. This problem is simplified for weak magnetic fields where London equation is applicable; nonetheless, strong magnetic field equations are only solvable through numerical methods. This is while, both the  $\Psi$  and  $\lambda$  vary with film thickness as varies with  $x$ , which is due to the film thickness, while again depends on  $|\Psi|^2$ .

The critical magnetic field can be calculated by the usual method of equating the free energy of the film in the superconducting state with that in the normal state. The general expression for  $H'_c$  is complicated, but simplifies in two special cases:

(i)  $a \gg \lambda$ , in this case

$$H'_c = H_c \left( 1 + \frac{\alpha \lambda}{2a} \right), \quad (2.11)$$

where  $2a$  is the thickness of the film,  $\lambda$  is the penetration depth in a weak magnetic field, and  $\alpha$  is a coefficient very close to unity. This is essentially the same as the London result.

(ii)  $a < \lambda$ , this case causes  $\Psi$  to be approximately constant throughout the film resulting in,

$$H'_c = \left[ \frac{\sqrt{(6)\lambda}}{a} \right] H_c. \quad (2.12)$$

This differs from the London result by factor of  $\sqrt{2}$ . As  $H$  approaches  $H'_c$ ,  $\Psi$  gradually falls to zero which brought out a surprising consequence of the Ginzburg theory showing the transition as a second-order one.

The major advantage of the Ginzburg-Landau theory is that it allows the study of spatially inhomogeneous systems, such as proximity systems, thin films, and others. If small amount of static (and nonmagnetic) impurities is introduced into a superconductor, this will have practically no effect on its thermodynamic properties and will not change its critical temperature. The electromagnetic properties are another matter to be considered separately. The processes of electron impurity scattering which will change the electronic momenta are important and will affect the coherence length,  $\zeta$ . The latter will become equal to  $(\zeta_0 l)^2$ , where  $l$  is the mean free path defined by the impurity density. Thus doping will lead to a decrease in  $\zeta$  and a corresponding rise in  $\kappa$ . In this way, a pure Type I superconductors can, by doping, be turned into a Type II superconductors, resulting in a radical change of its behaviour in an external magnetic field.

Even though the experimental accuracy of Ginzburg-Landau theory has not exceeded London theory if values of  $\lambda$  obtained from measurements on large



specimens are used. The greatest success of the Ginzburg-Landau theory still remains to be the correct predictor of the first to second order transition change with decreasing thickness, which London Theory fails to achieve.

### **BCS theory:**

Any successful microscopic theory of superconductivity must be able to explain the following basic characteristics of superconductor;

- (i) Superconductor is essentially bound up with some profound change in the behaviour of the conduction electrons which marked by the appearance of long range order and a gap in their energy spectrum of the order of  $10^{-4}eV$ .
- (ii) The crystal lattice does not show any change of properties, but must nevertheless play a very important part in establishing superconductivity because the critical temperature depends on the atomic mass.
- (iii) The superconducting to normal transition is a phase change of the second order.

Almost half a century after the discovery of superconductivity, a comprehensive, microscopic theory was proposed by Bardeen, Cooper, and Schrieffer (1957), which is called the BCS theory. This theory gives an excellent account of the equilibrium properties of superconductors and, to quote from their conclusion section, "this quantitative agreement, as well as the fact that we can account for the main features of superconductivity, is convincing evidence that our model is essentially correct."

The BCS results involve complicated, many-body, quantum-mechanical equations and a study would take us far a field.

**Cooper Pairs and Principle of BCS theory:** In 1956 Cooper considered a non-interacting Fermi gas at  $\sim 0\text{K}$ , so all the states are filled for  $k \leq k_F$ . To this Fermi gas, two electrons are added, which occupy states with  $k > k_F$  because of the Pauli-exclusion principle. Then it is assumed that a net attractive electron-electron interaction exists between these two electrons when their energies are within  $\hbar\omega_c$  of the Fermi energy  $E_F$ . This attraction occurs because as the first electron moves through the crystal, it distorts (by means of a phonon) the structure in such a manner that a second electron reduces its energy by moving through the distorted structure. For electrons in this energy range, it is suggested that the interaction is attractive and larger than the repulsive, screened-Coulomb interaction and this is called phonon-mediated pairing.

The electron-electron interaction,  $U$ , scatters a pair of electrons with crystal momenta  $(k, -k)$  to  $(k', -k')$ . The scattering matrix element is  $U_{k,k'}$ . Cooper assumed that  $U_{k,k'} = -U_0$  (independent of  $k$ , called weak coupling) for states within a cutoff energy  $\hbar\omega_c$  of  $E_F$ . The matrix element was taken as zero for energies outside the range  $E_F$ . Cooper showed that though electrons are restricted to having momenta outside the Fermi sphere, they will have a bound state lying below  $2E_F$ . This bound state is called a Cooper pair. Thus, clearly there may be an instability in the electron system if this interaction is operative.

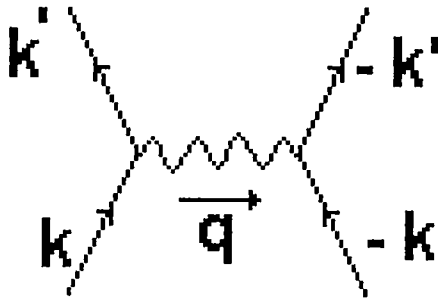


Figure 2.6: Schematic representation of electron-electron interaction transmitted by a phonon.

**BCS Results:** If we consider; the density of states at energy  $E$  of one-spin orientation as  $N(E)$ , that is, the number of states between energy  $E$  and  $E+dE$  for electrons of one-spin orientation. by writing a many-body wave function BCS were able to show that there is a second order phase transition to a new electron state with the transition temperature expressed as

$$k_B T_c = 1.14 \hbar \omega_c e^{-1/N(E_F)U_0}, \quad (2.13)$$

where  $N(E_F)$  is the density of normal state electrons at the Fermi energy. The cutoff phonon energy  $\hbar \omega_c$  is related to the Debye energy  $\hbar \omega_D$  in which  $\omega_D \propto M^{-1/2}$ , where  $M$  is the atomic mass. Thus, the isotope effect comes out of the theory in a natural manner, namely,  $T_c \propto M^{-1/2}$ , which had been suggested by Frohlich in 1950 and was found to be in excellent agreement with experiments on mercury isotopes (1950).

According to the BCS theory the calculated energy gap at 0K is:

$$2\Delta(0) = \frac{\hbar\omega_c}{\sinh [1/N(E_F)U_0]} \approx 4\hbar\omega_c e^{-1/N(E_F)U_0}. \quad (2.14)$$

The idea of a gap in the density of state is shown in Fig. 2.7, in a greatly exaggerated manner the normal state, quadratic, free-electron-like density of state is shown, which at 0K is filled up to  $E_F$ , for a superconductor. The 0K gap is centered at  $E_F$  and it 'pushes' allowed states into energy regions just below and above the gap, as indicated. The modified superconducting density of states,  $N_S(E)$ , for  $E > \Delta$  and  $E < -\Delta$ , is;

$$N_S(E) = N(0) \frac{E}{(E^2 - \Delta^2)^{-1/2}}, \quad |E| > \Delta. \quad (2.15)$$

For energies within the gap, the density of allowed states is zero. This expression is singular at the edges of the gap ( $E = \pm\Delta$ ), and for positive energies the result is shown in details in Fig. 2.7. Here it should be noted that the total number of state is unaltered by the interaction and those formally in the gap are 'pushed out' by the interaction. Thus, the number of superconducting state is much larger at  $T = 0K$  than just below  $T_c$ .

Since the expressions for  $k_B T_c$  and  $2\Delta(0)$  have the same form, their ratio is independent of the electron density of state and electron phonon matrix element, yielding the parameter-free result,

$$2\Delta(0)/k_B T_c = 3.52. \quad (2.16)$$

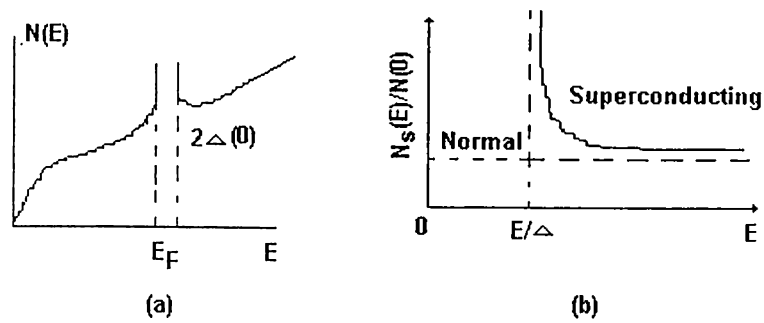


Figure 2.7: (a) normal-state, free electron, quadratic density of states is filled with electrons up to  $E_F$ . Then, the superconducting energy gap  $2\Delta(0)$  is shown and the allowed states that were in the gap are pushed into regions just above and below the gap. (b) More detail of the density of states above the Fermi energy (taken as zero).

Table B.2 (see appendix) shows that experimental results for many elemental superconductors are close to 3.5, as are results for many compound superconductors.

By solving the gap equation at elevated temperatures, the temperature dependence of gap,  $2\Delta(T)$ , can be calculated. The gap vanishes at  $T_c$ , and just below this value,  $\Delta(T)$  can be approximated by;

$$\Delta(T) \approx AT_c(1 - T/T_c)^{1/2} \quad T < T_c$$

where  $A = 3.06$ .

### Band Theory:

The invention of high  $T_c$  superconductors has led the solid state physicists to take interest in complicated superconducting alloys. This has resulted in even energy band calculations yielding results that may be called spaghetti diagrams because of the large number of dispersionless electron energy levels vs. crystal

momentum involved. Special attention will be given to Fermi levels  $E_F$  since they have a direct consequence on the conduction process and superconductivity.

We begin with band diagrams. Band diagrams are essentially always for one-electron bands. In these calculations electron-electron repulsion is treated in an averaged manner as the electron orbital are largely extended compared to the nearest neighbor atoms which makes Coulomb's repulsion forces approximation quite feasible. Hence on average electron-electron correlation can be considered as mere perturbations. For a high  $T_c$  material, the electron-electron interaction is much larger than in ordinary metals, hence electrons are found to be strongly correlated and one electron band has little or no significance. A Hubbard type or resonating valance band model probably is a more sensible starting point to describe the electronic energies. This point of view is supported by the fact that one electron band calculation prefect metallic behaviour for all the high  $T_c$  type materials even the insulator ones. Cuprate materials on the other hand has a reasonable agreement between the one-electron band structure and experimental results. We shall focus on one-electron bands of these high  $T_c$  systems and their metallic properties. A particular approach is required for behaviors of the carriers within these materials. We will present the simplest viewpoint that reasonably agrees with the experimental values.

## Energy Gap:

Superconductors being different from other materials have different energy band origin and nature as well. In a superconductor the electron-electron interaction is significant and plays a vital role in ordering the electrons in K space with respect to the Fermi gas of electrons. Insulators, have an electron-lattice interaction, which is responsible for electron-lattice ties as well. The argument of the exponential factor in the electronic heat capacity of a superconductor is found to be  $-E_g/2K_B T$  instead of  $-E_g/K_B T$ . Comparing the optical and electron tunneling determinations of the band gap,  $E_g$  have been calculated.

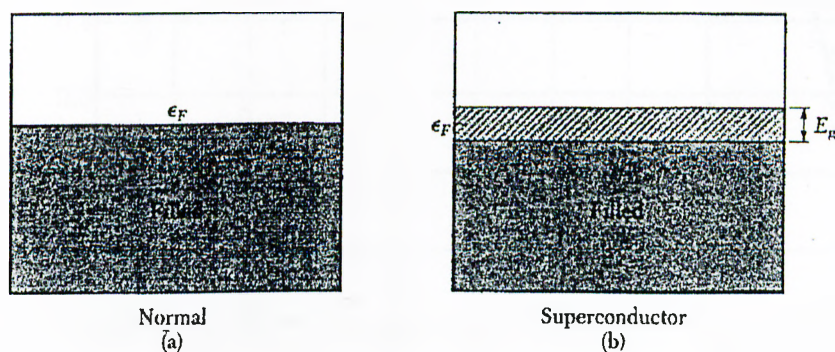


Figure 2.8: (a) Conduction band in the normal state, (b) energy gap at the Fermi level in the superconducting state. Electrons in excited states above the gap behave as normal electrons in rf fields: they cause resistance; at dc they are shorted out by the superconducting electrons. The gap  $E_g$  is exaggerated in the figure: typically  $E_g \sim 10^{-4} \epsilon_F$ .

The transition in zero magnetic field from the superconducting state to the normal state is observed to be second-order phase transition. At a second order transition there is no latent heat, but there is a discontinuity in the heat capacity, evident in Fig. 2.7a. Furthermore, the energy gap decreases continuously to zero as the temperature is increased to the transition temperature  $T_c$ , as in

Fig. 2.9. A first-order transition would be characterized by a latent heat and by a discontinuity in the energy gap.

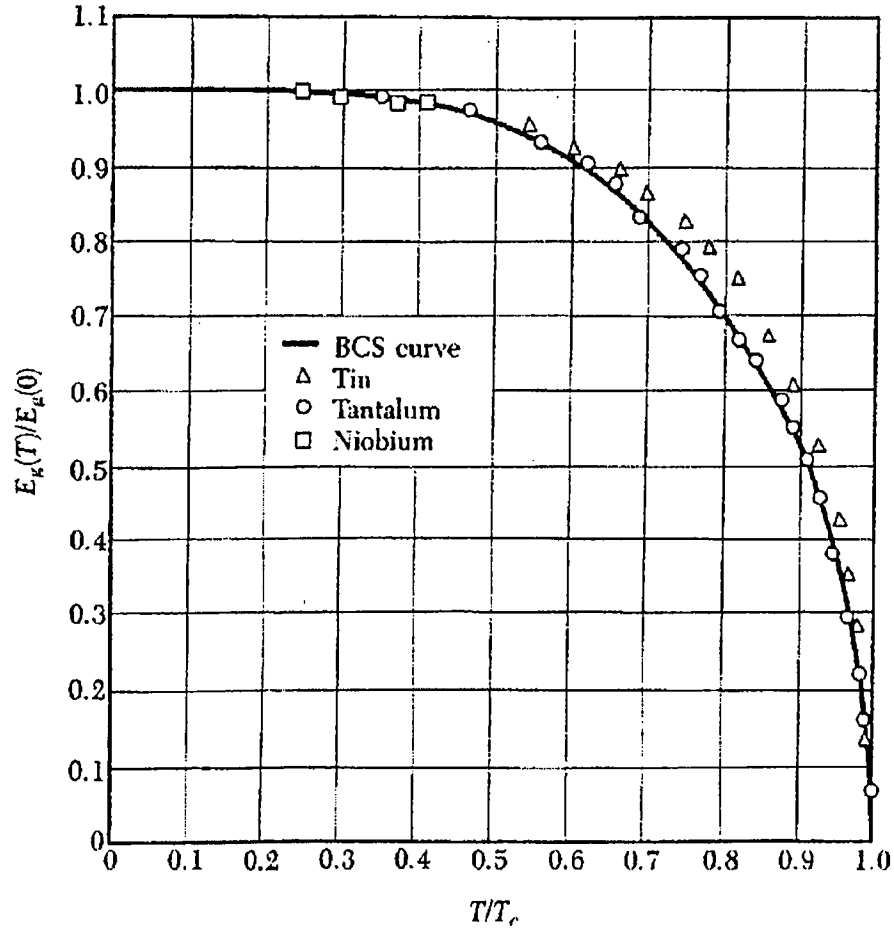


Figure 2.9: Reduced values of the observed energy gap as a function of the reduced temperature  $T/T_c$ , after Townsend and Sutton. The solid curve is drawn for the BCS theory Type of superconductors with the structure for YBCO (e.g. low  $T_c$  metals, alloys, HTSC oxides, C60).

### Electronic and Band Structure:

The cause of superconductivity in the copper-oxide systems occurs mainly due to metal insulator controlled by doping or oxygen stoichiometry as well as



due to structural instability (orthorhombic  $\leftrightarrow$  tetragonal). At low temperatures, the metallic phase becomes superconducting, while the insulating phase show long-range anti-ferromagnetic order. The structure of most of the high- $T_c$  superconductors are layered perovskite with large anisotropy [1] and most unique feature is the presence of Cu- $O_2$  layers which seem to be crucial for the high temperature superconductivity. The exception is the cubic perovskite  $Ba_{1-x}K_xBiO_{3-y}$ , which has an onset temperature of 30K with the Cu- $O_2$  layers missing. In this section we will see some of the basic electronic properties and band structure of most famous high-temperature superconductors,  $YBa_2Cu_3O_{7-x}$ .

**Electronic properties of  $YBa_2Cu_3O_{7-x}$ :** The unique feature of the structure of  $YBa_2Cu_3O_{7-x}$  is the absence of the  $2+y$  oxygen atoms for the perfect triple perovskite  $YCuO_3(BaCuO_3)_2$  [2]. In the limit  $x = 0$ , the vacancies are due to the absences of the oxygen atoms from the Y plane which separates the adjoining Cu- $O_2$  layers, and half of the oxygen sites in the Cu-O plane between the Ba-O layers which leads to the formation of the Cu-O chain. There are three weakly coupled Cu-O layers in the unit cell, consisting of two quasi-two-dimensional Cu- $O_2$  planes and a one-dimensional Cu-O chain. Along the c-axis, the oxygen atom in the Ba-O plane ( $O_{Ba}$ ) is significantly close to the fourfold coordinated Cu atoms in the chains ( $1.85\text{\AA}$ ) than the fivefold coordinated Cu atom in the planes ( $2.30\text{\AA}$ ). As  $x$  is increased from 0 to 1, the oxygen atoms, in the chain layers, are removed and some of the oxygen atoms are moved to the empty sites, which eventually leads the orthorhombic to tetragonal transformation. One notable change in the structure as the oxygen atoms

are removed is that  $O_{Ba}$  atom moves away from the Cu- $O_2$  plane towards the Cu-O chain along the c-axis, so that the Cu atoms in the chain layer are more isolated and the interlayer coupling between Cu- $O_2$  planes are further reduced. There is a remarkable correlation between  $T_c$  and the oxygen vacancy concentration [3]  $T_c$  is around 90 K for  $0 \leq x \leq 0.2$  before decreasing sharply to 60 K, where it remains up to  $x = 0.5$ . Beyond  $x = 0.5$ ,  $T_c$  drops sharply and anti-ferromagnetic order has been observed near  $x = 0.7, 0.85$  and 1.

**Band Structure of  $YBa_2Cu_3O_7$ :** Band structure of  $YBa_2Cu_3O_7$  was first presented by Mattheiss and Hamann and by Massidda et al. [4]. Mattheiss and Hamann chose the Cu-O chain along the a-axis rather than the experimentally determined b-axis in their calculation. Since detailed neutron analysis was not available at the time. Hence the resulting band structure and subsequent calculations especially near  $E_F$  differ somewhat from that of Massidda et al due to slightly different Cu-O distance in the chain. They found that the electronic structure of  $YBa_2Cu_3O_7$  consists of occupied  $O_{2s}$  bands, away from  $E_F$ , centered at -15 eV,  $Ba_{5p}$  bands centered at -10 eV, as well as unoccupied  $Ba_{5d}$  and  $Y_{4d}$  bands above 3.4 eV. More than 60 % of their charge on the Cu-O chains are emphasized with the large symbols in Fig. 2.10a, while states with more than 80 % charge on the two Cu-O layers are shown in Fig. 2.10b. Among the four bands that cross  $E_F$ , two of them have the majority of their charge on the Cu- $O_2$  plane corresponding to one band for each layer. The Cu-O chains are responsible for the two other bands; a steep, band crossing  $E_F$ , which

is strongly dispersive only in the chain Direction, that is, along the X-S and  $\Gamma$ -Y directions, and a flat band just at  $E_F$  along the Y-S direction.

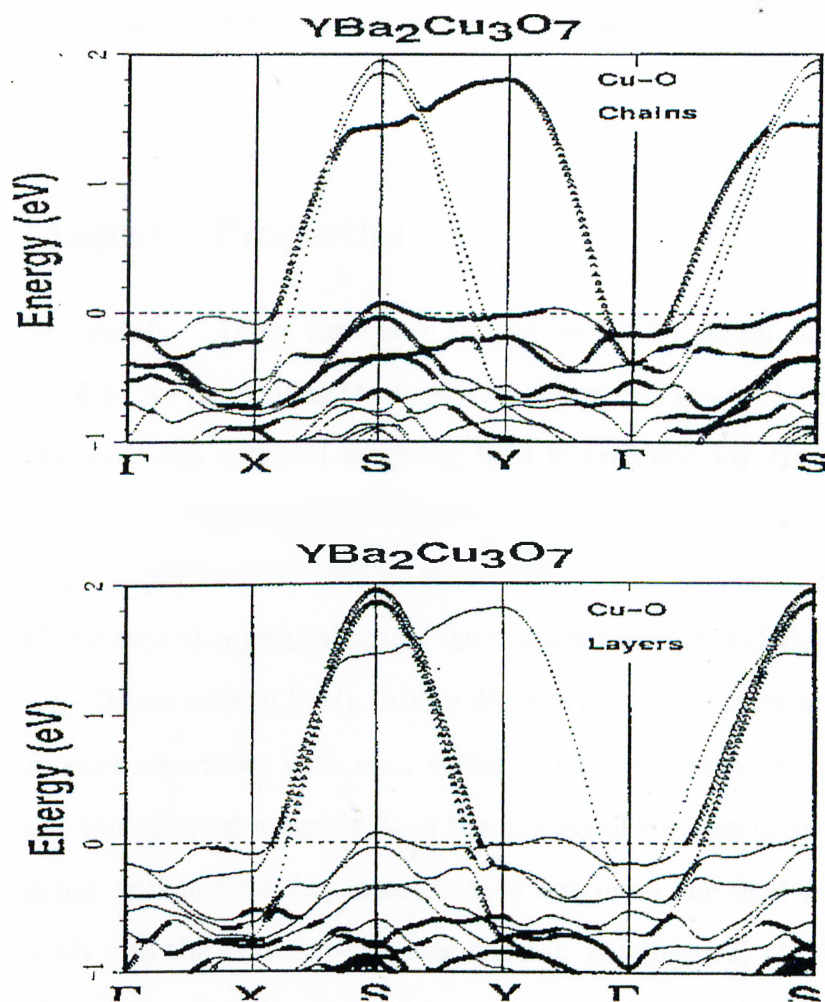


Figure 2.10: Energy bands of  $YBa_2Cu_3O_7$  along some high symmetry directions for  $k_z = 0$  of the orthorhombic BZ, from Krakauer and Pickett.

The one-dimensional nature of Cu-O chain as well as the two-dimensional nature of the Cu- $O_2$  planes was confirmed by the detailed analysis of the charge density distribution. The ionic Y and Ba atoms were found to act as electron donors and are not active participants otherwise, even if the

fully substituted material is ordered magnetically at very low temperature. The lack of conduction electron density near the Y site explains the stability of the high superconducting critical temperature when the isolated Y atoms are replaced by strongly magnetic rare-earth such as Gd or Er.

### 2.1.3 Magnetic Properties

**Type II Materials:** As we have seen in section 2.2.2 that on the basis of critical field we can divide the superconductor two types. In type I superconductor the external magnetic field is excluded for  $H < H_c$ , for  $H$  above  $H_c$ , the field penetrates the entire sample and superconductivity is completely destroyed as shown in the Fig. 2.3a. On the other hand for a type II superconductor, the magnetic field is excluded only for  $H < H_{c1}$  (lower critical field). Above  $H_{c1}$  the field penetrates in vortices, and fluxoid associated with each vortex is one flux quantum [5]. If we increase the external magnetic field the density of vortices increases until the upper critical field  $H_{c2}$  is reached, where upon the field penetrates uniformly and the material becomes normal. All High-  $T_c$  materials are type II superconductors.

**Penetration Depth:** Below  $H_c$  or  $H_{c1}$ , the external magnetic field is excluded from the bulk of the material by a persistent supercurrent in the surface region which induces a field that exactly cancels the applied field. The depth of this surface layer is called the penetration depth and is given by the London theory (section 2.2.2). The temperature dependence of the

penetration depth was first calculated with the two-fluid model, which yields;

$$\lambda(T) = \lambda(0)[1 - (T/T_c)^4]^{-1/2}. \quad (2.17)$$

where  $\lambda(0)$  is the value at absolute zero. Figure 2.11 is a schematic diagram of the behaviour of  $\lambda(T)$ , where it can be seen that (and also the coherence length) become very large near  $T_c$ .  $\lambda(T)$  can be directly measured for  $H < H_c$  or  $H_{c1}$  by using  $H_z = H_z(0) \exp(-x/\lambda L)$ .

The relation between the susceptibility  $\chi \equiv M/H$  and  $\lambda$  is given by;

$$\frac{\chi(T)}{\chi_0} = 1 - \frac{2\lambda}{d} \tanh(d/2\lambda). \quad (2.18)$$

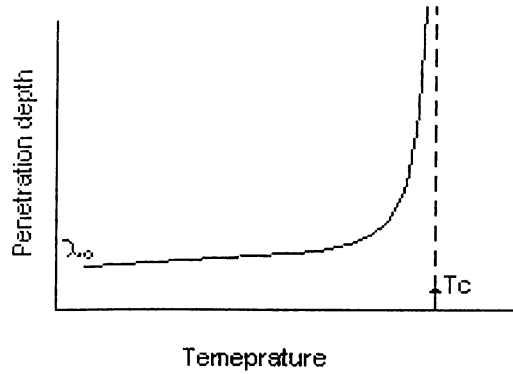


Figure 2.11: Dependence of penetration depth on the temperature.

Where  $\chi_0$  is the zero-temperature susceptibility and the hyperbolic tangent factor is a correction term close to unity for  $2/d \ll 1$  ( $d$  = thickness of the ab plane in the direction of c-axis for Y123). This equation shows how the susceptibility is reduced by the volume fraction of the sample penetrated by the field; the factor 2 arising from penetration on both

sides of the sample.

BCS predicts a temperature dependent penetration depth similar to the Eq. 2.17, with small changes in the strong-coupled limit, and small changes in the dirty limit.

$H_{c1}$  : Both  $H_{c1}$  and  $\lambda$  are closely related theoretically and in the way that they can be measured. For an isotropic superconductor, the lower critical field ( $H_{c1}$ ) is related to the penetration depth by,

$$H_{c1} \approx \phi_0/4\pi\lambda^2. \quad (2.19)$$

where  $\phi_0$  is the fluxoid quantum (GL free energy expression).

**Coherence Length and  $H_{c2}$  :** The coherence length is essentially the spatial range, or the decay distance, of the superconducting wavefunction. One may also think of it as the average diameter, or range, of a Cooper pair which for conventional superconductors, typically varies from ( $\sim 500$  to  $10^4 \text{ \AA}$ ). As we have discussed in Ginzburg-Landau theory an important parameter is  $\kappa = \lambda/\zeta$ , which relates the penetration depth to the coherence length. According to Abrikosov if  $\kappa > 1/\sqrt{2}$ , the superconductor is type II. For most elemental superconductors, the GL parameter  $\kappa \ll 1$  and therefore they are type I. The compound conventional superconductors and certainly all high-  $T_c$  materials are type II superconductors with

$\kappa \sim 100$  (extreme type II limit), and they are in the clean limit.

The measurement of coherence length ( $\zeta$ ) is difficult. It can be extracted from fluctuation contribution to the specific heat, susceptibility, or conductivity. However for the HTSC reliable values can be calculated by using the simple expression,

$$H_{c2} \approx \phi_0/4\pi\zeta^2, \quad (2.20)$$

where  $\phi_0$  is the fluxoid quantum.

## 2.2 HTSC physical and electrical properties, and the YBCO superconducting material

### 2.2.1 Overview of HTSC

Since the discovery of superconductivity in 1911 the search for superconductivity with a high transition temperature, namely above the liquid nitrogen temperature of 77K, has been one of the most challenging tasks. However, before 1986, the highest transition temperature achieved was only 23.2K for Nb<sub>3</sub>Ge (1973). In 1975 superconductivity was observed in BaPb<sub>1-x</sub>Bi<sub>x</sub>O<sub>3</sub> with critical temperature above 13K. This compound is the predecessor of the current high-T<sub>c</sub> superconductors.

In 1986 Bednorz and Muller, made a remarkable discovery. According to their point of views  $T_c$  can be raised by increasing the electron-phonon interaction by using Jahn-Teller effect. In 1986, they achieved superconductivity at around 30K in the Ba-La-Cu-O system the first materials in a class of cuprates (Cu oxides). The material they used was  $\text{La}_2\text{CuO}_4$  in which Ba, Sr or Ca were introduced to replace some of the La.

The superconducting phase was found to crystallize in the  $\text{K}_2\text{NiF}_4$  structure, which is a layered perovskite with a strongly anisotropic crystal structure. The Ba-doped materials is usually written as  $\text{La}_{2-x}\text{Ba}_x\text{CuO}_4$  and the superconducting properties depend strongly on the doping  $x$ . A record high  $T_c$  of nearly 40K was achieved in the material  $\text{La}_{1.85}\text{Ba}_{0.15}\text{CuO}_4$ .

Several months after the discovery of the Ba-La-Cu-O system, Y-Ba-Cu-O (YBCO) was discover with a  $T_c$  above 77K. Subsequent magnetic field effect measurements indicated a record-high upper critical field  $H_{c2} \sim 1430\text{T}$  at 0K for these compounds. The identification of the phase responsible for the superconductivity led to the chemical formula  $\text{YBa}_2\text{Cu}_3\text{O}_{7-\delta}$  and to the evidence for a layered structure. This crystal structure is an oxygen-defect perovskite and is very anisotropic. Cu-O planes and linear Cu-O chains along the b axis were found to exist.

With the exact stoichiometry and the general structure of the superconducting phase determined, attempts were made to replace Y by the rare-earth elements to examine their role in high-temperature superconductivity. Thus a new class of superconductors,  $\text{ABa}_2\text{Cu}_3\text{O}_{7-\delta}$  with  $A = \text{Y, La, Nd, Sm, Eu, Gd}$ ,



$H_o$ , Er or Lu, with  $T_c$  above 90K was discovered.

Since 1988, many more new compounds as well as new classes of compounds are discovered. Notable among these are the Bi-Sr-Cu-O and the Bi-Sr-Ca-Cu-O (BSCCO) compounds with transition temperatures up to 115K, and the Tl-Ba-Ca-Cu-O (TBCCO) compounds, with transition temperatures up to 125K. The general formula for the thallium compounds is  $Tl_mBa_2Ca_{n-1}Cu_nO_{2n+m+2}$  where  $n$  denotes the numbers of Cu atoms and  $m$  is the number of Tl atoms.  $T_c$  increases with increasing number for  $CuO_2$  planes in the elementary unit cell which is the general rule for all cuprate compounds. With time, the discovery of other cuprates has resulted in a large number of superconducting compounds and a maximum  $T_c$  of about 140K.

There are many other widely known high- $T_c$  superconductors. In the lead-substituted TBCCO or BSCCO compounds Tl or Bi are partially substituted by Pb, such that the chemical formula begins  $(Tl_xPb_{1-x}...)$ . In mercury compounds Tl is substituted by Hg (Putalin et al. 1993). The resulting compound  $HgBa_2CuO_{4+\delta}$  has  $T_c = 94K$ , which is exceptionally high for a single- $CuO_2$ -layer compound. In oxycarbonates a carbonate group ( $CO_3$ ) is introduced in the conventional copper oxide configuration which results in the general chemical formula  $(Y,Ca)_n(Ba,Sr)_{2n}Cu_{3n-1}(CO_3)O_{7n-3}$  (Raveau et al 1993) with typical  $T_c$  values below 77K.

$\text{BaPb}_{0.75}\text{Bi}_{0.25}\text{O}_3$	$T_c = 12K$	BPBO
$\text{La}_{1.85}\text{Ba}_{0.15}\text{CuO}_4$	$T_c = 36K$	LBCO
$\text{YBa}_2\text{Cu}_3\text{O}_7$	$T_c = 90K$	YBCO
$\text{Tl}_2\text{Ba}_2\text{Ca}_2\text{Cu}_3\text{O}_{10}$	$T_c = 120K$	TBCO
$\text{HgBaCaCuO}$	$T_c = 133K$	HBCO

Table 2.1: Memorable steps in the history of Superconductor structures.

The family of high- $T_c$  superconductors is very large. Despite high- $T_c$  compounds having many different structures with a variety of chemical substitutions the general property is the presence of the copper oxide layers.

## 2.2.2 Basic Structure

### Y123

High  $T_c$  denotes superconductivity in material, chiefly oxides, with high transition temperatures, accompanied by high critical currents and magnetic fields. Memorable steps in the adaced include:

The crystal structures of these materials, except for BPBO, are oxygen-defect modifications of the perovskite structure, with about one-third of the oxygen positions vacant. The primitive cell is developed from that of a tetragonal perovskite tripled along the  $c$  axis. Per formula unit of  $\text{YBa}_2\text{Cu}_3\text{O}_7$ , the positive ion valences based on  $Y^{+3}$ ,  $Ba^{+2}$ ,  $Cu^{+2}$  are  $3 \times 1 + 2 \times 2 + 2 \times 3 = 13$  and the negative (oxygen) valency is  $-2$  times  $7 = -14$ .

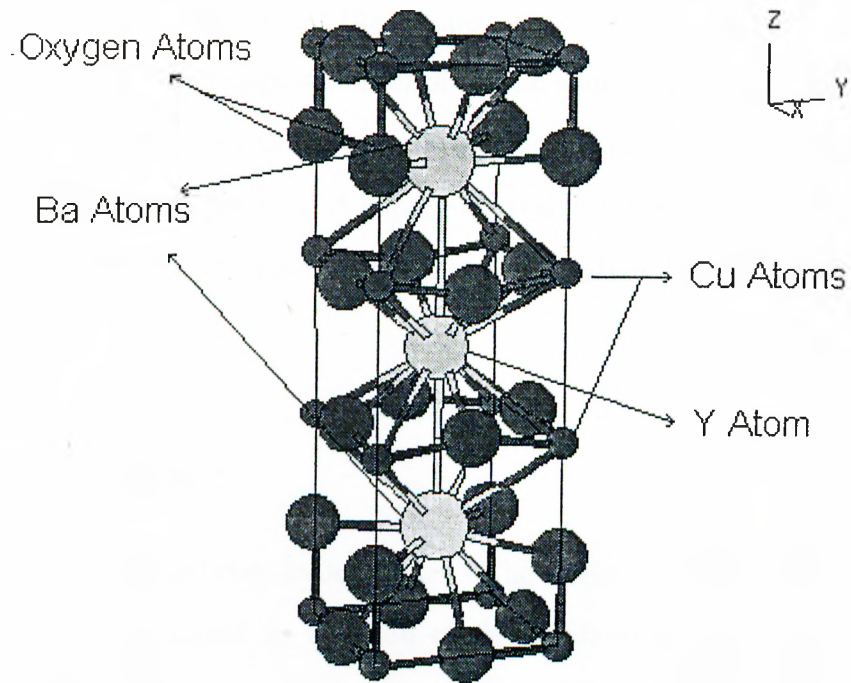


Figure 2.12: Experimental set-up for laser ablation deposition.

The quasitragonal or orthorhombic cell dimensions of YBCO are, in nm,  $a = 0.388$ ,  $b = 0.384$ ,  $c = 1.163$ , with cell volume  $0.173 \text{ nm}^3$ ; if there is one excess charge carrier in this volume the carrier concentration is  $n_0 = 5.77 \times 10^{21} \text{ cm}^{-3}$ . The excess carriers typically are holes embedded in doped antiferromagnetic insulators.

The Parallel sheets of  $\text{CuO}_2$  are a structural feature of all HTS. In YBCO crystal structure shown in Figure 2.12, the  $\text{CuO}_2$  planes are parallel to the plane of the  $ab$  axes in the orthorhombic primitive cell. Two of these planes, those through the interior of the cell, are the dominant conducting pathways. The oxygen content per cell can be changed reversibly from 7.0 to 6.0 atoms, simply by pumping oxygen in and out of the parallel chains of  $\text{CuO}$  that run

along the b-axis of the figure. At the composition  $YBa_2Cu_3O_6$  the crystal is an insulator, with antiferromagnetic order of the Cu spins. An increase in the oxygen content above  $O_{6.5}$  makes the crystal metallic and non-magnetic; the crystal is superconducting above  $O_{6.64}$ . A charge-neutral formula for  $YBa_2Cu_3O_7$  can be written as  $YBa_2(Cu^{2+})_2(Cu^{3+})(O_7^{2-})$  or as  $YBa_2(Cu^{2+})_3(O^{2-})_6(O^-)$ . [5]

### 2.2.3 Resistance

**Conventional Resistivity Behaviour:** The electric resistivity of most metals is dominated by collision of the conduction electrons with lattice phonons at room temperature and by collisions with impurity atoms and mechanical imperfections in the lattice at liquid helium temperature. The net overall resistivity is given by:

$$\rho = \rho_l + \rho_i, \quad (2.21)$$

where  $\rho_l$  is the resistivity caused by the thermal phonons and  $\rho_i$  is the resistivity caused by scattering of the electrons due to static defects that disturb the periodicity of the lattice.

The temperature dependency of the electrical resistivity is proportional to the rate at which an electron collides with thermal phonons and thermal electrons. Concentration of phonons is proportional to the collision rate. One simple limit is at temperatures over the Debye temperature  $\theta_D$ : [6] here the phonon concentration is proportional to the temperature

T, so that  $\rho \propto T$  for  $T > \theta_D$ .

At low temperatures, however, we cannot analyze the electron scattering in terms of classical departures of atoms from their equilibrium position, rather, scattering from their quantized lattice vibration, which needs to be taken into account. Umklapp scattering [6] accounts for most of electrical resistance at low temperatures in which phonon contribution is due to the phonons of the type;

$$K_i + q \leftrightarrow K_f, \quad (2.22)$$

where  $K_i$  and  $K_f$  are initial and final wave vectors respectively and 'q' is phonon wave vector. Hence with low temperature range, both small and conservative crystal momentum strongly reduce the possible channels for electron scattering ultimately reducing the resistance

$$\rho \propto T^5 \quad \text{where } T \gg 0.2\theta. \quad (2.23)$$

The interaction of electrons with other deviations from perfect translational symmetry also gives rise to electron scattering and finite resistance. So at low temperatures a resistivity of the form

$$\rho \approx C + DT^5 \quad (2.24)$$

is expected. Where C is called the residual resistivity.

Grüneisen-Bloch obtained an analytic result for the normal scattering as:

$$\rho_l \propto \frac{T^5}{\theta^6} \quad (2.25)$$

at very low temperature. These normal processes contribute to the resistivity in all metals.

**Resistivity of High-  $T_c$  materials:** The effect on the resistance by changing the temperature for high temperature superconductors (HTSC) is different. The resistivity of single crystal Y123 perpendicular to c-axis is shown in Fig. 2.13 where and is measured separately.

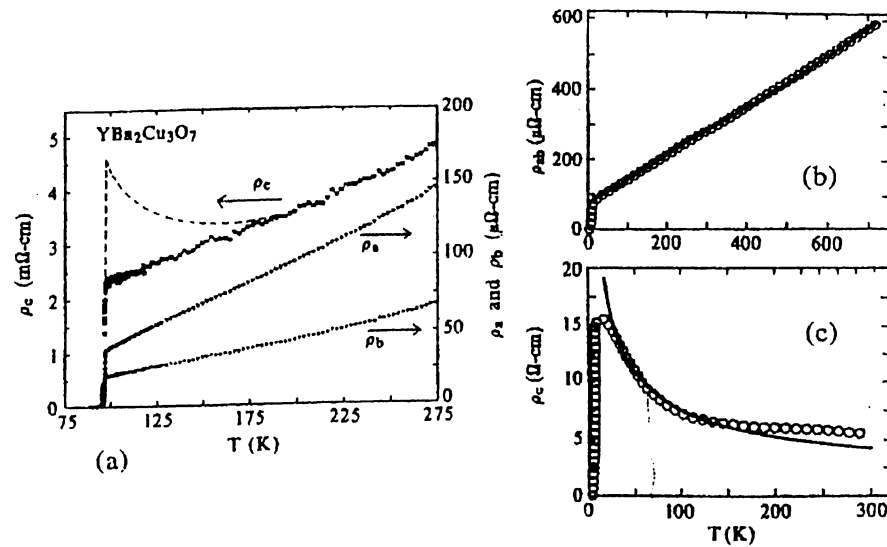


Figure 2.13: (a) The a-, b-, c-direction resistivities. { For detail, see T.A.Friedmann, Phys. Rev. B42, 6217(1990)}. The dashed curve is a schematic result for  $\rho_c$ . (b) and (c)  $\rho_{ab}$  and  $\rho_c$  for 2-Bi ( $n=1$ ) superconductor with  $T_c$  (7K). { For details, see S. Marten, Phys. Rev. B41,846(1990)}.

We observe the behaviour to be linear with temperature. But at low temperatures, resistivity is closer to the relation,  $\rho \approx C + DT^5$  while the resistivity for c-axis is somewhat controversial. It is interesting to note that most of the high-  $T_c$  crystals and oriented films yield similar B values  $\sim 1\mu\Omega cm/K$ . This suggests common scattering mechanism in

Cu-O planes for ordinary metals.(we only expect linear  $\rho_{ab}$  behaviour for  $T \gg 0.2$  but here understanding most is different). One explanation of the linear T behavior has been found by considering the resistivity to be two-dimensional(i.e., ab plane) and due to two carries that interacts with each other.

Early results of Hall coefficient measurements on HTSC material were presented in a review article by Tanaka. For Y-Ba-Cu-O,  $R_H$  increases with decreasing temperature and with decreasing oxygen content. Early single crystal measurement show linear normal state resistance in ab-plane and semiconductor behaviour in the c direction and may be taken as indication of quite good crystal quality although the resistivity is larger than that for the current best crystals. The hall coefficient for magnetic field along the c-axis show that  $1/R_H$  is linear in T. For a field applied in the ab-plane the Hall coefficient is negative or electron like and is  $-2 \times 10^4$  cm/C.

For Bi-Sr-Ca-Cu-O (a mixture of 2212 and 2223 phases) the Hall coefficient is found to be positive and decreasing from 5 to  $3(\times 10^{-9}m^3/c)$  between 120 to 280K. In the case of Tl-Ba-Ca-Cu-O (2223 phase) positive  $R_H$  decreasing from 5 to  $3(\times 10^{-9}m^3/c)$  is measured by One group. [5]

These results, are fairly consistent in indicating that the carriers are holes in the ab plane of the Y-Ba-Cu-O and the Bi-Sr-Ca-Cu-O materials at temperatures just above  $T_c$ . Extrapolation to below  $T_c$  is assumed. The

Hall coefficient in a single crystal suggest electron transport in the c direction for Y-Ba-Cu-O and for newer materials class,  $Nd_{2-x}Ce_xCuO_{4-y}$ ; the indication of electron pairing is also suggested by these measurements.

## 2.2.4 Magnetism

**Insulator Phase:** The Cu ion magnetic moments are ordered antiferromagnetically in the insulator phases of all of the high-  $T_c$  materials at relatively high temperatures. Within a Cu-O plane, the nearest-neighbour Cu moments are aligned in opposite direction.

To understand the effects clearly, we see some examples: Fig. 2.14 shows the ordering of the Cu magnetic moment of La ( $n=1$ ), with Neel temperature  $T_N \approx 340K$ . Where Neel Temperature is defined as the temperature at which Ferimagnetic and antiferromagnetic materials become paramagnetic. While for Y123 insulating ( $T_N \approx 500K$ ) the anti-ferromagnetic ordering of the magnetic moments on the planer Cu atoms is essentially the same as in La ( $n=1$ ); adjacent spins in the plane are anti-parallel.

Many of the other high-  $T_c$  materials also can be made insulating for example, by partially replacing the  $Ca^{2+}$  between the Cu-O planes with  $Y^{3+}$ , or vice versa, depending whether one starts with 2-Tl(n) or Y123.

**Superconducting Phase:** Anti-ferromagnetic order is observed below  $T_c$  without drastically affecting the superconductivity in some rather special conventional superconductors. In high-  $T_c$  materials, the coexistence of



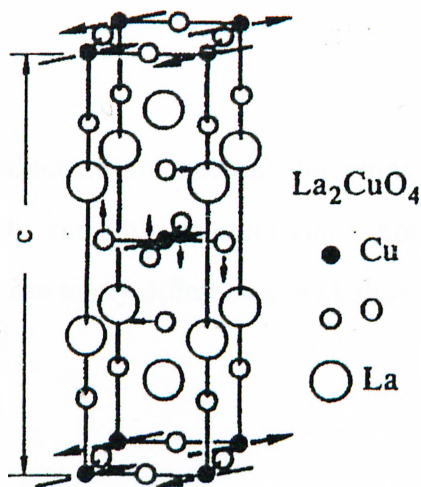


Figure 2.14: A unit cell of  $\text{La}_2\text{CuO}_4$ . The larger black arrows in the Cu atoms denote the spin directions below  $T_N$ . The smaller arrows attached to the O atoms surrounding the central Cu atom indicate the tilts that cause the tetragonal material to become orthorhombic at low temperatures.

anti-ferromagnetism at temperatures well below  $T_c$  is not unusual. We may take Y123 as an example. Rare earth atoms can replace the Y atoms with essentially no effect on  $T_c$ . In fact,  $T_c$  increases slightly, perhaps up to 95K, which is probably associated with ionic-size effects.

For conventional superconductors, magnetic impurities or external magnetic fields tend to destroy superconductivity. This also tends to imply that a magnetic moment on the Cu atom site and superconductivity are mutually exclusive. On the other hand, it can be argued that the close proximity of anti-ferromagnetic and superconductive states may indicate a common origin, or at least a closely related origin. This thought has led to the idea, currently under study, that the electron-electron attraction required to form Cooper pairs might arise not from phonons, but from some kind of anti-ferromagnetic magnons (i.e., magnon-mediated

pairing).

Some of superconductors are not anti-ferromagnetic in their insulating phases like  $BaBiO_3$ , and superconductivity is not absorbed above 30K. In such superconductors many different aspect show that pairing mechanism is different.

## 2.3 Applications

### 2.3.1 Introduction

Since the discovery of high-temperature superconductors, tremendous efforts and considerable research have been taken in the field to understand their properties for the use of these materials in applications. In general, applications of superconductors can be divided into two types, large scale and small scale.

**Large-scale applications**, in which large currents and long lengths of superconducting cables are required in working environments where the magnetic field may be several tesla ( $1 \text{ T} = 10^4 \text{ Oe}$ ). Examples include magnets and power transmission lines, transformers, and generators where current densities of at least  $10^5 \text{ amps/cm}$  are required. The second type of application is **small-scale applications**, where the required currents are much smaller, and more specialised properties of superconductors tend to be exploited. Example include detection systems, and analog and digital process; millimeter wave mixers, amplifiers, picosecond sampling circuits, ultra-precise voltage standards, very

sensitive magnetometers, dispersive delay lines and possible low power linear A/D converters.

The application point of view for high-temperature superconductors is extremely exciting on the basis of the fact that these superconducting materials have a working range 77K (i.e.  $T_c$  77K). Hence inexpensive and easy-to-use liquid nitrogen can be used as a coolant. Moreover, high-  $T_c$  materials are all type II superconductors with high  $H_{c2}$  values. As high-  $T_c$  materials are not ductile hence making it very difficult to form wires, a pre-requisite for many applications their impact is still ambiguous.

### 2.3.2 Large-scale applications

For many of the large-scale applications, superconductors are advantageous over normal metals only because of lower resistance and hence smaller power loss as energy consumption in the world and electrical energy in particular are staggering. Hence, elimination of even a small fraction of the resistive load can have significant impact. On the other hand manufacturing the strong magnetic fields above 2 tesla by using high-  $T_c$  superconductors could eliminate the iron cores in motors, generators, and transformers, which will result in reduced size, weight, and losses from the iron cores.

Eventually, the electric utility industry may be one the largest user of superconductor by utilization of superconductors in transmission cables, generators,

and energy storage.

**Wires and superconducting Magnets** As we have discussed in the first section, three important parameters,  $T_c$ ,  $H_{c2}$ , and  $J_c$  can characterize a superconductor. The former two characters for the high-  $T_c$  superconductors are very large. The former two are very large; it is the latter quantity that is still problematic. Wires of silver sheath 2-Bi (n=3) can now be made with properties that are superior to those of conventional superconductors at 4K to 20 K and at high magnetic field. It might be anticipated that laboratory high field magnetics with this wire will replace those presently sold that use conventional superconductors. These wires can be used in energy storage devices, electric motor windings, electromagnetic, pumps, and magnets for magnetic separation, magnetic heat pumps, and others.

While on the other hand in all high frequency and high performance applications of superconducting devices, there is a requirement to transfer signal from one point to another. A unique important advantage of superconductivity is the prospect of doing this via transmission lines of very high bandwidth, which have exceptionally low loss and dispersion. In addition, this seems feasible for physically small and closely packed configurations, which normally would result in unacceptable level of cross talk between the lines. Finally, because of these features one can even build long delay lines and deliberately coupled lines in order to perform

some important signal processing functions.

**Levitation:** This is, perhaps, one instance in which large-scale applications of superconductivity seem close to becoming reality. Incidentally, non-superconducting magnets could be used in trains as well, as in German maglev train concept. However, the Japanese prototypes and most of the American feasibility studies employ superconducting technology.

There are two major lines of design currently pursued by Japanese manufacturers. Both schemes essentially use magnetic forces to lift a train off the railroad tracks. In Attractive levitation train scheme, as shown in Figure 2.15, a T shape rail lies in the middle of two conventional rails.

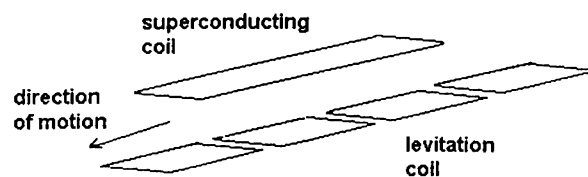


Figure 2.15: First way used to levitate the train.

The train jugs the T rail from beneath, where superconducting magnets are placed (the magnets are located on the train). These superconducting magnets generate a magnetic field, which attracts the rail; since the rail is rigidly bolted to the ground, it is the train that moves toward the rail, thus lifting itself away from the ground. A delicate balance between downward gravitational and upward magnetic forces has to be achieved by carefully adjusting the magnetic field; otherwise the train would slam into the rail. In the second scheme, the repulsive levitation train, there are nonsuperconducting coils on the each side of the railroad bed. Superconducting coils lie just above on the train. As the train moves, the

magnetic field generated by the superconducting coils on the train passes over the coils on the ground. The magnetic field generated by the coils in the railbed has the polarity needed to oppose the magnetic field generated on the train. Thus lifting the train from the tracks, as the pole of a magnet would repel the end of another magnet with the same polarity.

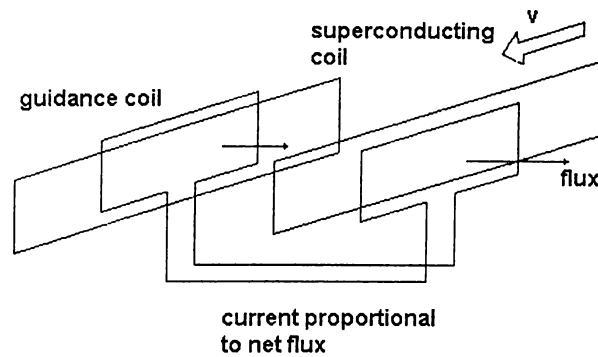


Figure 2.16: Second possible technique for magnetic laveitaton for train.

### 2.3.3 Small-scale applications

The first attempt is attributable to Dudley Buck for the invention of the cryotron switching device for digital computing. This device demonstrated to work, was later modified and developed into a manufacturable form and thus becoming an incipient technology. Its inherent speed limitations were demolished by the discovery of superconductive tunneling, quasi-particle techniques, which launched a major attempt to evaluate devices, which exploited these phenomena and then create a technology. In this section we will try to investigate some of the small-scale application to superconductors.

## SQUIDS:

Superconducting Quantum Interference Devices (SQUIDS) are among the first major applications of High-  $T_c$  Superconductivity (HTS). SQUIDS may be considered as model circuits for superconducting electronics because they contain all the vital components (Josephson junctions, resistors, capacitors, inductors, striplines, crossovers, vias). They require the basic process technologies necessary for even highly complex cryoelectronic circuits. This, customising HTS SQUIDS, will be the essential first step in establishing any electronic applications of HTS.

SQUID is a magnetic flux sensor, which converts magnetic flux into voltage. There are two types of SQUIDS: dc-SQUID and rf-SQUID. A dc-SQUID consists of two Josephson junctions interrupting a superconducting ring, as shown in Figure 2.17a. The prefix "dc" implies that the device is biased with a direct current. The total critical current of a dc-SQUID varies periodically with the magnetic flux passing through the ring, with a period of one flux quantum,

$$\phi_0 = \frac{h}{2e} (\approx 2.07 \times 10^{-7} \text{ Gauss} - \text{cm}^2); \quad (2.26)$$

$h$  is Planck's constant and  $e$ , the electronic charge. Figure 2.17b shows I-V characteristics of the SQUID for  $\phi = n\phi_0$  and  $\phi = (n + 1/2)\phi_0$  where  $n = 0, 1, 2, \dots$ . Maximum change in the critical current of the SQUID is obtained by applying a flux of  $(n + 1/2)\phi_0$ . If the dc-SQUID is biased with a constant current, which is greater than the critical current of the SQUID, the voltage

drop across the SQUID also varies periodically with flux (Figure 2.17c).

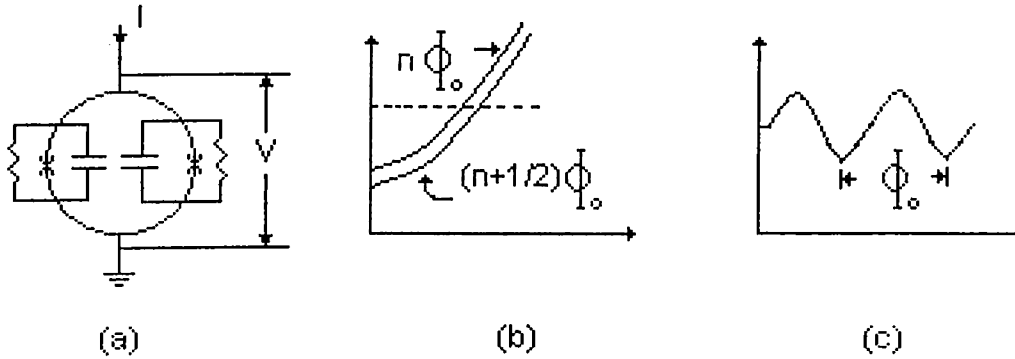


Figure 2.17: (a) Schematic diagram of a dc-SQUID, (b) I-V characteristic for  $\phi = n\phi_0$  and  $\phi = (n + 1/2)\phi_0$ , (c)  $V - \phi$  characteristic for a constant bias current.

An rf-SQUID consists of a superconducting loop interrupted by Josephson junction (Figure 2.18a). The prefix "rf" implies that the device is biased with a radio frequency signal. The SQUID is inductively coupled to a tank circuit, which is driven, with a rf current. The reflected signal is amplified using a low noise amplifier and is detected by a diode detector. Figure 2.18b shows the variation of the peak amplitude of the voltage,  $V_{rf}$ , across the tank circuit versus the peak amplitude of the  $I_{rf}$ . For an applied flux  $\phi = n\phi_0$ , the characteristic consists of a set of steps and risers. Here  $n$  is an integer. As one increases (or decreases) the flux, each step splits into two, with a maximum separation in voltage occurring for a flux of  $(n + 1/2)\phi_0$ . As the flux is further increased to  $(n + 1)\phi_0$  or decreased to  $(n - 1)\phi_0$ , the  $V_{rf} - I_{rf}$  curve is restored to the solid line in Figure 2.18b. Thus, at a constant value of  $I_{rf}$ , the period of oscillations being  $\phi_0$  Figure 2.18c. The amplitude of the triangular voltage-flux ( $V-\phi$ ) oscillations gradually decreases, becomes zero and then again starts increasing to attain the maximum value. The triangular pattern,



now have its maxima at points where the old characteristic had its minima. This phenomenon, known as the "phase reversal" is due to the change of rf-bias current from one step to the next higher step in the  $V_{rf} - I_{rf}$  characteristic.

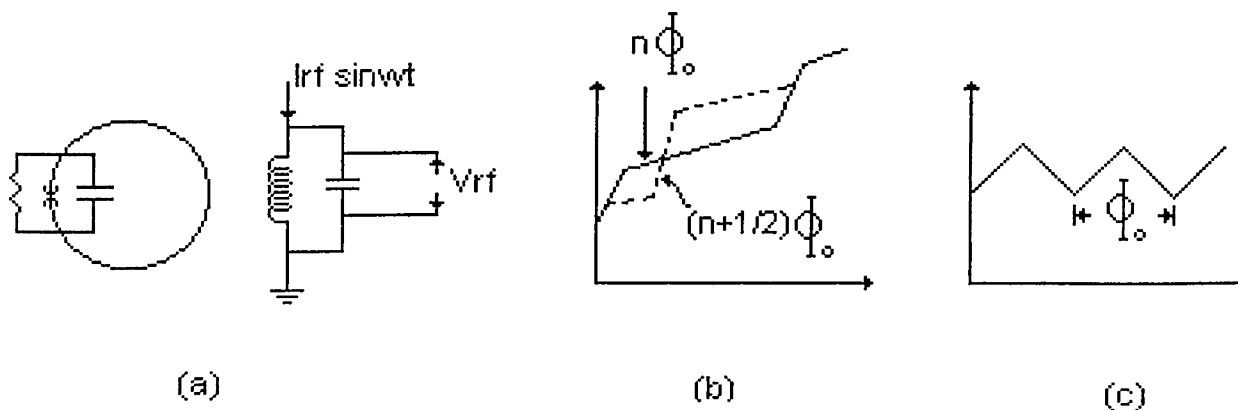


Figure 2.18: (a) Schematic representation of an rf-SQUID, (b) peak amplitude of  $V_{rf}$  versus  $I_{rf}$  for  $\phi = n\phi_0$  and  $\phi = (n + 1/2)\phi_0$  (c) peak amplitude of  $V_{rf}$  vs. flux for fixed  $I_{rf}$ .

Magnetic field sensitivity of a SQUID can be increased by using a superconducting flux transformer. It is a closed superconducting loop consisting of a large area pick-up coil connected in series with a small area input coil, which is inductively coupled to the SQUID as shown in Figure 2.19a. For an efficient flux transformer, inductance ( $L_p$ ) of the pick up coil should be nearly equal to the inductance ( $L_i$ ) of the input coil. Thus the input coil should be multi-turn. By a proper design of the flux transformer, field sensitivity of about  $10^{-15} T/\sqrt{Hz}$  is achieved for Nb based low- $T_c$  dc-SQUID.

An important extension of flux transformer is a gradiometer used to measure field gradient as shown in Figure 2.19b. This arrangement enables to

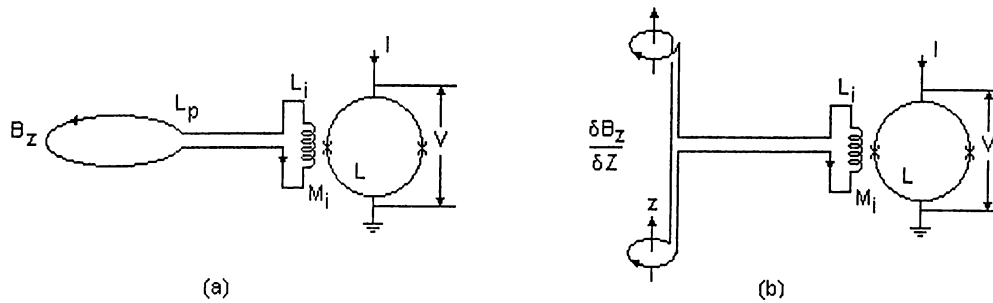


Figure 2.19: (a) Superconducting flux transformer for measuring a field  $B_z$ ; (b) superconducting first order gradiometer for measuring a field gradient  $\frac{\partial B_z}{\partial z}$ ;  $L_i$  is inductance of the input coil of the transformer and  $M_i$  is mutual inductance between the input coil and the SQUID loop.

measure minutes localized magnetic signals, as low as  $10^{-13}$  T even when a uniform magnetic field of  $10^{-8}$  T is present. For a uniform magnetic field,  $B_z$ , equal and opposite fluxes in the gradiometer produce no signal to the SQUID, whereas gradient  $\frac{\partial B_z}{\partial z}$  links a net flux to the transformer, producing a signal in the SQUID. Since gradients from a magnetic dipole fall off as  $1/r^4$ , the gradiometer discriminates magnetic interference arising from distant sources in favor of locally generated signals.

### Other Superconductor applications

Here are listed some other applications;

- Superconducting edge transition Bolometers.
- Antenna coupled superconducting bolometers.
- Josephson junction bolometers.
- Kinetic inductance bolometer.
- Magnetic-susceptibility bolometer.

- Intrinsic superconducting thermal detector.
- Microwave Application (Passive Device ):
- Superconducting High-Q Resonators (strip-line & Ring resonators).
- Superconducting Resonator-Stabilized Oscillators.
- Superconducting Bandpass Filters (High-Q & Small Size). Resonators -based Filters
- Superconducting Delay Lines (Tapped Delay Lines & Chirp Filters).
- Superconducting Antenna Feed Networks.
- Superconducting Spiral Antenna.
- Superconducting Multichip Modules.
- Active HTSC Microwave Devices (Superconducting Flux-Flow Transistors (SFFT))
- Hybrid Superconductor/Semiconductor devices & systems.
- Superconducting Circuits (GHz A/D Units. Memory Cells, Flip-Flops & logic circuits, Neural Networks, 10GHz Oscilloscope, Picovoltmeter, ...)
- Superconducting Maglev Trains (Magnetic Levitation: Electromagnetic systems(- EMS) & Electrodynamic systems (EDS)).
- Superconducting Magnetic Energy Storage (SMES for momentary outage, Stabilization & energy storage).
- Super ship (Magneto hydrodynamic (MHD) Ship Propulsion).
- Superconducting Bearings (Flywheel Energy Storage, ...)
- Superconducting Super Collider (SSC) & Synchrotron Magnets.
- Superconducting Refrigeration & Supercooling (Magnetic Refrigeration).
- Superconducting Electrical Motors & Super cooling (Magnetic Refrigeration).
- Superconducting Fault Current Limbers.

- Superconducting Transmission Lines.

The superconducting radiation detector which are the focus of this work is discussed thoroughly in the next chapter.

## Chapter 3

# DETECTORS AND DETECTORS PARAMETERS

### 3.1 Infrared Radiation

Electromagnetic radiations having a wavelength in the range from  $c.75 \times 10^{-6}$  cm to  $c.100,000 \times 10^{-6}$  cm (0.000075–0.1 cm). Infrared rays thus occupy that part of the electromagnetic spectrum with a frequency less than that of visible light and greater than that of most radio waves, although there is some overlap.

The name infrared means “below the red,” i.e., beyond the red, or lower-frequency (longer wavelength), end of the visible spectrum. Infrared radiation is thermal, or heat, radiation. It was first discovered in 1800 by Sir William Herschel, who was attempting to determine the part of the visible spectrum

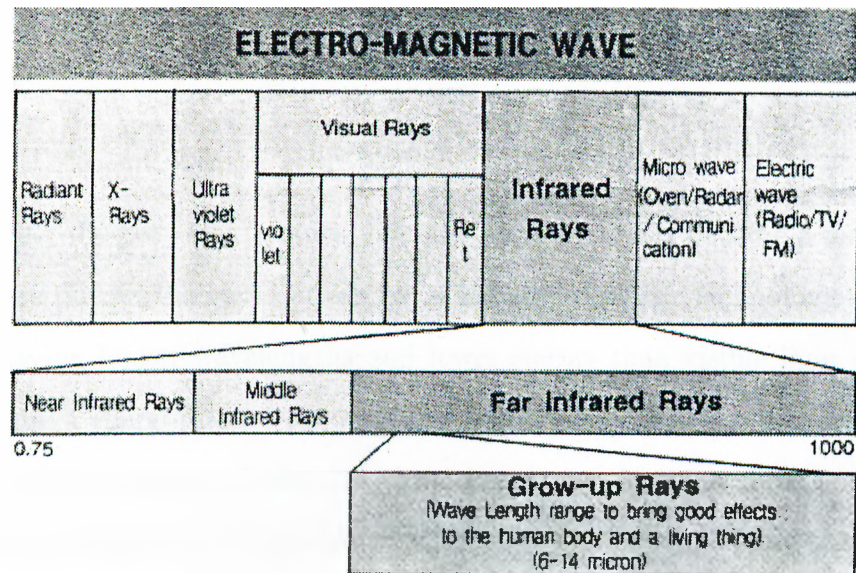


Figure 3.1: Infrared radiation spectrum.

with the minimum associated heat in connection with astronomical observations he was making. In 1847, A. H. L. Fizeau and J. B. L. Foucault showed that infrared radiation has the same properties as visible light, being reflected, refracted, and capable of forming an interference pattern. Infrared radiation is typically produced by objects whose temperature is above.

There are many applications of infrared radiation. In the field of infrared astronomy, new and fascinating discoveries are being made about the Universe. Medical infrared imaging is a very useful diagnostic tool. Infrared cameras are used for police and security work as well as in fire fighting and in the military. Infrared imaging is used to detect heat loss in buildings and in testing electronic systems. Infrared satellites have been used to monitor the Earth's weather, to study vegetation patterns, and to study geology and ocean temperatures. In industry, infrared spectroscopy forms an increasingly important part of metal

and alloy research, and infrared photography is used to regulate the quality of products.

During the past few decades, infrared astronomy has become a major field of science due to the rapid advances in infrared detector technology. Infrared light, having longer wavelengths and lower energy than visible light does not have enough energy to interact with the photographic plates, which are used in visible light astronomy. Instead we have to rely on electronic devices to detect radiation. Early infrared detection was done by thermocouples and thermopiles (a group of thermocouples combined in one cell).

In the 1950's astronomers started to use Lead-sulphide (PbS) detectors to study infrared radiation in the 1 to 4 micron range. A major breakthrough came in 1961, with the development of the germanium bolometer. This instrument was hundreds of times more sensitive than previous detectors and was capable of detecting all infrared wavelengths. To study a particular wavelength of infrared emission filters can be used, which filter out all but the desired wavelengths.

Infrared detector technology continues to advance at a rapid rate. Now we use InSb and HgCdTe detectors for the 1 to 5 micron ranges. The development of infrared array detectors in the 1980's caused another giant leap in the sensitivity of infrared observations. Basically a detector array is a combination of several single detectors. These arrays allow to produce images containing

tens of thousands of pixels at the same time. Infrared arrays have been used on several infrared satellite missions.

## 3.2 Detector Parameters

### 3.2.1 Responsivity

The basic function of the detector is to convert radiant input to an output signal of some convenient type. The responsivity  $\mathfrak{R}$  is the ratio between the output signal and the radiant input. Low responsivity is not itself an insurmountable problem; it is always possible to increase signal levels by adding amplifiers to the signal processing. A limitation that cannot be overcome with additional gain is the presence of noise.

### 3.2.2 Noise

When the electrical output signal is randomly fluctuating, may it be voltage, current or power, it is called 'Noise'. The noise level of the detector determines the limit to the sensitivity, and it must be considered in order to determine the detectable incident power. In general we can subdivide the noise associated with a detector system as,

#### Photon Noise

- a) Noise due to the radiation signal.



- b) Noise due to background radiation.

**Intrinsic Noise:**

- a) Johnson Noise.
- b) Shot Noise.
- c) Generation-Recombination Noise.
- d)  $1/f$  Noise.
- e) Temperature Fluctuations (phonon) noise.
- f) Microphonics.

**Post-detector Electronic Noise:**

- a) Johnson Noise.
- b) Shot Noise.
- c) Generation -Recombination 'Noise.
- d)  $1/f$  Noise .
- e) Temperature Fluctuations (phonon) noise.
- f) Popcorn Noise.
- g) Microphonics.

Three major noises are present in photoconductive applications namely, 1/f noise, Johnson noise, and generation-recombination noise. The 1/f dependence holds for noise power, the noise voltage varying as one over the square root of frequency. The empirical formula for mean square noise current is;

$$\bar{i}_{1/f}^2 = \frac{B_1 I_b^2 \Delta f}{f^\beta}, \quad (3.1)$$

where  $B_1$  is proportionality constant,  $I_b$  is DC current through detector  $\Delta f$  is electrical bandwidth,  $f$  is the frequency and  $\beta$  is constant which is usually taken as 1.

Johnson noise is caused by the thermal agitation of electrons in a resistor. It is also called Nyquist or thermal noise. The Johnson noise is calculated as,

$$\bar{i}_J^2 = \frac{4K_B T \Delta f}{R_d}, \quad (3.2)$$

where  $K_B$  is the Boltzmann constant,  $T$  is temperature  $R_d$  is detector resistance and  $\Delta f$  is electrical bandwidth.

Fluctuations in generation rates, recombination rates and/or trapping rates are responsible for wavering in free carrier current concentration hence giving rise to the generation-recombination noise. The expression for the combination of G-R noise due to both photon and thermal excitation is given by

$$\bar{i}_{GR}^2 = 4q(\eta E_P^B A_d G^2 + g_{th} G^2) \Delta f, \quad (3.3)$$

where  $q$  is the electron charge,  $\eta$  is quantum efficiency,  $E_p^B$  is photon irradiance and  $A_d$  is detector area,  $G$  is a photoconductive gain, and  $G_{th}$  is the thermal generation rate.

**Noise in YBCO superconductors bolometers:** Noise characteristics, which depend on the operating temperatures, bias current, and modulation frequency, determine the ultimate sensitivity of a superconducting bolometer. In bolometers we can subdivide the noise in two three types which are based on the experimental results. [7]

**(a) Type (i) noise:** Upon investigating the effect of bias current on the noise above  $T_{c\_onset}$  region (the normal region), the noise was revealed to be consistent with Johnson noise. Low frequency range also makes the noise dependent on the bias current hence accounting the fluctuations in the material. For bias current of (about 200  $\text{\AA}$ ), the noise voltages are linearly proportional to bias current which suggests that the resistance fluctuation is not dependent on bias current. Since we are aware of the transition temperature, the Cooper pairs having a finite life time, and the conductivity being the sum of the conductivity of normal electrons and of Cooper pairs, the conductivity fluctuation in this region can be interpreted to be due to fluctuation in the density of the carriers.

**(b) Type (ii) noise:** A second noise phenomena is revealed upon observing the bias current - temperature relationship at about  $T_{c\_zero}$ . When

bias current is increased the noise region in the temperature widens, and this region shifts to lower temperatures at higher currents. The reason may arise from the presence of weak links and associated superconductor-normal-superconductor (SNS) junctions. Whereas noise region broadening in this temperature region with increasing current can be due to the effect of the bias current on the weak links of the film. This should also occur with increasing magnetic field.

(c) **Type (iii) noise:** For less granular sample yet another noise characteristics are observed at temperature right below  $T_{c\_zero}$ . This kind of noise peaks right below the onset temperature of the excess noise. This noise peak below  $T_{c\_zero}$  increases with increasing bias current, but approaches zero for zero bias current, and hence differ from the type (ii) noise.

In the temperature region below  $T_{c\_zero}$ , at low bias currents, a continuous superconducting path is expected to exist between the probes of the sample. This fact, and the strong dependence of the noise on the bias current, suggests vortex motion as the source for noise in this region. It can be due to thermally activated two-level or diffusive vortex motion that may also be enhanced by a strong Lorentz force due to applied current.

(d) **Type (iv) noise:** Another noise is a noise in the temperature region between  $T_{c\_zero}$  and  $T_{c\_onset}$ , where the slope and responsivity is high. This noise also depends on the substrate chosen like it is observed that

films on MgO show higher noise than films on  $SrTiO_3$ , which is less granular than the former. It has been observed below some frequency (400Hz) the noise voltage increases by increasing the frequency, and also it is dependent on the bias current. A possible cause of noise in all the samples in the transition region is conductance fluctuations due to variations in the volume fraction of the superconducting phase in the current path through the material.

### 3.2.3 Signal to Noise Ratio

A simple way to describe the "cleanliness" of a given signal level, we use the term signal-to-noise ratio (S/N). It can be easily imagined that S/N is nothing but the signal voltage divided by the rms noise voltage. Though helpful, S/N can not characterize the detector itself. We can get a better S/N for the same detector just by applying a higher incidence level. It just reveals the conditions under which the sample is working.

### 3.2.4 Noise Equivalent Power

The noise equivalent power (NEP) of a detector is the required power incident on the detector to produce a signal output equal to the rms noise output.

$$\text{NEP} = \text{noise}/\text{responsivity}. \quad (3.4)$$

Stated another way, The NEP is the signal level that produces a signal-to-noise ratio of 1. The current signal out put is;

$$i_s = \mathfrak{R}_i \phi_e. \quad (3.5)$$

So the signal-to-noise ratio is;

$$\frac{S}{N} = \frac{\mathfrak{R}_i \phi_e}{I_{rms}}. \quad (3.6)$$

The NEP is the incident radiant power,  $\phi_e$ , for a signal-to-noise ratio of 1, NEP is where  $i_{rms}$  is the root-mean-square noise current in amperes and  $\mathfrak{R}_i$  is the current responsivity in amperes per watt. Either the spectral responsivity  $\mathfrak{R}_i(\lambda, f)$  (or the blackbody responsivity  $\mathfrak{R}_f(\lambda, f)$ ) may be inserted in to above equation to define two different noise equivalent powers. Even though noise equivalent power is a useful parameter for comparing similar detectors under identical conditions, it cannot be used as a summarized performance measure for dissimilar detectors.

### 3.2.5 Specific Detectivity

The NEP (noise equivalent power) formula helps us in calculating the minimum detection power of a system. However, because of these undesirable features: (1) a good detector will have a small NEP, and (2) detectors of different sizes will have different NEPs. We cannot say in general what a good NEP should be unless we specify the size of the detector. The specific detectivity ( $D^*$ ) eliminates the above mentioned drawbacks. A large  $D^*$  is good, and for a given environment all good detectors should have about the same  $D^*$ .  $D^*$  is

the responsivity times the square root of the area, divided by the noise spectral density:

$$\begin{aligned}
 D^* &= \frac{\text{responsivity} \times \sqrt{\text{area}}}{\text{noise}/\sqrt{\Delta f}} = \frac{\Re\sqrt{A_d}}{N/\sqrt{\Delta f}} \\
 &= \frac{\text{Signal} \times \sqrt{\Delta f}}{\text{noise} \times \text{incidence} \times \sqrt{\text{area}}} = \frac{S\sqrt{\Delta f}}{NE\sqrt{A_d}} \quad (3.7)
 \end{aligned}$$

In units of  $\text{cm.}(Hz)_{1/2}/W$ .

In case of superconductor the detectivity can be defined in terms of responsivity and noise, as;

$$D^* = \frac{\sqrt{A(\Delta f)r_v}}{V_n}, \quad (3.8)$$

where  $A$  is the radiation absorbing area of the detector,  $r_v$  is the reponsitivity,  $V_n$  is the voltage noise, and  $\Delta f$  is the frequency range used to obtain the noise measurement. Keeping in mind that the value of  $r_v$  is proportional to slope of resistance versus temperature curve  $dR/dT$  and the bias current, the detectivity of superconducting transition bolometers is found to be a function of the bias temperature through the slope mentioned above. It also depends on frequency. Higher detectivity can be obtained by changing with the parameters like thickness of the film, substrate, etc.

### 3.2.6 Dynamic Range

When electrical signals are plotted versus radiometric input, curve levels off after increasing linearly hence displaying that the detector outputs will increase linearly with input signal over some range of incidences, and fail to be linear at some large incidence. Linearity describes the exactness with which this is true. A major source of deviation from linearity is saturation of the detector or electronic circuit. The Dynamic range is the ratio of the highest useful signal to the lowest measurable signal. One of the possible Highest useful signal might be defined as the point at which a given linearity specification is exceeded, and lowest measurable signal might be the signal at which  $S/N = 1$ .

### 3.2.7 Spatial Considerations

**Uniformity of Response:** It is also a matter of importance for the detector to be uniformly responsive over its surface while considering its applications. Since no detector can be perfectly uniform, it is actually a matter of how non-uniform it is and how much of non-uniformity can the customer afford. A response profile is one way to report uniformity.

**Modulation Transfer Function (MTF):** Considering a target made up of alternation hot and cold lines, with the hot lines repeating at some frequency 'k' every millimeter. We call 'k' the 'spatial frequency' of the target. MTF is a measure of how much the detector signal will vary as we scan a target with that spatial frequency. MTF is sometimes called



the spatial equivalent of the frequency response of a detector, or the spatial frequency response. It is a measure of how well the detector can sense small details. MTF depends on detector size and the uniformity of response across the detector. A small detector with uniform response will have better MTF and be able to see smaller features than will a large one, or one with a response that tapers off near the detector edges.

### 3.2.8 Cross Talk

If one has an array of detectors and if we image a spot on one detector, there should be no signal from the other detector. In practice, some signal will be present on the others, although it should be very small. This excess signal is said to be due to crosstalk. Cross talk is generally measured as a percentage of the input or driving signal. A requirement that cross talk be less than 5 % would be fairly easy to meet, whereas a requirement as small as 0.05 % is very hard for now. Crosstalk can be due to optical effects and electrical effects as illustrated in Figure 3.2.

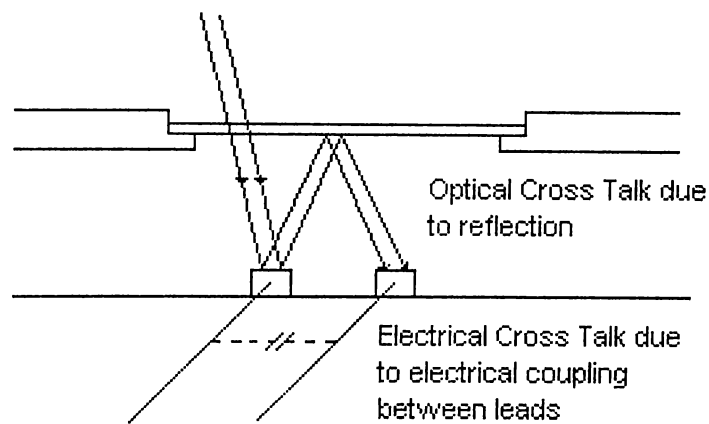


Figure 3.2: Cross talk.

### 3.3 Detectors' type

#### 3.3.1 Photon Detector

Quantum or photon detectors generally respond to incident radiation on an electronic level. It is not necessary to heat the entire atomic structure, so these detectors are normally much faster than thermal detectors.

It can be shown that for semiconducting materials the electrons can have low energies or higher energies but cannot have energies in between. Thus there is a gap in the allowed energies. At low temperatures, with no incident radiation, all of the electrons are in the lower bands. It can be shown that when all the carriers are in the valance bands, no conduction occurs. Thus at low temperatures the electrical resistance of semiconductors is very high. At

higher temperatures, motion of the atoms can give some electrons enough energy to "jump" up into the conduction bands, where they conduct electricity. The result is a characteristic decrease in electrical resistance as the temperature increases.

The energy gaps described above are characteristic of all semiconductors. Semiconductor detectors that rely on that gap for their operation are called intrinsic detectors. Additional energy levels can be created by deliberately adding impurities; this is referred to as doping the material, and the resulting detectors are called extrinsic detectors.

**Carrier Generation:** Carriers can be given enough energy to cross the gap into the conducting bands if they collide with an incoming "packet" of electromagnetic radiation- a photon. This generation of carriers in the conduction band is the detection mechanism for both the photoconducting (PC) and photovoltaic (PV) infrared detector. Although the responsivity expression is different for PC and PV detectors, the rate at which carriers are generated is the same for both.

**Diode and Photovoltaic Detectors:** Photovoltaic (PV) detectors are diodes made from materials with a band gap less than the energy of the incident photons to be detected. Any material that can work as a photoconductive detector can, in theory, be made into a photovoltaic detector. For practical reasons Si, InSb, and HgCdTe are the common photovoltaic detector materials. As infrared radiation passes near the junction, it is

absorbed and gives an electron enough energy to reach the conduction band. This generates an electron in the conduction band and leaves behind a hole that can also contribute to the conduction. This process is sometimes referred to as kicking the electron into the conduction band, or as creating an electron-hole pair. The presence of an electron-hole pair changes the current-voltage relationship of the diode. That change can be monitored to provide infrared detection.

Advantages of PV detectors over PC detectors include a better theoretical limit to the signal-to-noise ratio, simpler biasing, and more accurately predictable responsivity. (how about the speed) Photovoltaic detectors are generally more fragile than photoconductors. They are susceptible to electrostatic discharge and to physical damage during handling.

**Photoconductive Detectors:** Photoconductive detectors include the doped germanium and silicon detectors (Ge: Xx, Si: Xx) and the lead salts (PbS and PbSe). (The ternary compounds HgCdTe and PbSnTe can be used for PC detectors is greater than for the photovoltaics by a factor known as photoconductive gain).

### 3.3.2 Thermal Detector

**Principles:** The performance of a thermal detector is calculated in two stages. First by consideration of the thermal characteristics of the system the temperature rise produced by the incident radiations is determined.

Secondly this temperature rise is used to determine the change in the property which is being used to indicate the signal.

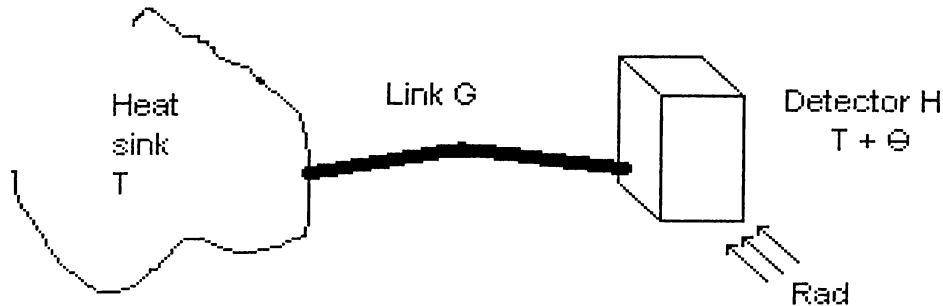


Figure 3.3: Thermal detector.

The simplest representation of the thermal circuit of an infrared detector is shown in Fig. 3.3. The detector is represented by a thermal mass  $H$  coupled via a conductance  $G$  to a heat sink at a constant temperature  $T$ . In the absence of radiation input the average temperature of the detector will also be  $T$ , although it will exhibit a fluctuation about this value. This fluctuation gives rise to a source of detector noise, which sets the ultimate limit to the minimum signal detected by a perfect thermal detector. When the detector receives radiation input, the rise in temperature is found by solving the equation:

$$\eta I = H \left( \frac{d\theta}{dt} \right) + G\theta, \quad (3.9)$$

where  $I$  is radiation power incident upon the detector,  $\eta$  of which the fraction is actually absorbed, and the fraction  $(1 - \eta)$  being either reflected from the front surface or transmitted through the detector. The

temperature of the detector at the time  $t$  is

$$T_D = T + \theta. \quad (3.10)$$

Current may be time independent but more generally will consist of a time independent component  $I_0$  plus at least one component modulated at an angular frequency  $\omega$ . Hence we can write,

$$I = I_0 + I_\omega e^{i\omega t}, \quad (3.11)$$

where  $I_0$ . Solving the above equation for the amplitude of the excess temperature component corresponding to  $I_\omega$  and for its phase  $\theta_\omega$  difference  $\phi$  from  $I_\omega$ ;

$$\theta_\omega = \eta I_\omega (G^2 + \omega^2 H^2)^{-1/2} \quad (3.12)$$

and

$$\phi = \tan^{-1}\left(\frac{\omega H}{G}\right). \quad (3.13)$$

Equation 3.12 illustrate several features of thermal detector. Clearly it is advantageous to make  $\theta_\omega$  as large as possible. To do this  $I_\omega$  should be as small as possible and  $\omega$  sufficiently low that  $\omega H < G$ . In other words both the thermal capacity of the detector and its thermal coupling to its surroundings should be as small as possible.

Equation 3.12 shows that as  $\omega$  is increased, the term  $\omega^2 H^2$  will eventually exceed  $G$  and then  $\theta_\omega$  will fall inversely as  $\omega$ . A characteristic thermal

response time for the detector can therefore be defined as ;

$$\tau_T = \frac{H}{G}. \quad (3.14)$$

For typical detector design  $\tau_T$  falls within the range of milliseconds to seconds. Equation 3.13 also shows that  $G$  should be made as small as possible. However if we have already made  $H$  as small as we can, equation 3.14 shows that reducing  $G$  will increase  $\tau_T$ , which may be undesirable. Thus it may be necessary to adopt a compromise in the choice of  $G$ .

If the thermal detector has a receiving area "a" of emissivity then when it is in thermal equilibrium with its surroundings it will radiate a total flux where  $\sigma$  is the Stefan-Boltzmann constant  $\Theta = dT$ . If now the temperature of the detector is increased by a small amount, the flux radiated is increased by

$$4\alpha\eta\sigma T^3 dT = 4\alpha\eta\sigma T^3 \theta. \quad (3.15)$$

Hence the radiative component of the thermal conductance is  $GR$ ,

$$GR = 4\alpha\eta\sigma T^3. \quad (3.16)$$

When the detector is in thermal equilibrium with the heat sink the rms fluctuation in the power flowing through the thermal conductance into the detector is;

$$\Delta\omega_T = (4\Pi T^2 G)^{1/2}, \quad (3.17)$$

which will be smallest when G assumes its minimum value, i.e. GR. Then it will be a minimum and its value gives the minimum detectable power for an ideal thermal detector. The minimum detectable signal power  $P_N$  is defined as the signal power incident upon the detector required to equal the thermal noise power. Hence if the temperature fluctuation associated with GR is the only noise source,

$$\eta P_N = \Delta\omega_T (16\alpha\eta\sigma kT^5)^{1/2}. \quad (3.18)$$

The definition of  $W_T$  and of  $P_N$  assumes the amplified noise bandwidth  $\Delta f$  is reduced to 1 Hz. For wider bandwidth  $\Delta f$  the rms. noise increases as  $(\Delta f)^2$ . Equation 3.18 represents the best performance attainable from a thermal detector.

**The Thermopile:** The thermopile is one of the oldest infrared detectors, being first described by Melloni but it is still widely used and in its latest form (the thin film thermopile) is used in space instrumentation.

The basic element in a thermopile is a junction between two dissimilar conductors having a large Seebeck coefficient,  $\Theta$ . To perform efficiently a large electrical conductivity  $\sigma$  is required to minimize Joulean heat loss



and a small thermal conductivity  $K$  to minimize heat conduction loss between the hot and cold junctions of the thermopile. These requirements are incompatible and we find that in common with other thermoelectric devices the best choice of thermoelectric material is that for which  $\frac{\sigma\Theta^2}{K}$  is a maximum and that this occurs for certain heavily doped semiconductors, for example  $Bi_2Te_3$  and related compounds. To make an efficient thermal infrared detector the device must also be an efficient absorber of the incident radiation and must have a small thermal mass to give as short a response time as possible.

The recent development of thin film techniques has enabled cheap thermopile to be designed, which can be fabricated as complex arrays with good reliability.

**The Golay Cell and Related detectors:** The Golay cell is widely used in laboratory instruments. It is still one of the most sensitive room temperature detectors. But its bulkiness, comparative fragility, sensitivity to vibration and rather slow response time limit it to laboratory applications. In a Golay cell as shown in Fig. 3.4, radiation absorbed by a receiver inside a closed capsule of gas (usually xenon for its low thermal conductivity) heats the gas causing its pressure to rise which distorts a flexible membrane on which a mirror is mounted. The movement of the mirror is used to deflect a beam of light shining on a photocell and so producing a change in the photocell current as the output. In modern Golay cell the beam of light is provided by a light emitting diode and a solid state photodiode is used to detect it. The reliability and stability of this

arrangement is significantly better than that of the earlier Golay cells, which used a tungsten filament lamp and vacuum photocell. Apart from the greater reliability of the modern components, the lower heat dissipation with the device probably increases the reliability of the gas cell itself.

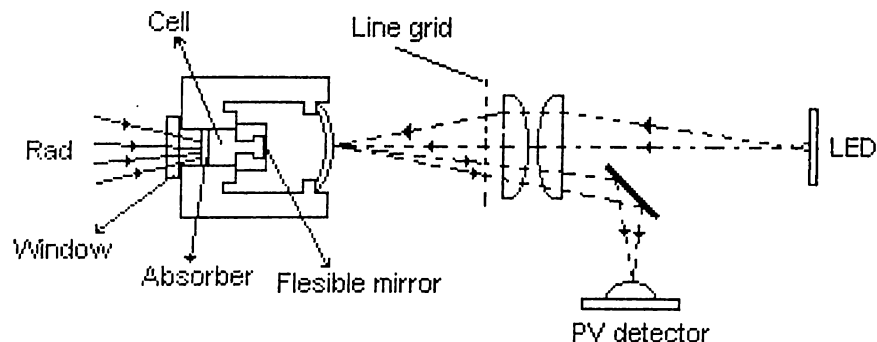


Figure 3.4: Golay cell.

Another method of obtaining an electrical output from the gas cell is to place a fixed conductor near the distorting membrane forming a variable condenser, which can be measured with a suitable circuit. The Golay cell is still the basic detector used in a large amount of laboratory instrumentation and the gas analysis technique employing the Luft cell is widely used. The Golay cell, being used from the visible to wavelengths of several  $\mu\text{m}$  has been used over a broader band of the spectrum than any other detector, except possibly the pyroelectric.

**Pyroelectric Detector:** A pyroelectric material is one of low enough crystalline symmetry to be able to possess an internal electric dipole moment. Although the external field produced by this dipole will normally be neutralized by an extrinsic charge distribution near the surface of the

material. In good pyroelectric material this extrinsic charge distribution is relatively stable so that even quite slow changes in the sample's temperature, which produces changes in the internal dipole moment, produce a measurable change in surface charge. Hence if a small capacitor is fabricated by applying a pair of electrodes to the sample the change in temperature and hence the incident thermal radiation can be detected by measuring the charge on the condenser. The magnitude of the pyroelectric effect is such that the sensitivity of the best detectors is comparable with that of the Golary cell or of a high sensitivity thermopile. But an element embodying this performance is considerably more robust than the other thermal detectors of comparable sensitivity.

Figure 3.5 is the equivalent electrical circuit of a pyroelectric detector. If  $A$  is the area normal to the polar axis of the material and this produces a modulated temperature rise.

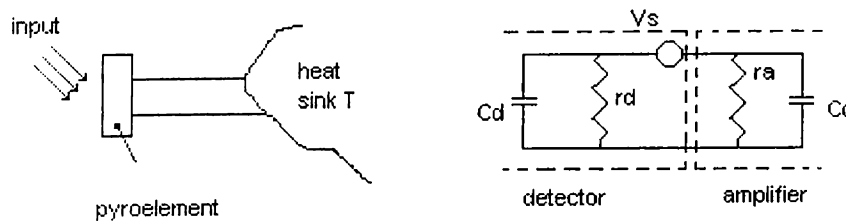


Figure 3.5: Schematic circuit of pyroelectric detector.

The corresponding voltage developed across the amplifier input is;

$$V = \omega \rho A \theta_{\omega} r (1 + \omega^2 \tau_T^2)^{-1/2}, \quad (3.19)$$

where  $p$  is the pyroelectric coefficient and  $\tau_T = rC$  is the electrical time constant of the output circuit of the detector. Substituting for  $\theta_{\omega}$  gives the voltage responsivity;

$$R = \eta(\omega \rho A r / G)(1 + \omega^2 \tau_T^2)^{-1/2} \quad (3.20)$$

where the thermal time constant  $\tau_T$  is given by  $\tau_T = H/G$ . For most applications the high frequency approximation is valid, i.e.,  $R = \rho A / HC$ , which shows for high responsivity a pyroelectric material with a large value of  $(\rho / \epsilon \dot{C})$  is required. This quantity is one of the figure merit for selecting pyroelectric material. When noise consideration are included it may be necessary to modify it.

**The Bolometer:** The bolometer is a resistive element constructed from a material with a large temperature coefficient so that the absorbed radiation produces a large change in resistance.

To operate a bolometer (Fig. 3.6) an accurately controlled bias current  $I$  from a suitable source and regulating impedance is passed through the

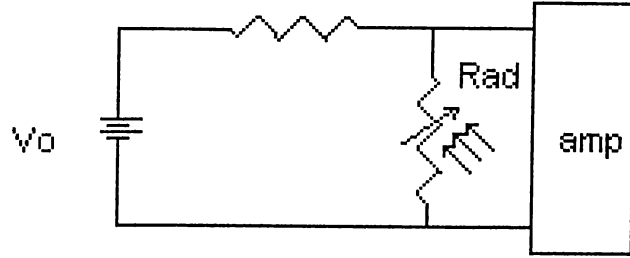


Figure 3.6: Schematic circuit of bolometer.

element. If the incident radiation input produces a small change  $r$  in the resistance  $\partial r$  of the bolometer then an output voltage is generated as;

$$V_s = i\partial r. \quad (3.21)$$

If the input radiation produces an increase in  $\theta$  the temperature of the element and the temperature coefficient of resistance;  $(\frac{1}{r})(\frac{dr}{dT})$  is  $\alpha$  then

$$V_s = \eta I_\omega i \alpha r (G^2 + \omega^2 H^2)^{1/2} \quad (3.22)$$

corresponding to a voltage responsivity

$$R = \eta i \alpha r (G^2 + \omega^2 H^2)^{1/2}. \quad (3.23)$$

The above equation shows the desirability of having large values for  $\alpha$ ,  $r$ , and  $I$  as well as small values for  $G$  and  $H$ . This equation implies that the input impedance of the amplifier is large compared with  $r$ . This sets a limit on  $r$  so that the resistance cannot be increased independently. Also with very high resistance elements the input capacity of the connecting leads and the amplifier can produce a time constant longer than the thermal time constant. The bias current  $I$  cannot be increased independently. When it becomes large, Joule heating will raise the temperature of the element and if  $\alpha$  is negative destructive thermal run away may occur, but apart from this an increase in noise with increasing  $I$  will set an optimum value. (The problem of maximizing  $\alpha$  then comes to choosing suitable material.) The same basic materials that are used for resistance thermometers are the obvious choices and in fact when constructed in a suitable configuration they have all been used.

In addition to radiation noise and temperature noise associated with the thermal impedance of the element, Johnson noise associated with the resistance  $r$  is one of the most important noise sources. With some types of bolometer low frequency current noise is important and is the principal factor limiting  $I$ . With room temperature bolometers amplifier noise should not be important but with cryogenic devices it is usually the dominant noise source, especially when operating with cooled filters to limit the radiation noise to the sub-mm band.

With the need for high performance far infrared detectors, attention was given to the development of much higher performance bolometers making use of the fact that at very low temperatures it is possible to obtain much larger relative changes in resistance than near room temperature. The specific heat is much smaller and that if the detector and its surrounding are cooled to a very low temperature the ultimate sensitivity can be orders higher than that for a room temperature device. Putely has derived an expression for the ultimate sensitivity of helium cooled detectors taking into account the effects of room temperature radiation and has shown that the best NEPs, which can be achieved in the sub mm regions are within the range  $10^{-13} - 10^{-14}$ W, depending upon the spectral filtering and field of view.

Figure 3.4 gives more detailed information on the cryogenic bolometers. In comparing different results it must be remembered that it is not very meaningful to use  $D^*$  or other figures of merit. This is because two of the principal noise sources are independent of the detectors' area. Thus the main thermal conductance contributing to the temperature noise term is usually that of the electrical lead and in many cases the amplifier noise is still the largest noise source.

Figure 1: Typical Spectral Response of Infrared Detectors

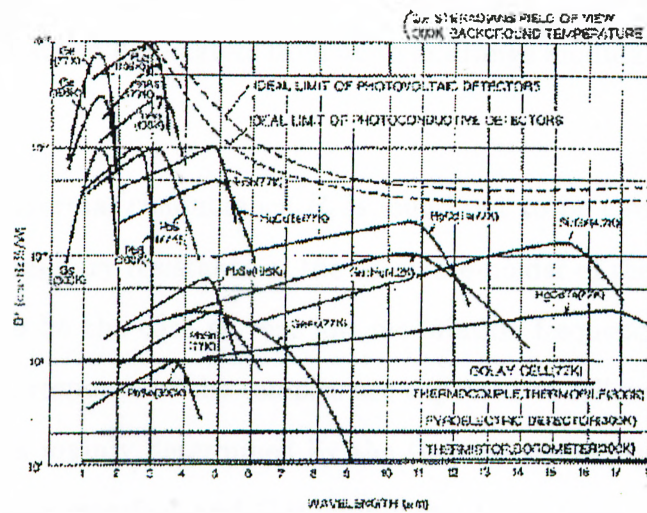


Figure 3.7: Performance of cooled bolometer NEP of carbon, germanium, silicon and thallium selenide semiconducting bolometers and tin, aluminum and titanium superconducting bolometers..

### 3.4 HTSC Bolometers and the Thermal model

#### Introduction

In order to understand the relation between magnitude (and phase) response and thermal parameters of the cryogenic systems, which are usually frequency dependent, we need some kind of thermal model. Which can predict the effect of different parameters related to the bolometers. The frequency response and effects of the thermal boundary resistance at the interfaces of the substrate on the versus modulation frequency of the edge-transition bolometers, has already been studied and proposed in different works. There have been already some efforts to predict the thermal response behaviour using different thermal



models. In this study we will try to understand the thermal model and its closed form solution for the bolometers of the mentioned High-  $T_c$  superconducting edge-transition bolometers from dc to midrange modulation frequency.

As the total thermal conductance  $R_t$  is found out to be close to the value of the thermal boundary resistance at the substrate-holder of the samples,  $R_{sc}$ , which is found to be the case at very low modulation frequencies. In such a configuration the response of the samples are expected to follow a simple R-C model where R is mainly determined by the thermal boundary resistance at the substrate-holder interface and C is mainly due to the heat capacity of the substrate materials,  $C_s$ , which is much higher than that of the film. It has been found that this would be the case up to frequencies where the thermal diffusion length,  $L$ , into the substrate materials is more than the substrate thickness,  $L_s$ , and the effect of the substrate-cold finger interface can be seen by the heat wave propagating into the substrate. The increase of the modulation frequency beyond the values where the thermal diffusion length is less than the substrate thickness can cause a change in the slope of the response magnitude versus modulation frequency compared to that of the basic R-C model. This found to happen at a frequency,  $f_L$ , called the knee frequency which is dependent on the substrate material and its thickness. Considering the thermal diffusion length as the characteristics penetration depth of the temperature variation into the substrate, the Knee frequency can be determined from,

$$f_L = \frac{D}{\pi L_s^2}, \quad (3.24)$$

where  $L_s$  is the substrate thickness,  $D = K_s / C_s$  is the thermal diffusivity of the substrate materials, and  $K_s$  and  $C_s$  are the thermal conductivity and the

specific heat (per unit volume) of the substrate materials respectively. It has been found that for the frequencies less than  $f_L$ , the response is found to scale as  $f^{-1}$  following the response for a simple R-C model. For frequencies higher than  $f_L$  the response is found to scale as  $f^{-1/2}$  due to the variation of the effective penetration depth of the temperature variation into the substrate. The response follows the  $f^{-1/2}$  dependence up to frequencies where the thermal resistance of the superconducting film-substrate boundary,  $R_{fs}$ , is negligible compared to that of the substrate materials,  $R_s$ . The frequency dependent total thermal conductance of the substrate,  $R_s$ , is determined from the thermal diffusion length as;

$$R_s = \frac{1}{A\beta\sqrt{C_s K_s \pi f}}, \quad (3.25)$$

where  $A$  is the effective area of the conductive path,  $f$  is the modulation frequency in Hz, and  $\beta$  is a correction factor for the above approximation of the effective length of the ac heat flow. The effects of the substrate thermal boundary resistance and its temperature dependency is also proposed to be partly responsible for the response versus temperature which was interpreted as the non-equilibrium response of such devices. [8]

### The Thermal Modeling

As shown in the experimental configuration of the thin film samples on crystalline substrates with contact to the holder and the temperature sensor in the figure below.

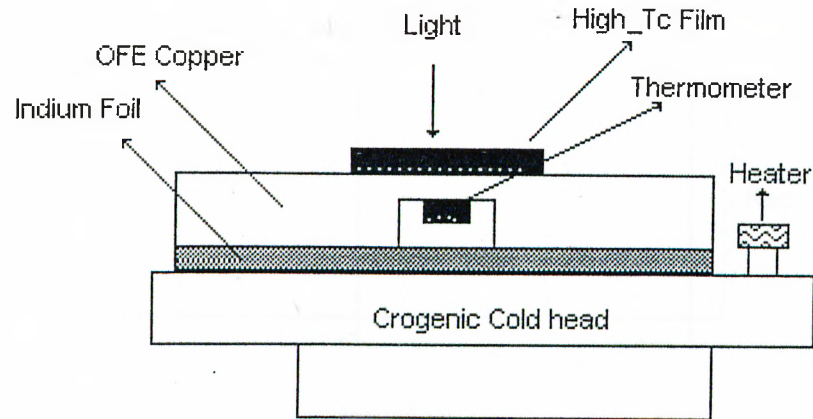


Figure 3.8: Configuration of superconducting sample, heater, sample holder and the cryogenic cold head.

In most of the cases the area of the superconducting pattern with respect to the substrate thickness is large, so we could consider the superconducting pattern as a lumped film on top of the substrate material and substrate as a continuous uniform media. By the use of electrical analogue discussed in previous chapter, the thermal equivalent circuit of the samples in contact with the holder can be shown as in the Fig. 3.9.

Where  $q$  is the absorbed radiation intensity at the surface of the sample. In this equivalent diagram, two thermal boundary resistance is considered at the substrate interfaces while only the heat capacity of the superconducting film is calculated and found to be negligible compared to that of the substrate and the interfaces. For samples with thicker superconducting film as for the screen-printed materials, the limited heat conductivity of the superconducting

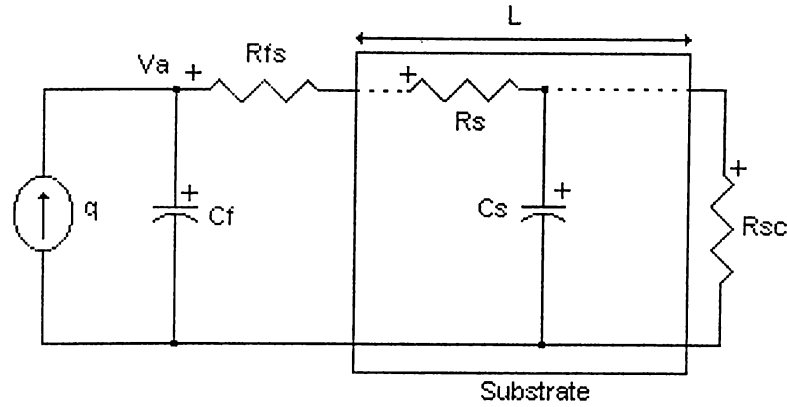


Figure 3.9: Equivalent thermophysical diagram of the sample in contact to the cryogenics holder,  $q$  is the input radiation power,  $C_{fs}$  is a lumped heat capacitance of the film,  $C_s$  and  $R_s$  are the heat capacity and thermal conductivity of the substrate material, and  $R_{fs}$  and  $R_{sc}$  are the thermal boundary resistance values at the film-substrate and the substrate-holder respectively..

material same as for the substrate, should also be considered.

There exist lateral heat diffusion in the substrate before the heat wave from the film reaches the substrate-holder boundary resistance, a correction factor,  $\alpha$ , can be obtained to be applied to the measured  $R_{sc}$  values. The value of the  $\alpha$  depends mainly on two things, firstly it increases by increasing the thermal conductivity of the substrate thickness and secondly it increases by decreasing the superconducting pattern area with respect to the substrate thickness which is consistent with the above interpretation for the cause of the correction factor,  $\alpha$ .

In order to achieve the complete close form solution to the model as in the figure above, we need to concentrate on the following three important calculations,

### Temperature variation in the substrate:

As we know for very low modulation frequencies where  $C_f$  is much smaller than the contributing heat capacity of the substrate and the film-substrate thermal boundary resistance  $R_{fs}$ , is much smaller than that of the substrate-holder and /or the thermal resistance of the substrate,  $R_s$ , we can assume that the absorbed radiation power,  $q$ , is directly applied to the surface of the substrate ignoring the effects of the  $C_f$  and  $R_{fs}$ .

Substrate can be thought as a continues media of R and C elements. So in order to find the temperature variation at the surface for the substrate, we can use the general heat propagation equation with boundary condition  $R_{sc}$ . For one dimensional heat propagation in a material we have;

$$\frac{\partial T}{\partial t} = D \frac{\partial^2 T}{\partial x^2}, \quad (3.26)$$

where  $D = k/c$  is the thermal diffusivity of the material and  $k$  and  $c$  are the thermal conductivity and the specific heat per unit volume of the material which is substrate in this case. A quantity  $L$ , called the "thermal diffusion length", is defined as:

$$L = \left(\frac{D}{\pi f}\right)^2. \quad (3.27)$$

By definition  $L$  represents the characteristic penetration depth of the temperature variation into the substrate. Considering the thermal diffusion length as the effective length for heat flow into the substrate, the corresponding thermal conductance can be found as a

$$G = ak_s \frac{A}{L}. \quad (3.28)$$

Then the thermal conductance of the substrate can be found by plugging the value of  $D = k_s / c_s$

$$G_s = aA \sqrt{c_s k_s \pi f}, \quad (3.29)$$

which shows that  $G_s$  is a function of the frequency and scales as  $f^{-1/2}$ . We can calculate the total heat capacity of the substrate as,

$$C_s = bc_s AL = bA \sqrt{c_s k_s l \pi f}, \quad (3.30)$$

where  $b$  is a constant to compensate for the drop of the amplitude of the temperature variation along  $L$ .

The temperature at the surface of the substrate without the consideration of the effect of the heat capacity of the superconducting film,  $C_f$ , and the thermal boundary resistance at its interface,  $R_{fs}$ , is obtained to follows;

$$\Delta T = q \frac{\exp(\gamma L) + \Gamma \exp(-\gamma L)}{\exp(\gamma L) - \Gamma \exp(-\gamma L)}, \quad (3.31)$$

where  $\gamma$  is the characteristic thermal impedance of the substrate material defined as;

$$\gamma = \frac{1+i}{\sqrt{2}} \sqrt{\frac{\omega c_s}{k_s}} \quad (3.32)$$

and the  $\Gamma$  is defined as:

$$\Gamma = \frac{R_{sc} - \sqrt{\frac{1}{i\omega c_s k_s}}}{R_{sc} + \sqrt{\frac{1}{i\omega c_s k_s}}} \quad (3.33)$$

$\omega$  is the angular modulation frequency, and  $k_s$  and  $c_s$  are the heat conductivity and the heat capacity of the substrate materials, respectively. The value of  $R_{sc}$  can be found from;

$$R_{sc} = \frac{1}{G(W/K)} \quad (3.34)$$

where  $G$  is the thermal conductance of the device at very low frequencies,  $G(0)$ . It has been taken at the assumption of  $G_{fs} \gg G_s \gg G_{sc}$  where  $G_{fs} = 1/R_{fs}$ .

#### Temperature variation at the film:

In order to obtain the voltage response of the current biased samples to the modulated radiation intensity at all frequency ranges, we need to find the temperature variation in the superconducting film which is considered to be the temperature variation across  $C_f$  in the equivalent circuit of Figure 3.9 . Hence the only temperature gradient from top of the superconducting film to the substrate would be that across the film-substrate interface,  $R_{fs}$ . Solving the one dimensional thermal differential equation with the complete boundary condition, the temperature variation in the superconducting film is found to follow;

$$\Delta T = q \left( \frac{\frac{\exp(\gamma L) + \Gamma \exp(-\gamma L)}{\exp(\gamma L) - \Gamma \exp(-\gamma L)} \sqrt{\frac{1}{i\omega c_s k_s}} + R_{fs}}{\frac{\exp(\gamma L) + \Gamma \exp(-\gamma L)}{\exp(\gamma L) - \Gamma \exp(-\gamma L)} \sqrt{\frac{i\omega}{c_s k_s}} C_f + 1 + i\omega C_f R_{fs}} \right), \quad (3.35)$$

where  $q$  is the absorbed radiation power in the film per unit area, and  $C_f$  and  $R_{fs}$  are the total heat capacity of the superconducting film and the thermal

boundary resistance at the film-substrate interface per unit area, respectively.

This equation is valid only for the low frequency up to values where the thermal diffusion length into the superconducting film becomes smaller and/or comparable to the thickness of the film. This is while the penetration depth and/or the absorption coefficient length in the superconducting film is still considered to be much smaller than the film thickness or otherwise considered. If we try to investigate the effect of the  $R_{fs}$  in equation 3.35 then at very low frequencies the denominator will approach one and  $R_{fs}$  will become negligible compared to the first term leading to the results of the one boundary conduction problem as in equation 3.35. The basic reason behind this is, at very low modulation frequencies the temperature variation reaches the bottom of the substrate, hence the heat capacity of the film with respect to that of the whole substrate material under the pattern and the thermal boundary resistance at the film-substrate with respect to  $R_s$  and  $R_{sc}$  becomes negligible.

#### **The voltage response and bias current dependence:**

If we consider the temperature variation in the film caused by the absorbed radiation to be uniform all across the pattern, the voltage response in a dc current bias configuration can be obtained from;

$$dV = I_b \Delta T \frac{dR}{dT}, \quad (3.36)$$

where  $I_b$  is the dc bias current,  $dR/dT$  is the slope of the R versus T curve at the bias temperature, and  $\Delta T$  is the temperature variation in the superconducting



film as given in equation 3.36. This is valid within the temperature variation range where  $dR/dT$  can be considered to be constant which is about one tenth of the transition width at the middle of the superconducting to normal transition temperatures in our samples. Considering the maximum temperature variations being below about 1mV as measured during the characterizations presented in this work and the transition widths typically of few degrees of Kelvin in our samples, the variation of  $dR/dT$  and/or the non-linearity of equations is found to be negligible in our measured and calculated response. This would not be the case for devices exposed to high radiation intensities which are normally voltage biased for further stability's.

There might also be a consecutive temperature variation due to ac Joule heating in the film caused by the resistance variation in the superconducting film caused by the input radiation power. This effect on the response which is in the form of a positive feedback in the used current-biased configuration here, can be considered either in the model as a dependent radiation source in parallel to the radiation source,  $q$ , in the equivalent diagram of Figure 3.9, or simply as an additional term in the overall responsivity of the samples as given in the following form,

$$r_{V-t} = \frac{r_V}{(1 - I r_V / \eta)}, \quad (3.37)$$

$r_{V-t}$  is the overall responsivity in volts per watt and  $\eta$  is the absorption coefficient in the film. Considering the effect of the absorption coefficient in the  $q$  factor in equation 3.37 .  $r_V$  will be the same as  $dV$  as given in equation.

### 3.5 Conclusion

For the measurements of objects emanating photons on the range of 2 eV or higher, quantum detectors having room temperature are generally used. For the smaller energies (longer wavelengths) narrower band gap semiconductors are required. However, even if a quantum detector has a sufficiently small energy band gap, at room temperatures its own intrinsic noise is much higher than a photoconductive signal. Noise level is temperature dependent, therefore, when detecting long wavelength photons, a signal-to-noise ratio may become so small that accurate measurement becomes impossible. This is the reason, why for the operation in the near and far infrared spectral ranges a detector not only should have a sufficiently narrow energy gap, but its temperature has to be lowered to the level where intrinsic noise is reduced to an acceptable level.

The operating principle of a cooled detector is about the same as that of a photoresistor, except that it operates at far longer wavelengths and at much lower temperatures. Cooling shifts the response to longer wavelengths and increases sensitivity. Application of the cooled quantum detectors include measurements of optical power over a broad spectral range, thermal temperature measurement, thermal imaging, detection of water content, and gas analysis. The behaviour of cryogenic detectors can be characterized by thermal model. The characteristic parameters which effect the responsivity or in other words the sensitivity of the detector can be found by these thermal equivalent models.

In this chapter we have seen a branch of superconductor detectors named as bolometers or edge-transition detectors. According to the thermal equivalent model, the thermal boundary resistance between film and substrate ( $R_{fs}$ ), thermal conductance ( $G$ ), and the slope  $dR/dT$  are the important parameters. So either by increasing the  $R_{fs}$ ,  $dR/dT$  ratio, or by decreasing  $G$  we can increase the responsivity and detectivity of the system.

## Chapter 4

# CRYOGENICS AND INSTRUMENTATION

### 4.1 Introduction

There are two basic needs in order to characterize the superconductors. Cryogenic system is one of them, which can be used to cool down the system to liquid nitrogen temperature. It should be capable of providing means to apply and receive the signal from the detector in an efficient manner. Secondly electrical setup is required to convert the out put signal into useful information, to characterize the superconductor detector.

Initially basic thermal properties are considered in this chapter. This provides insight to the importance of thermal parameter, which is to be taken care in designing the Dewar. The cryogenic system is explained with a proposed thermal equivalent model. Electrical setup is discussed in the end, where the focus is mainly on the dc characterization.

## 4.2 Thermal Properties Consideration

### 4.2.1 Thermal Expansion

As the temperature of the materials change, the linear dimensions of them change. Therefore a changed dimension (length, width, or thickness) is equal to the original dimension times the coefficient of expansion,  $\alpha$ . The coefficient of expansion has the units of reciprocal degrees. To emphasize the dependence on original length, the units of (are sometimes written as (in./in.)/K or (cm/cm)/K).

Since thermal mismatches stresses the parts bonded together, the expansion issue is hence more significant to us. Hence initiating a great care in selecting substrates for film material which we are going to deposit on it, special care should be taken in mounting of windows that will be cooled, and in solder or glue joints.

The coefficient of expansion,  $\alpha$ , is temperature dependent, going to zero at very low temperatures. Because the coefficient of expansion is temperature dependent, average or integrated values are required, then if  $\Delta T$  is not small, we get:

$$\Delta x = x_0 \int_{T_1}^{T_2} \alpha dT \equiv x_0 \alpha_{T_1} (T_2 - T_1). \quad (4.1)$$

We may understand thermal expansion by considering for a classical oscillator the effect of anharmonic terms in the potential energy on the mean separation of a pair of atoms at a temperature  $T$ . Consider the potential energy of the atoms at a displacement  $x$  from their equilibrium then separation at absolute zero in:

$$U(x) = cx^2 - gx^3 - fx^4 \quad (4.2)$$

with  $c$ ,  $g$ , and  $f$  all positive. The term in  $x^3$  represents the asymmetry of the mutual repulsion of the atoms and the term in  $x^4$  represents the softening of the vibration at large amplitudes.

We can calculate the average displacement by using the Boltzmann distribution function, which weights the possible values of  $x$  according to their thermal dynamic probability;

$$\langle x \rangle = \frac{\int_{-\infty}^{\infty} x \exp[-\beta U(x)] dx}{\int_{-\infty}^{\infty} \exp[-\beta U(x)] dx}, \quad (4.3)$$

with  $\beta = 1/K_B T$ . In the classical region the thermal expansion after some simplifications becomes,

$$\langle x \rangle = \frac{3g}{4c^2} k_B T. \quad (4.4)$$

## 4.2.2 Thermal Conductivity

The measuring of heat transfer ability through conductors is called 'thermal conductivity'. Consider the bar of uniform cross-sectional area  $A$  and length  $l$  shown in the Figure 4.1. If the temperature difference  $\Delta T$  between the ends of the bar is small, the heat transferred by conduction through the bar is given by,

$$P = k \frac{A}{L} \Delta T, \quad (4.5)$$

where  $\Delta T$  is the temperature difference across the bar and 'k' is the thermal conductivity. The units of thermal conductivity are  $W/(cm.K)$ .

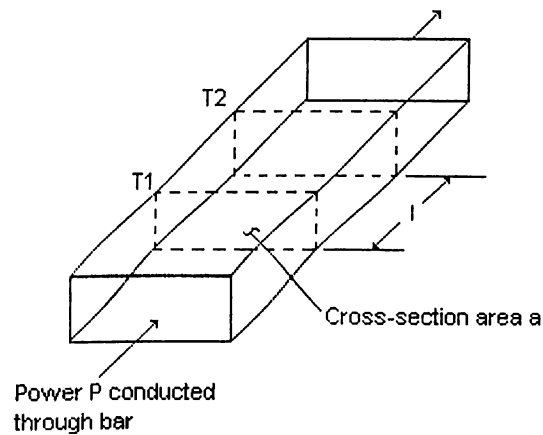


Figure 4.1: Definition of thermal conductivity.

The thermal conductivity of most materials varies dramatically with temperature in the cryogenic temperature ranges (see Figure 4.2). Thermal conductivity at cryogenic temperatures is also a strong function of the material purity and heat-treatment. The above formula can be used for heat conduction provided that the temperature difference  $\Delta T$  is small. When the temperature

difference range is large (300K to 77K), the use of an average conductivity in the above formula replaces the product of factor k and  $(T_2 - T_1)$  by integrated values as:

$$P = \int_{T_1}^{T_2} k(T) dT \frac{A}{L}$$

$$\equiv k(T_1)(T_2 - T_1) \frac{A}{L} \quad \text{if } T_2 - T_1 \text{ is small.} \quad (4.6)$$

The steps in performing thermal conductivity calculations are then:

- (1) determine the material and temperature range of interest, and locate a conductivity values or curve appropriate to that material and temperature; and
- (2) if the temperature range is small enough, or if the accuracy requirements are not demanding, use formula 4.5. To predict the conducted heat, if more accuracy is desired, obtain the integrated conductivity value or do the integration yourself.

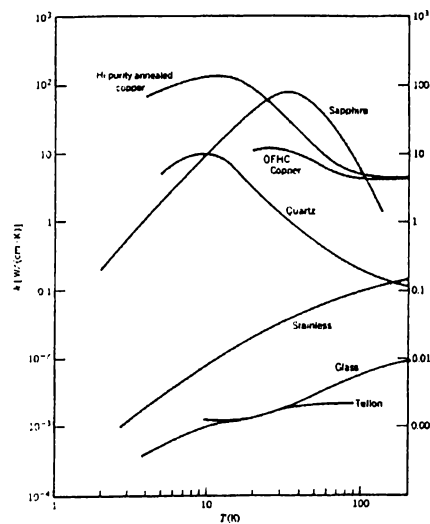


Figure 7.6. Thermal conductivity for common cryogenic building materials.

Figure 4.2: Thermal conductivity for common cryogenic building materials..



It is some time convenient to combine the conductivity with the area to length ratio in a thermal conductance ( $K$ ) or a thermal impedance ( $Z$ ):

$$K = k \frac{A}{L} \quad (4.7)$$

$$Z = \frac{1}{K}. \quad (4.8)$$

Units of thermal conductance  $K$  are  $W/K$ . In the this representation form heat transfer can be written as,

$$P = K \Delta T = \frac{\Delta T}{Z} \quad (4.9)$$

$$\Delta T = P Z = \frac{P}{K}. \quad (4.10)$$

If the thermal conductivity cannot be measure or predicted in any other way, Wiedemann-Franz Law [9] can be useful to estimate the thermal conductivity:

$$K = L \sigma T, \quad (4.11)$$

where the ratio of  $k$  to  $\sigma T$  is the Lorenz ratio  $L$ .

As seen from the formula itself, this law limits the applicability to such a stringent level that accuracy cannot be guaranteed. This leads the law to being used only as a last resort. This law holds when the electrons dominate the heat transfer process and when the lifetimes associated with thermal and electronic conduction are same. The first condition does not hold for insulators and impure metal, and thermal conductivity of insulators will be higher than that

predicted from the Wiedeman-Franz law. The second condition does not hold at low temperatures [10]; at low temperature according to the Wiedeman-Franz law, thermal conductivity of good conductors will be less than that predicted.

### 4.2.3 Specific Heat

The amount of heat required to make a one-degree change in the temperature of an object is its heat capacity. The usual symbol is  $C$  and the common units are joule per Kelvin:  $J/K$ . The specific heat capacity 'c' is the heat capacity per unit mass, and common units are joule per gram per Kelvin:  $J/(g.K)$ . The amount of heat required to cause an arbitrary temperature change in an object of mass 'm' is described in equation below,

$$Q = m \int_{T_1}^{T_2} c(T) dT$$

$$\equiv mc(T_1)(T_2 - T_1) \quad \text{if } T_2 - T_1 \text{ is small.} \quad (4.12)$$

For cryogenic temperatures the heat capacity is a strong function of temperature, so average or integrated values are necessary if large temperature changes are involved. The specific heat unlike the thermal conductivity is not sensitive to sample purity or preparation technique making the selection of appropriate values for a particular problem very much a less of a difficulty. Table B.3 (see appendix) lists the representative values. In case the specific heat capacity of some material cannot be located in the table we can use Debye temperature  $\theta_D$ , in which case the heat capacity can be estimated from the Debye theory, the procedure will be as follow,

- (1) First calculate the ratio  $T/\theta_D$ ,
- (2) Then refer to tables or graphs of the Debye function-specific heat capacity per mole as a function of  $T/\theta_D$ ,
- (3) Divide that value by the molecular mass  $M$  (grams per mole) to obtain the specific heat in  $J/(g.K)$

$$c[J/(g.K)] = \frac{c[J/(g.K)]}{M/(g/mol)}. \quad (4.13)$$

At temperatures much below both the Debye temperature and the Fermi temperature, the heat capacity of metals may be written as the sum of electron and phonon contribution:

$$c = \gamma T + AT^3, \quad (4.14)$$

where  $\gamma$  and  $A$  are constants characteristic of the material. The electronic term is linear in  $T$  and is dominant at sufficiently low temperatures. It is convenient to exhibit the experimental values of  $c$  as a plot of  $c/T$  versus  $T^2$ :

$$c/T = \gamma + AT^2. \quad (4.15)$$

For then the points should lie on a straight line with slope  $A$  and intercept  $\gamma$ .

## 4.2.4 Electrical Analogous

With the following substitutions implying same mathematics, one with electronic experiences can visualize the thermal performance and calculations in terms of one's own field:

Charge (C)	→	heat energy (J)
Current (C/s,A)	→	heat flow (J/s,W)
Voltage (V)	→	temperature (K)
Impedance (V/A, $\Omega$ )	→	thermal impedance (K/W)
Conductance (1/ $\Omega$ )	→	thermal conductance (W/K)
Capacitance (C/V)	→	heat capacity (J/K)

Table 4.1: Electrical Analogous.

Once these substitutions are made, the electrical formulas and intuition can be applied to thermal problems.

## 4.2.5 Liquid Nitrogen

The common cryogens for IR detector work are listed in table B.4 (see appendix), the most common are liquid nitrogen and liquid helium. Helium is the coldest known cryogen. Under normal atmospheric pressure it boils at 4.2K. Helium though has the lowest cooling capacity of the common cryogens; it boils very quickly, so requires very careful insulation in order to store, while on the other hand Nitrogen is relatively inexpensive and has a relatively high

cooling capacity.

**Nitrogen:** It constitutes 78.03% of the air, has a gaseous specific gravity of 0.967 and has a boiling point of  $-320.5^{\circ}F$  ( $-195.8^{\circ}C$ , 77K) at atmospheric pressure. It is colorless, odourless, and tasteless. From an inexhaustible source in our atmosphere, liquefaction and fractional distillation can obtain it. It can also be easily prepared by heating a water solution of ammonium nitrite.

It is less expensive than Helium and Neon, and is used in large quantities both to thermally insulate the more expensive cryogens, and to cool detectors and hence used in this work. At this point we will like to introduce two definitions, as

**Heat of Vaporization:** The energy required to vaporize a given quantity of liquid is called the heat of vaporization  $h$ .

$$Q = hM = h\rho V. \quad (4.16)$$

where  $M$  and  $V$  are the mass and volume of liquid vaporized by heat  $Q$ .

**Enthalpy:** A cryogen, when used in a cooling system first vaporizes and finally rises in temperature to that of the room absorbing heat from the surroundings. The total heat absorbed is the heat of vaporization plus the specific heat integrated from the boiling point to the final temperature of the gas given as;

$$Q = [H(T_2) - H(T_1)]\rho_l V_l. \quad (4.17)$$

This total heat can be calculate form tables of the enthalpy H of the cryogen. The total heat is the difference in the enthalpy of the material at the starting and ending temperatures.

So it is obvious that heat of vaporization is only a small part of the cooling capacity of cryogens. The vapor can provide a great deal of useful cooling if used efficiently. This cooling capability is lost if the vapor is allowed to vent directly to the atmosphere.

#### 4.2.6 Temperature Sensors

In qualitative manner temperature of any object implies that how cold or wart the object is. Temperature on the other hand can be generalized as a system's temperature if the measured quantity for a number of systems is the same under thermal equilibrium. A thermometer is an instrument, which measures the temperature of a system in a quantitative way. There are many different types of temperature sensors as listed below,

**Thermocouples:** Thermocouples are pairs of dissimilar metal alloy wires joined at least end to end generating a net thermoelectric voltage between the two ends according to the size of the temperature difference

between the ends. The relative Seebeck coefficients of the wire pair and the uniformity of the wire's relative Seebeck coefficient.

There are many different types of thermocouples, which have different application ranges, which is shown in the table above.

**Thermistors:** Thermistors are tiny bits of inexpensive semiconductor materials with highly temperature sensitive electrical resistance.

**Liquid-In-Glass Thermometers:** Liquid in glass thermometers are the sensors one visualizes most often for temperature measurement. A glass cylinder with a bulb at one end, a capillary hole down the axis, connected to the reservoir in the bulb filled with silvery mercury or perhaps a red-colored fluid, an engraved temperature scale. There are many designs and a significant range of capabilities and uses of those designs.

**Resistance Temperature Detectors (RTDs):** RTDs are wire wound and thin film devices that work on the physical principle of the temperature coefficient of electrical resistance of metals. They are nearly linear over a wide range of temperatures and can be made small enough to have response times of a fraction of a second. They require an electrical current to produce a voltage drop across the sensor that can be then measured by a calibrated read-out device.

Platinum is the material used in most RTDs. It is highly resistant to contamination and has a predictable resistance change as a function of temperature. Other materials used in RTDs are tungsten, copper, nickel and nickel alloys. While some RTDs are constructed by depositing a platinum film on a substrate. It is then encapsulated for protection. Because these thin-film devices are small, they respond rapidly to changes in temperature.

**Radiation Thermometers :** Radiation Thermometers (Pyrometers, if you will) are non-contact temperature sensors that measure temperature from the amount of thermal electromagnetic radiation received from a spot on the object of measurement. This group of sensors includes both spot or point measuring devices in addition to line measuring radiation thermometers, which produce 1-D and, with known relative motion, can produce 2-D temperature distributions, and thermal imaging, or area measuring, thermometers which measure over an area from which the resulting image can be displayed as a 2-D temperature map of the region viewed.

**Fibre Optic Temperature Sensors:** There are a wide number of devices that utilize fiber optics to aid in measuring temperature. Most are actually slight variation of radiation thermometers, but not all. Most all depends upon a temperature-sensing component being placed on the tip of the fiber optics "free end". The other end is attached to a measuring system that collects the desired radiation and processes it into a temperature value. Like a lot of things there are some notable exceptions: the



bulk fiber optic sensors, which measure the temperature of the fiber along its length and produce either an average temperature or some measure of the temperature distribution along the length of the fiber.

**Filled system Thermometers:** They look like small metal tubes with bulges on the end-filled system thermometers-much like liquid-in-glass-but different.

**Bimetallic thermometers:** Bimets, as they are often called, are based on differential thermal expansion of metals. They are simple rugged devices usually used as spot checking devices by lab, QA and maintenance staff, or to control your home heating/cooling system.

**Semiconductor Temperature Sensors:** Commercial temperature sensors have been made from semiconductors for a number of years now. Working over a limited temperature range, they are simple, linear, accurate and low cost devices with many uses.

In our mechanical set up we have used both the Thermocouple and Resistance Temperature Detector (RTD) pt100 as the temperature sensor. As we have discussed above that for RTDs are the most accurate and more linear so we can use the conversion table as given in the appendix. We can also approximate the temperature dependence with a straight line, which can be defined by measuring two data points, the ice water temperature and the liquid nitrogen temperature. In this case, we only need to find the  $dR/dT$  of the sensor

and then a computerized system can convert the measured resistance into the corresponding temperature.

## **4.3 Mechanical Setup and the Cryogenics**

### **4.3.1 Introduction**

Work at low temperature will require calculations of the time required for components to cool, the ultimate temperature they will reach, and the amount of cryogen used in cooling process. Those calculations depend on the ability of the materials to conduct heat, the amount of heat they store, and the cooling capacity of the cryogens. Thermal modeling of the cryogenic system helps to investigate the critical parameter which determines the above mentioned problems.

In this section a thermal model has been proposed though close form solutions have not been found. After considering the design rule proposed Dewar has been evaluated upon these rules.

### **4.3.2 Thermal modeling**

In the following designed cryogenic system, shown in Fig. 4.3., there are two possible ways for the heat to flow toward the outer environment or vice versa.

One is through the walls of the liquid nitrogen container (made of stainless steel) and the other is through the base plate of the container into the environment. The temperature of liquid nitrogen, represented by  $q$ , is considered to be relative ground of the thermal equivalent circuit.

Considering first the conduction through the walls of the container, heat flows from liquid nitrogen to the walls by convection ( $R_{conv}$ ) and then the stainless steel ( $R_{ss}$ ). Then the heat flow is further divided into three branches, which, starting from the upper portion towards the lower portion of the dewar, are as follows:

1. Walls of liquid nitrogen container to the Teflon through conduction ( $R_{tef}$ ) and then to the environment, through convection.
2. From walls to the insulating Styrofoam ( $R_{sf}$ ) by conduction and to the environment by convection.
3. A large part of liquid nitrogen container is conducting heat by conduction in series through Styrofoam, then stainless steel, styrofoam, teflon and finally to the outer environment by convection.

This is shown in Figure 4.4, where all three possibilities are considered together.

Considering now the second possibility, we have copper at the base plate of the liquid nitrogen container. Most of this base plate is directly exposed to the

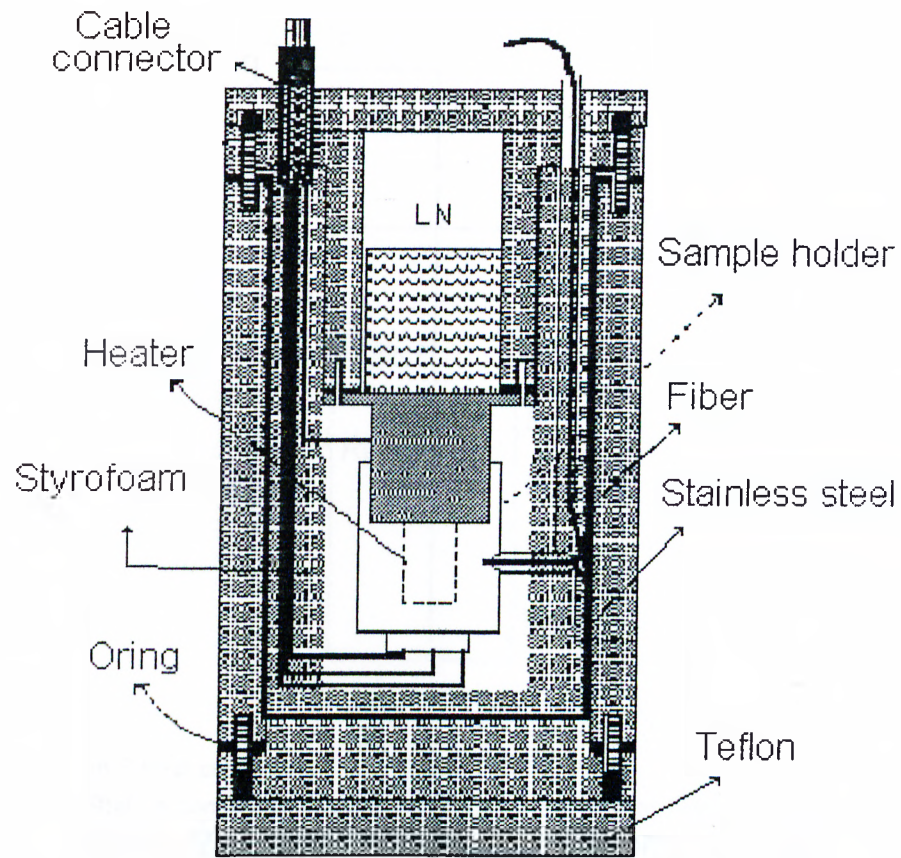


Figure 4.3: Cross section of the Dewar.

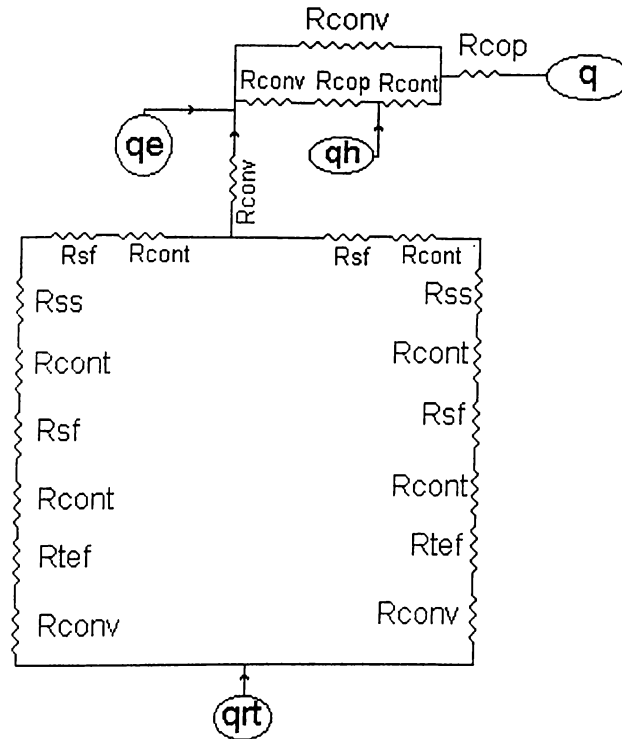
inner environment of the Dewar. So there is additional heating at this point as shown in Figure 4.4 by " $q_e$ ". Heat also flows by conduction to the sample holder, which is connected to the base plate and this holder is also directly exposed to inner environment. So the second main branch is conducting heat from the base plate to inner environment by two ways, which in terms of sequence, of their resistances are as,

1. " $R_{conv} - R_{cop} - R_{conv}$ "



provide the temperature stability at the holder.

**Thermal model for the second branch**



- |   |   |
|---|---|
| $q_h$ = Heat conduction due to heater         | $q = 77K$   |
| $R_{tef}$ = conduction through teflon         | $q_{rt}$ = Room Temperature                       |
| $R_{sf}$ = conduction through styrofoam       | $R_{conv}$ = thermal resistance due to convection |
| $R_{ss}$ = conduction through stainless steel | $R_{cop}$ = conduction through copper             |
| $R_{cont}$ = conduction through contacts      |   |

Figure 4.5: Thermal model for the dewar where the heat transfer involves the inner environment.

Due to continuous flow of heat, steady state cannot be achieved and hence representing the heat capacity of the involved masses, capacitors are inserted at each inter connecting resistance node. Systematic approval can be used to find the detailed thermal parameters. Normally following formulae are used to find the particular thermal resistances:

For thermal resistance,  $R_{ij}$  we have;

$$R_{ij} = \begin{cases} \frac{\delta_{ij}}{kA_{kij}} & \text{for conduction} \\ \frac{1}{h_{ij}A_{c_{ij}}} & \text{for convection} \end{cases}$$

where  $k$  is the thermal conductivity,  $h_{ij}$  is the heat transfer coefficient,  $A_k$  conduction area and  $A_c$  convection area. For the thermal capacitance

$$C_i = V_i \rho c_p \quad (4.18)$$

The following expression must be satisfied at each nodal point  $i$ : [11]

$$\text{Explicit : } \sum_j \frac{t_j - t_i}{R_{ij}} + q_i = \frac{C_i}{\partial \tau} (t'_i - t_i) \quad (4.19)$$

$$\text{Implicit : } \sum_j \frac{t'_j - t'_i}{R_{ij}} + q_i = \frac{C_i}{\partial \tau} (t'_i - t_i), \quad (4.20)$$

where  $q_i$  denotes the rate of heat exchange (external or internal) at the node.

### 4.3.3 Dewar design

In Dewar design there are some basic but important points which should be taken into consideration. In this section we will try to focus on these parameters and try to explain the changes in the approach to improve the reliability of our Dewar, working at environmental pressure.

As shown in the Figure 4.7, **Conduction** from room temperature into the cryogen is minimized by using supports with the smallest possible cross section and as long as possible. Materials with low thermal conductivity are used.

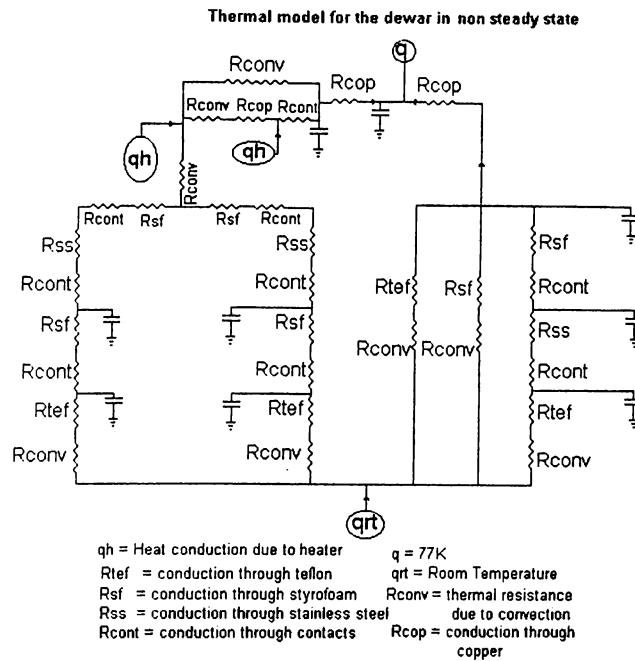


Figure 4.6: Non steady state model for the dewar.

Stainless steel is the most common material. So for the purpose of low conduction from outer environment, we have used Stainless steel for inner wall of the Dewar. The liquid Nitrogen container is also made of Stainless steel in order to reduce the heat conduction through the wall of the container. The base of liquid nitrogen container is made of copper with holes (groves) in the sample holder in order to increase the conduction to the sample holder. It has been observed that making the container in this way decreases the Nitrogen boiling and provides better conductivity to the sample.

In order to reduce the volume inside the Dewar, which should be cooled down, we have filled the space between the liquid nitrogen container and the Stainless steel inner wall of the dewar. By doing so we could reach down to  $-194^{\circ}C$  (81K) in the first step. This also further reduces the boiling of the



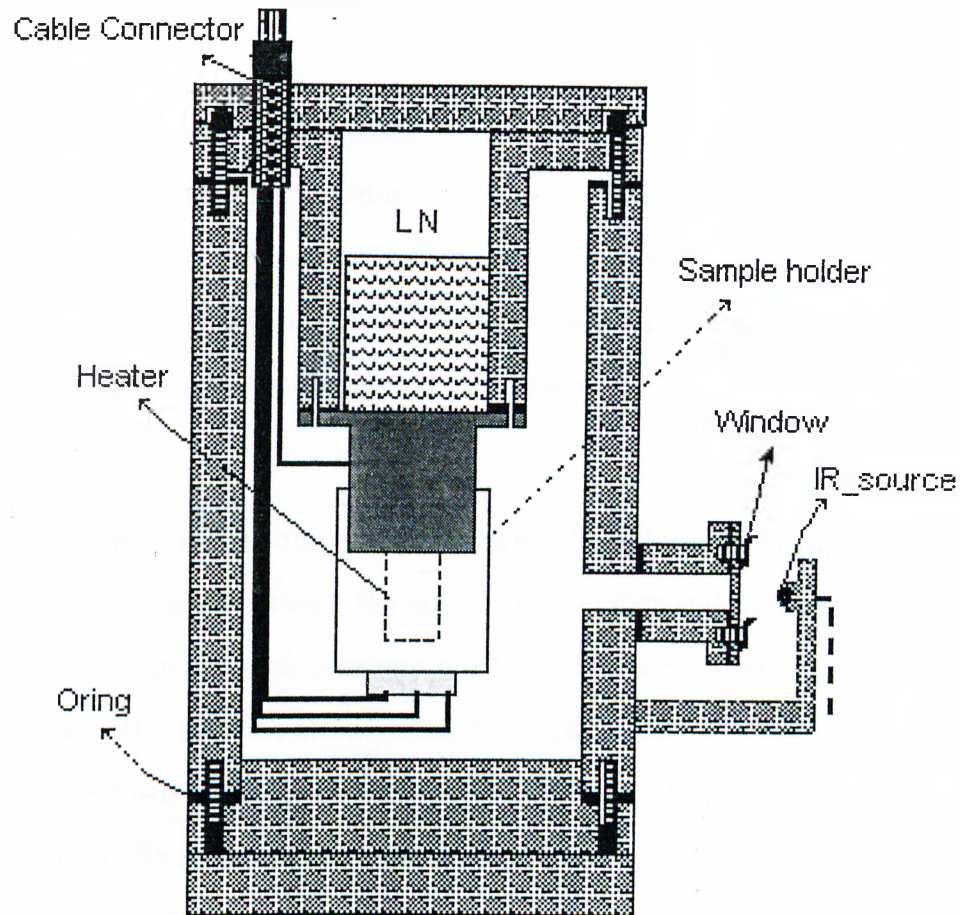


Figure 4.7: Cross section of the Dewar.

liquid nitrogen or in other words increases the lifetime of liquid Nitrogen.

Conduction through electrical leads is also considerable. Using leads made of manganin or constantan can reduce the thermal conductivity. Unfortunately materials with low thermal conductivity also have low electrical conductivities, so electrical requirements must be balanced against cryogenic considerations. We have used the twisted copper wires, which are rolled across the liquid nitrogen container in order to prevent the flow of heat from outer environment

to the sample holder.

**Power dissipation** in the leads is a source of heat that should be considered; large diameter leads reduce the power dissipation but increase the conducted heat load. So in order to reduce the power dissipation and not to conduct the heat, we have use 28 and 26 gauge wires have rolled them around the liquid nitrogen container as mentioned above.

**Convection and gaseous conduction** can be reduced to negligible values by evacuating the space between the inner cold chamber and the outer chamber walls. To maintain that vacuum one must use materials that do not outgas and must keep the surfaces clean. Even fingerprints can generate enough gas to slow pump down or spoil the vacuum shortly after the dewar disconnected from the pump. By means of the following formulas we can see how gases helps in thermal conduction.

**Case I:** High pressure (mean free path < spacing between walls)

$$Q = k \frac{A}{d} \Delta T, \quad (4.21)$$

where  $A$  is the area of surfaces facing each other,  $d$  is the distance between the hot and cold surfaces,  $\Delta T$  is temperature difference between the warm and cold surfaces, and  $k$  is the thermal conductivity of the gas.

**Case II:** Low pressures (mean free path > spacing between walls)

$$Q = K_1 a \sqrt{\frac{273K}{T_i}} P A \Delta T, \quad (4.22)$$

where  $K_1$  is free molecular conductivity,  $a$  is accommodation coefficient,  $T_i$  is the temperature of the cold surface,  $P$  is Dewar pressure,  $A$  is area of the surfaces facing each other, and  $\Delta T$  is temperature difference between warm and cold surfaces.

In order to satisfy these requirements we have used the Styrofoam as discussed above, which not only reduces the condensation but also reduce the area which the liquid nitrogen has to cool down.

The heat conduction through radiation can be reduced by reducing the emissivity of the cold and warm surfaces that face each other, and also by introducing an intermediate temperature surface between the coldest and warmest surfaces. The radiative heat load to a spherical or cylindrical container of area  $A_1$ , temperature  $T_1$ , and emissivity  $\epsilon_1$  from a surrounding container of temperature  $T_2$  and emissivity  $\epsilon_2$  is given by:

$$P = \sigma(T_2 - T_1)\epsilon A_1. \quad (4.23)$$

where

$$\epsilon = \frac{\epsilon_1 \epsilon_2}{\epsilon_1 + \epsilon_2 - \epsilon_1 \epsilon_2}. \quad (4.24)$$

Additional refinements will improve the hold time of Nitrogen and perhaps allow us to add a little strength to the dewar neck: multilayer insulation (MLI)

can be wrapped loosely around the inner wall. It is a blanket of alternating layers of aluminized Mylar and veil-like material to keep the layers from touching. The escaping Nitrogen gas can be channeled along the neck walls, cooling them and compensating for some of the conducted heat. We did not consider these improvements in our dewars because they complicate the calculations, but they can improve dewar hold time substantially. Where the hold time is defined as the time for which the dewar is capable of holding the required temperature.

The power transferred by radiation, if MLI with  $N$  independent heat shields float in temperature between the planes at  $T_1$  and  $T_2$ , is:

$$P = \frac{\sigma(T_2^4 - T_1^4)}{N + 1} \epsilon A. \quad (4.25)$$

The proposed Dewar is shown in Figure 4.8. In this design we have used the copper sample holder which is attached to the copper cold head. This cold head is connected to Teflon cup, which provides the source for the liquid nitrogen. In order to couple the light from LED to the sample, multi mode fiber has been used.

For flexibility in handling, electrical connectors for the dc biasing of the sample, temperature measurement and controlling for the heater, is connected to the top plate of the liquid nitrogen holder. O-rings and Vacuum grease has been used to provide the good sealing for the expected self-vacuum.

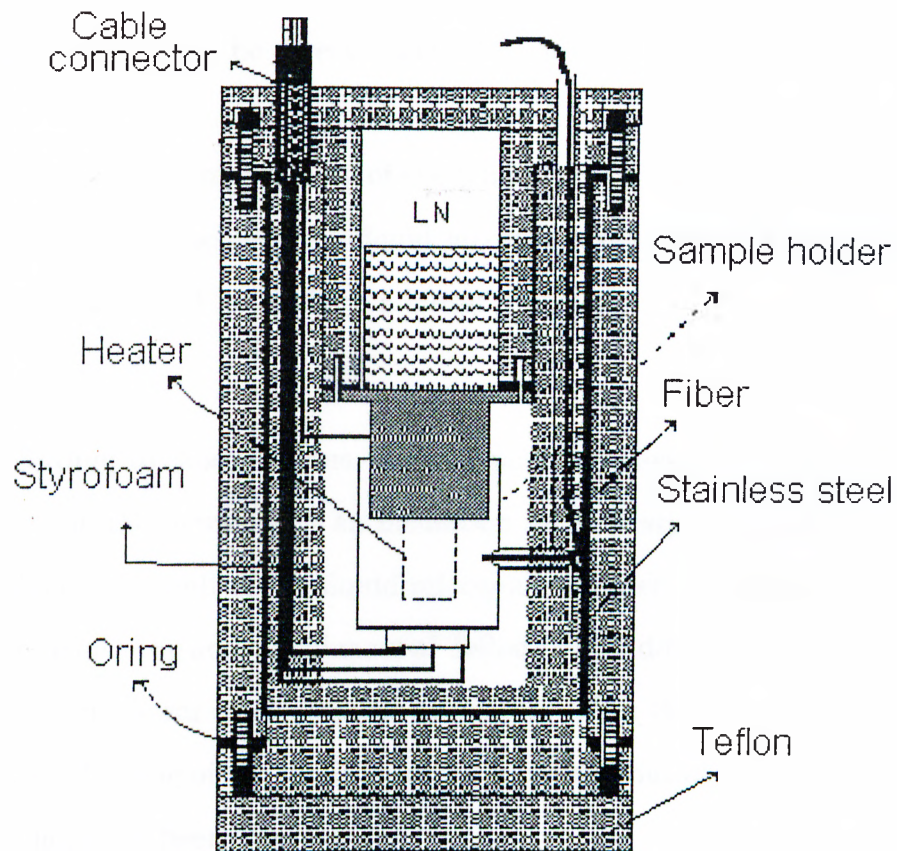


Figure 4.8: Cross section of the Dewar with modification..

The basic test for this configuration showed that there is a considerable consumption of liquid nitrogen in order to reach 77K. It was found out that this is basically due to the direct contact of liquid nitrogen with the Teflon, which has still very low thermal conductivity as compared to other materials. Secondly it was due to the fact that it has to cool down the whole environment inside before we can obtain the vacuum inside the dewar.

In order to improve this configuration we have changed the above design by considering the following few factors;

- 1) The volume inside the dewar should be small, in order to reduce the heat

conduction due to air circulation.

2) There should not be direct contact of the of the liquid nitrogen with the Teflon.

3) As the thermal conductivity of the teflon is very low, the inner environment take long time to achieve the liquid nitrogen temperature, so the inner walls of the dewar should be made of a better material.

According to modifications, we have put a stainless steel, SS, wall and the base in side the dewar with an insulation layer of styrofoam between the SS and teflon. The wall of the liquid nitrogen container has been changed to SS walls to reduce the additional mass of Teflon to cool down. To reduce the inside volume of the dewar styrofoam has been used. With this new configuration not only the hold time of the liquid nitrogen increased but also the temperature of sample hold has been improved.

## 4.4 Electrical setup

An electrical setup has been developed in order to characterize the edge transition infrared superconducting detectors, especially for Resistance vs. Temperature measurement, critical current measurement, and most important, for frequency response of the detectors at low temperatures.

#### 4.4.1 Resistance Vs. Temperature measurement

In order to measure the change in the resistance of the samples by decreasing the temperature, we have used two different methods; I ) Four probe method, and II ) mutual induction method explained as follows.

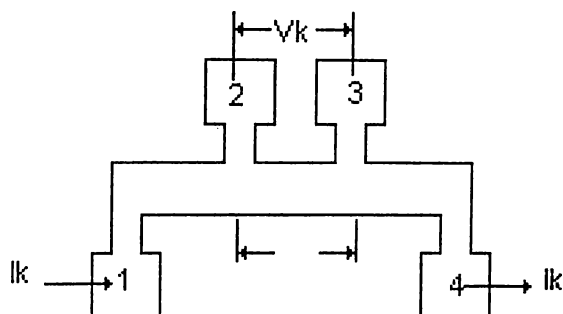


Figure 4.9: Basic setup for four probe measurement.

$$R_s = \frac{V}{I}CF. \quad (4.26)$$

**Method I: The Four-Point Probe Technique:** The resistance of a diffused layer can be measured by a four-point probe technique. The resistance of the sample can be expressed as,

$$R_s = \frac{V}{I}CF. \quad (4.27)$$

where  $R_s$  is the sheet resistance (in ohms/square);  $V$  is the dc voltage across the voltage probes (in volts);  $I$  is constant dc current passing

through the current probes (in amperes); and C.F. is the correction factor. In most common configuration the four probe points are in line with the dc current passing through the outer two probes and the voltage measured across the inner two probes.  $R_s \cdot x_j$  is the average resistivity of a diffused layer.

The correction factor for a circular sample (with a diameter  $d$ ) and a regular sample (with the side parallel to the probe line as  $a$  and that perpendicular to the probe line as  $d$ ) are given in Table 4.2 (where  $s$  is the probe spacing).

d/s	Circle	Square a/d=1	a/d	Rectangle a/d=3	a/d > 4
1.0				0.9988	0.9994
1.25				1.2467	1.2248
1.5			1.4788	1.4893	1.4893
1.75			1.7196	1.7238	1.7238
2.0			1.9475	1.9475	1.9475
2.5			2.3532	2.3541	2.3451
3.0	2.2662	2.4575	2.7000	2.7005	2.7005
4.0	2.9289	3.1127	3.2246	3.2248	3.2248
5.0	3.3625	3.5098	3.5749	3.5750	3.5750
7.5	3.9273	4.0095	4.0361	4.0362	4.0362
10.0	4.1716	4.2209	4.2357	4.2357	4.2357
15.0	4.3646	4.3882	4.3947	4.3947	4.3947
20.0	4.4364	4.4516	4.4553	4.4553	4.4553
40.0	4.5076	4.5120	4.5129	4.5129	4.5129
$\infty$	4.5324	4.5324	4.5325	4.5325	4.5325

Table 4.2: Correction factor C.F for the measurement of sheet resistances with the four-point probe.



Note that for a large  $d/s$ , the correction factor approaches that of a two-dimensional sheet extending to infinity in both directions, that is, C.F. = 4.53. For the correction factors to be insensitive to the sample size and the positions of the probe points with respect to the sample edge, a large  $d/s$  is desirable.

**Van der Pauw Technique:** The resistance of the sample with an irregular shape can be determined by using the Van der Pauw technique. For measurement four contact points along the periphery of a sample, as shown in Figure 4.10, current is forced to flow between two adjacent contacts,

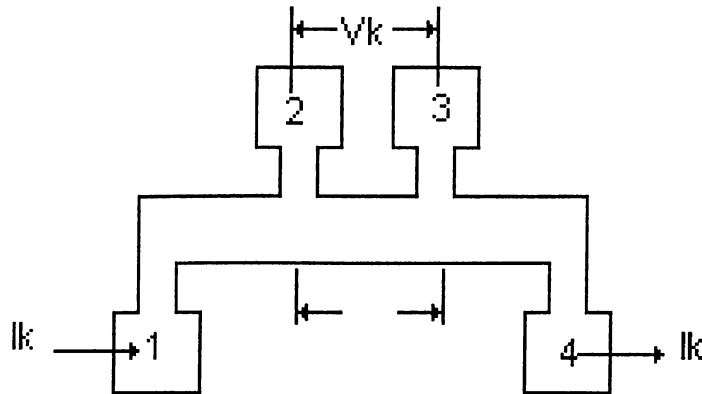


Figure 4.10: Basic configuration for four probe measurement.

and the voltage across the other pair of contacts is measured with a high-input impedance voltmeter. The resistivity of the sample is

$$\rho = \frac{\pi d}{\ln 2} \left( \frac{R_{12,34} R_{23,41}}{2} \right) F(Q). \quad (4.28)$$

where  $R_{12,34} = V_{12}/I_{34}$  and  $R_{23,41} = V_{23}/I_{41}$ .

$F(Q)$  is a correction factor and  $d$  is the sample thickness;

For the configuration shown in Figure 4.11. Current flows through two adjacent probes and the voltage is measured across the remaining two contacts. An average resistance is obtained by rotating the current and the voltage probes;

$$R = \frac{1}{4} \left( \frac{V_{12}}{I_{34}} + \frac{V_{23}}{I_{41}} + \frac{V_{34}}{I_{12}} + \frac{V_{41}}{I_{23}} \right) \Omega/\square. \quad (4.29)$$

Since the structure shown in figure b is symmetrical,  $F=Q = 1$ , and

$$R_s = \frac{\pi}{\ln 2} R = 4.53R. \quad (4.30)$$

In this measurement, the measured sheet resistance does not depend on the line width of the diffused region. When the resistance from a Kelvin resistor is measured, the effective line width of a diffused resistor can be determined from these two measurements. In a Kelvin resistor structure, a constant dc current flow through the two end contacts, and the voltage across the middle two contacts is measured with a high-input-impedance electrometer, which measures the potential difference across the center

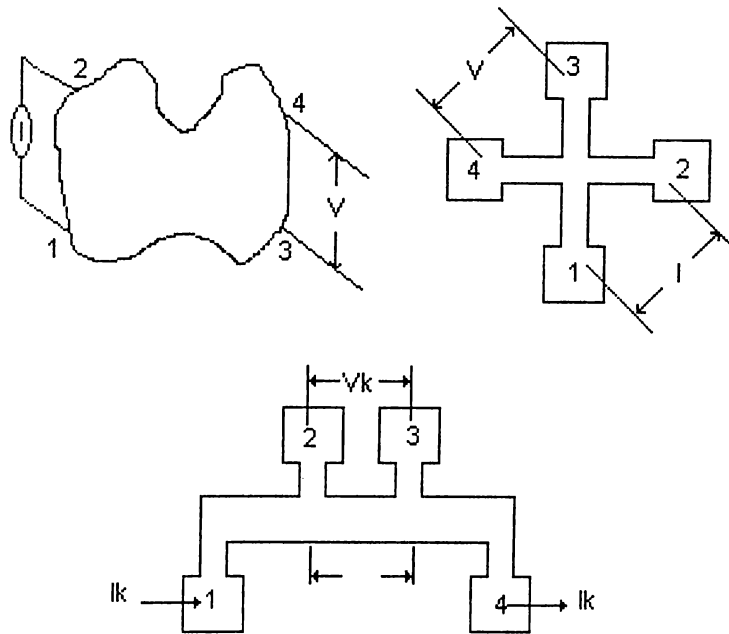


Figure 4.11: Van der Pauw and Kelvin resistor structures: (a) sample with an arbitrary shape; (b) an in-process tester design; (c) a Kelvin resistor design for measuring the effective window width..

probes without disturbing the equal potential lines or the current flow. The measured resistance from the Kelvin resistor,  $R_k$ , is  $V_k/I_k$ , with  $V_k$  the measured voltage across the voltage probes and  $I_k$  the current.

Dc analyses were done by switching the current through the sample in order to reduce the thermocouples effect of the measurement pins and this method is named as Quasi dc analysis. As shown in the Figure 4.12, the relay has been used to switch the current through the sample and the relay has been controlled by computerized system.

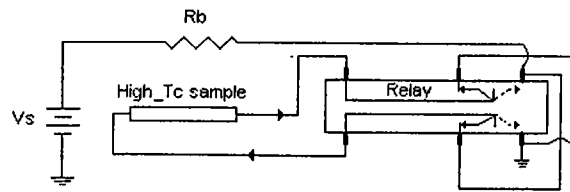


Figure 4.12: A relay configuration used to switch the current.

Thermocoupling effect can be reduced by switching, which can be explained as follows, If  $V_{plus}$  represent the voltage when the current direction is in positive direction then,  $V_{plus} = V_s + V_{th}$ . While if  $V_{neg}$  is the voltage when the current direction has been changed then  $V_{neg} = -V_s + V_{th}$ . As  $V_{th}$  is always being an additive part, so the coupling threshold can be discarded if we take the average of  $V_{plus}$  and  $V_{neg}$ , and the resulting voltage  $V_s = (V_{plus} + V_{neg})/2$  will be the true voltage.

For temperature readings we have used PT100, as we have discussed in article 4.3.6, which gives almost a linear decrease in the resistance by decreasing the temperature across it. Again for PT100 we have used the four-probe method in order to get more reliable temperature reading. For the purpose to read this voltage reading both from the sample as  $V_s$  and  $V_{pt}$  (from PT100) through the computer the analogue amplifier has been designed as shown in the Figure 4.13. To read out the data a 12 bit AD/DA Card has been used, which was programmed by using the Qbasic. [12]

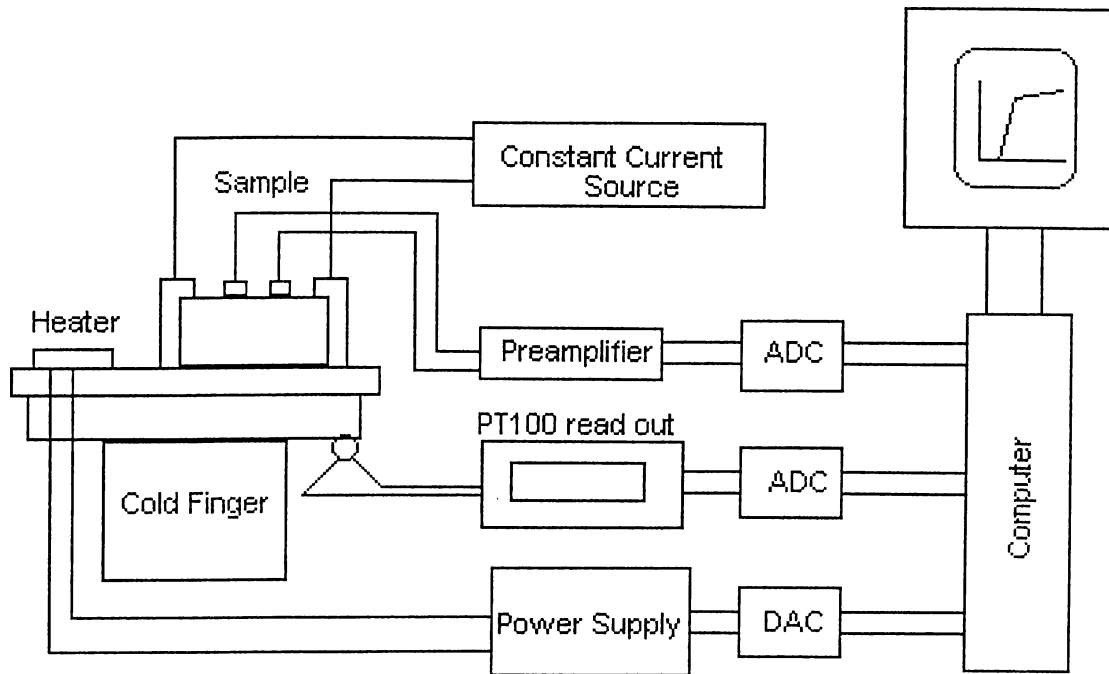


Figure 4.13: Computerized system for dc characterisation of superconducting thin and thick films.

**Method II:** Mutual Induction method: [13] An apparatus providing a non-contact method of probing the current-induced destruction of superconductivity in thick film samples has been developed. A schematic of the experimental set-up is shown in Figure 4.14.

A thick film sample is positioned between a primary coil, which induces a supercurrent in the film and a secondary coil that monitors flux penetration. As we can see from the diagram a sine wave current is applied to the primary coil, generating an ac magnetic field and inducing a shielding supercurrent in the film (if the sample is in the superconducting state). These supercurrents have the effect of reducing the magnetic flux linking to the secondary coil to a value less than a would have been in the normal

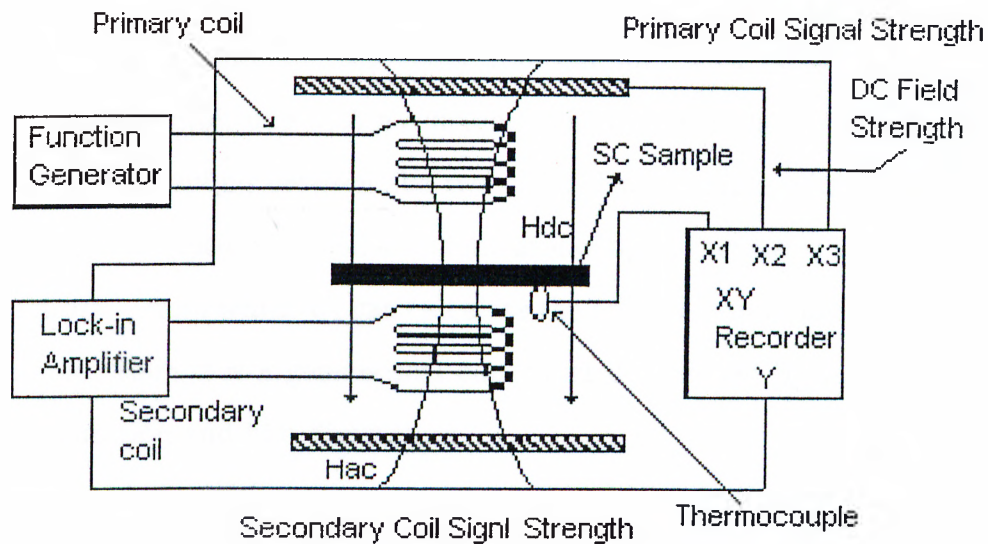


Figure 4.14: Schematic diagram for mutual induction measurement.

state. Therefore by monitoring the changes in the secondary coil signals we can detect at least the following information:

- a. The transition temperature,  $T_c$ . When we warm the sample above  $T_c$ , the magnetic shielding due to the supercurrent disappears. Hence we expect to see a signature for this change of state in the pick-up coil signals. If we plot pick-up coil signal vs. temperature, we should be able to identify the transition temperature of the samples.
- b. The critical current density,  $J_c$ . We can vary either the amplitude or the frequency of the ac current applied to the primary coil to change the induced supercurrent in the film. As the field amplitude due to the primary coil is increased, a signal proportional to that in the primary coil should be observed at the secondary coil. When the field amplitude

exceeds that just sufficient to induce a critical current in the film, the pick-up signal from the secondary coil will vary with further increases of the field amplitude with a different proportionality factor, due to the change in coupling between the two coils. This turning point in the response of the secondary coil is an indicator of flux penetration at a critical field  $\partial H_{c1}$ , from which we can calculate the critical current density of the sample. Here  $\partial$  is a geometrical parameter determined by the film-coil configuration and film dimensions.

c. The critical field,  $H_c$ . We can also apply an external dc magnetic field as shown in Figure 4.14. When this external dc magnetic field exceeds the critical field  $H_c$ , the transport supercurrent induced in the film will be destroyed and there will be a distinct change in magnetic flux linking to the secondary coil. It should be noted that this critical field is current dependent (induced by the ac field of the primary coil), and is the lower critical field  $H_{c1}$  in the case of the Type II superconductors. The geometry of the sample is such that, due to the demagnetisation coefficients, field will enter the superconductor well below the value of  $H_{c1}$ .

In experimental set-up [14], variable current source was used for the primary coil. The signal from the secondary coil is fed to an amplifier, which is a low noise feed back amplifier with a gain of about 1000. We can also directly use a lock in amplifier to amplify the induced voltage for a particular reference frequency. In case of amplifier we need to convert the output signal to be converted into the dc so that we can read this through the computer while on the other hand for lock-in amplifier the

out can be read by the computer together with the temperature readings from the PT100.

#### 4.4.2 Responsivity measurement

In order to measure the response vs. temperature, frequency response, and noise measurement, an electrical and mechanical set was required. According to requirement it should be capable of providing the following accessories;

- 1) Reliable way to apply the bias current to the sample.
- 2) Ability to shine light on the sample with out disturbing the dewar configuration.
- 3) Must be able to receive the modulated voltage and together with amplification average it.
- 4) Store the data and plot it according to desire.

These requirements have been achieved by the following setup;

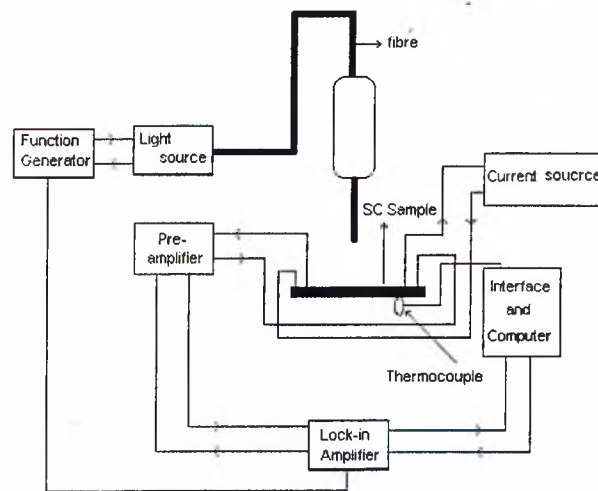


Figure 4.15: A setup for the response measurement for thick and thin film.



In this setup 3314A function generator from Hewlett Packard together with Infrared LED has been used to generate an infrared signal. Single mode fiber has been used in order to transmit the light from LED to the sample. Butt coupling method has been used to couple the light to the fiber. Although by this method the efficiency is not more than 10 % but still it is a cheap and simple way to couple light. A low noise preamplifier (Model SR560 by Stanford Research) is used to amplify the output modulated voltage. After amplification these voltages are feed to lock-in amplifier to average them and phase lock with the reference input signal. For temperature stabilisation a heater has been used which is operated by computer control power supply (6628A-system DC power supply). The output of the Lock-In amplifier is feed to computer by using the A/D card and matlab has been used to plot the data. The accuracy of this system is 10s of nV.

## Chapter 5

# FABRICATION AND CHARACTERISATION

### 5.1 High $T_c$ superconducting YBCO device fabrication and material development

After observing the basic properties, which are essential for the particular detector application and also considering the thermal model, it is necessary to use the appropriate manufacturing technology. In this section different fabrication techniques have been considered. In order to improve the important parameter which can effect the responsivity of the system, found from the one dimensional thermal model, a new method for the fabrication of the devices has been discussed. In order to check the validity of the annealing profile disk

fabrication was done first. After finding out the validity of the annealing profile, the device fabrication has been proceeded.

One of the important parameters which effects the properties of any detector is substrate material. Hence a brief literature survey has been given in order to understand the basics of substrate selection.

### **5.1.1 Overview of various thin-film deposition technologies**

The following is a brief description of the principles, salient features, applications, and selected literature references of the more important technologies for thin film deposition and formation, categorized in Table B.6 (see appendix.

#### **Evaporative Technologies:**

Although one of the oldest techniques used for depositing thin film, thermal evaporation or vacuum evaporation is still widely used in the laboratory and in industry for depositing metal and metal alloys. The following sequential basic steps take place:

- 1) A vapor is generated by boiling or subliming a source material;
- 2) the vapor is transported from the source to the substrate; and

3) the vapor is condensed to a solid film on the substrate surface.

Although deceptively simple in principle, the skilled practitioner must be well versed in vacuum physics, material science, mechanical and electrical engineering as well as in elements of thermodynamics, kinetic theory of gases, surface mobility, and condensation phenomena.

Evaporants cover an extraordinary range of varying chemical reactivity and vapor pressures. This variety leads to a large diversity of source components including resistance-heated filaments, electron beams; crucible heated by conduction, radiation, or rf-induction; arcs, exploding wires, and lasers. Additional complications include source container interactions; requirements for high vacuum precise substrate motion and the need for process monitoring and control.

**Molecular Beam epitaxy (MBE):** MBE is a sophisticated, finely controlled method for growing single-crystal epitaxial films in a high vacuum ( $10^{11}$  Torr). The films are formed on single-crystal substrate by slowly evaporating the elemental or molecular constituents of the film from separated Knudsen effusion source cells (deep crucibles in furnaces with cooled shrouds) on to substrate held at temperature appropriate for chemical reaction, epitaxy, and re-evaporation of excess reactants. The furnaces produce atomic or molecular beams of relatively small diameter, which are directed at the heated substrate, usually silicon or gallium arsenide. Fat shutters are interposed between the sources and the substrates. by controlling these shutters, one can grow superlattices with

precisely controlled uniformity, lattice match, composition, dopant concentrations thicknesses, and interfaces down to the level of atomic layers.

The expensive equipment are, at present, the major limitations for this promising deposition technology for production of the devices.

### **Glow-discharge Technologies:**

The electrode and gas-phase phenomena in various kinds of glow discharges represent a rich source of process used to deposit and etch thin films. Creative exploitation of these phenomena has resulted in the development of many useful processes for film deposition, as listed in Table B.6.

**Sputtering.** The most basic and well known of these processes is sputtering, the ejection of surface atoms from an electrode surface by momentum transfer from bombarding ions to surface atoms. From this definition, sputtering is clearly an etching process, and is, in fact, used as such for surface cleaning and for pattern delineation. Since sputtering produces a vapor of electrode material, it is also used as method of film deposition similar to evaporative deposition. Sputter-deposition has become a generic name for variety of processes.

- Diode Sputtering.
- Reactive Sputtering.

- Bias Sputtering.
- Magnetron Sputtering.
- Ion-Beam Sputtering.

**Plasma Processes.** The fact that some chemical reactions are accelerated at a given temperature in the presence of energetic reactive-ion bombardment is the basis of processes for surface treatments such as plasma oxidation, plasma nitriding and plasma carburising. A metal to be oxidized, nitrided or carburised is made the cathode of a glow discharge and is simultaneously heated by radiant of rf-induction means. The discharge gas is either  $O_2, N_2$  plus  $H_2$ , or  $CH_4$ . Very thick (0.1-2 mm) protective coatings on a variety of metals can be produced in this way to render surfaces hard and /or corrosion resistant.

- Anodization.
- Deposition of Inorganic/Organic Films.
- Microwave Electron Cyclotron Resonance Deposition.

**Cluster Beam Deposition.** Ionised cluster beam deposition (ICB) or cluster beam deposition is one of the most recent emerging technologies for the deposition of thin films with growth control capabilities not attainable by many of the other processes. ICB depositions are one of several techniques classifieds ion assisted thin-film formation. The material to be deposited emerges and expands in to a vacuum environment from a small nozzle of a heated confinement crucible, usually constructed of high-purity graphite. The vapor pressure within the crucible is several orders of magnitude higher than the pressure of the vacuum chamber so that the expanding vapor supercools. Homogeneous nucleation results in the

generation of atomic aggregates or clusters of up to a few thousand atoms held together by weak interatomic forces. The clusters passing through the vacuum towards the substrate can in part be positively charged by impact ionization with electron beam irradiation. Closely controlled acceleration voltages add energy to the ionized clusters which then impinge on the substrate, diffuse or migrate along the plane of the surface, and finally form a thin film of exceptional purity. The complete and detailed process is extremely complex but offers unprecedented possibilities of film formation once the fundamentals and engineering technology are fully understood and exploited.

#### **Gas Phase Chemical Processes:**

Method of film formation by purely chemical processes in the gas or vapor phases includes chemical vapor deposition and thermal oxidation. Chemical vapor deposition (CVD) is a materials synthesis process where by constituents of the vapor phase react chemically near or on a substrate surface to form a solid product. The main features of CVD are its versatility for synthesizing both simple and complex compounds with relative ease and at generally low temperatures. Both chemical composition and physical structure can be tailored by control of the reaction chemistry and deposition conditions.

Chemical reaction types basic to CVD include pyrolysis (thermal decomposition), oxidation, reduction, hydrolysis, nitride and carbide formation, synthesis reactions, disproportionation, and chemical transport. Deposition variables

such as temperature, pressure, input concentrations, gas flow rates and reactor geometry and operating principle determine the deposition rate and the properties of the film deposit. Thin-film materials that can be prepared by CVD cover a tremendous range of elements and compounds. Inorganic, organometallic, and organic reactants are used as starting materials. Materials deposited at low temperatures (e.g., below  $600^{\circ}\text{C}$  for silicon) are generally amorphous. Higher temperatures tend to lead to polycrystalline phases. Very high temperatures (typically  $900^{\circ}\text{C}$  to  $1100^{\circ}\text{C}$  in the case of silicon) are necessary for growing single-crystal films. These films are oriented according to the structure of the substrate crystal; this phenomenon, known as epitaxy, is of crucial practical importance in solid-state device technology.

**Ion Implantation.** Ion implantation has been used to form silicon-on-insulator structures by implanting large doses of atomic or molecular oxygen ions in single-crystal silicon substrates to produce a buried oxide layer with sharp interfaces after annealing. Simultaneous high dose implantation of low energy oxygen and nitrogen ions into silicon yields very thin films of silicon oxynitride, whereas low-energy implantation of nitrogen or ammonia into silicon yields a low-density silicon nitride layer.

In the Some of the many other techniques are thermal oxidation, liquid-phase chemical formation, electrolytic Anodization, and electroplating. The discussion of which is far beyond the scope of this work.



## 5.2 Fabrication

### 5.2.1 Fabrication of SC Disc, thick film and the Annealing profile

#### SC Disc fabrication:

Bulk superconducting discs were made by compressing the  $YBa_2Cu_3O_{7-x}$  powder using a home made compressor. The discs were annealed by using the following thermal treatment;

1. It was heated to 950 °C with heating rate of 10°C/min in the presence of  $O_2$ .
2. Changing the Gas atmosphere to Ar for 8 minutes at 950 °C.
3. Changing the gas again to  $O_2$  and stay at 950 °C for 1 hour.
4. Cooling down the disc with a cooling rate of -5°C down the 470 °C.
5. In the presence of Oxygen keeping the temperature at 470 °C for 2 hours, called the oxidation stage.
6. Cooling the down the system to room the temperature with a cooling rate of -1°C.

In order to observe the effect of the environmental gas, three different gases have been checked namely, Oxygen, Argon and air. The results obtained for the basic characteristics are given in section 6.1.2.

### Thick film fabrication:

**screen printing** Thick film pastes were formed by mixing powders of the superconducting materials with a printing vehicle composed of terpineol and ethyl cellulose. A three roll mill (Netzsch 272.00) mixed the compositions for at least one hour. The 123 powder was obtained from a commercial source (High  $T_c$  Superconco SP-5, 0.3 - 2.0  $\mu\text{m}$  diameter).

Pressed-powder MgO substrate were used for the samples. MgO was chosen for its low reactivity with the 123 material. Magnesia has a dielectric constant of approximately 9.5, a number similar to alumina and significantly lower than materials such as strontium titanate. The loss tangent is approximately  $10^{-4}$ . These properties make MgO a candidate for microwave applications.

Film were screen printed through 280 or 325 mesh stainless steel screens. After a short leveling period, a box oven was used to dry the films at 120 °C for one hour. A horizontal 75 mm (3 in) diameter quartz tube furnace equipped with a programmable temperature controller annealed the superconducting films. Films were heated to peak temperature at rates of 10 or 100 °C/min. Peak temperature of 850 to 980 °C were held for 10-30 minutes. Cooling occurred at a rate of 2 °C/min.

Exposing films to oxygen while cooling was expected to restore the oxygen stoichiometry to nearly  $YBa_2Cu_3O_7$ . Those films annealed in argon were also cooled in argon until their temperature dropped below 700 °C. We

believe Ar was effective in reducing the melting point of the powder, producing more effective sintering. [15]

**Post Annealed blow-assisted deposition** After getting familiarity with characteristic parameters (like  $R_{fs}$  and G) of the detectors which directly influence the responsivity and detectivity, in this study a simple but intuitively an effective idea for the fabrication of thick films has been proposed. The idea of settling down of dust with air has been explored. In order to deposit a thick film the following steps has been suggested:

1. A fine powder of  $YBa_2Cu_3O_7$  with a grain size of  $\sim 0.3 - 2. \mu\text{m}$  diameter was obtained from a commercial source.
2. For making the pattern, shadow masks have been placed on top of the substrate before starting the deposition.
3. With a help of fan, YBCO powder was blew in a closed container. After about 24 hours of blowing with a constant speed a thick layer of powder was settled on the substrate.
4. After obtaining the required thickness of the film this film was annealed using the annealing profile given below;
  - Heating the samples with a heating rate of  $10 \text{ }^\circ\text{C}/\text{min}$  up to  $950 \text{ }^\circ\text{C}$  in the presence of Oxygen.
  - Heating the samples at  $950 \text{ }^\circ\text{C}$  for 8 minutes in the presence of Ar gas environment.

- Changing the gas back to Oxygen and stay at the same temperature for 1 more hour .
- Cooling down the a system with cooling rate of 5 °C/min down the 470 °C.
- Oxidizing the sample at this temperature for 2 hours.
- Cooling down slowly with approximately a cooling rate of 1 °C/min. to the room temperature, in the presence of air or oxygen.

There are many advantage of using this method some of which are listed below;

- We don't have to use any kind of chemicals to make paste as we have to for screen printing method.
- The fabrication and patterning can be done at the same time for relatively large patterns.
- There is no need to apply heat during the deposition process, which prevents any cause for deoxidisation of the material.
- The film produced this way will have a prominent grain boundaries, which are assumed to be helpful to increase the Rfs, or in other words increase in the responsivity.
- Crystal formation will be perpendicular to the substrate which will increase the surface area for the radiation absorption.

Although this method seems very basic but it can be very useful to produce highly responsive detectors. Thermal modeling for this type of detectors is not trivial. In order to model these films we need a three dimensional version of the thermal model discussed in section 3.4.

## 5.2.2 Device Fabrication

Progress in fabrication of high temperature superconducting films has increased tremendously in the last few years. Film used in this study were mainly on  $\text{SrTiO}_3$ ,  $\text{LaAlO}_3$  and  $\text{MgO}$  substrates. Most of these films were prepared by Laser ablation. Laser ablation is one of the fastest and frequently used techniques for deposition of HITS films. In principal a high-energy pulse of laser beam is employed to vaporise the surface material of the target. This material is then deposited on the substrate. Using this technique a high growth rate for the film is obtained.

The Laser ablation system is shown schematically in Figure 5.1 [16]. The advantage of this system is that the laser can cause homogeneous ablation into a wide angle due to the geometry of the target and laser beam. The substrate is located on a heating stage within the homogeneous ablation plasma. The substrate is located on a heating stage within the homogeneous ablation plasma. The parameters of pulsed excimer laser used are about;

Wavelength	248 nm
Pulse duration	About 40 ns
Repetition rate	2 Hz
Energy density	2 Joule/ $\text{cm}^2$

Table 5.1: The parameters of pulsed excimer laser.

Resulting in a time for growth of a 50 nm thick film in less than 10 minutes.

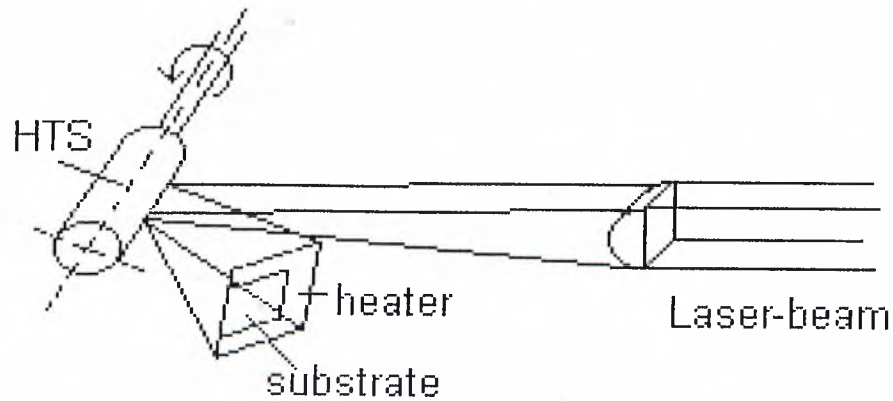


Figure 5.1: Experimental set-up for laser ablation deposition.

### 5.2.3 Substrate and Selection rules

In some materials systems, including HTS, the best films that can currently be produced are grown on materials that have serious limitations. The search for viable substrate materials is an active area of research that often accompanies the investigation and perfection of a film.

The quest for substrate materials that are capable of supporting excellent films of HTS materials has been in progress for nearly as long as HTS thin films have been prepared. In many cases it is desirable or even necessary for a film to be not only crystalline, often single crystalline, but also for the crystallographic axes of the film to have well-defined orientations with respect to the substrate. This usually requires that the film be epitaxial on its substrate, a constraint that introduces additional requirements that must be fulfilled by the substrate material.

**Chemical compatibility:** Ideally there should not be any chemical reactions between the film and substrate. The constraint is especially severe for HTS films since these materials are reactive with many substrates that might otherwise be good candidates.

**Thermal expansion match:** most combinations of substrates and films will be more or less mismatched in regard to the thermal expansion. This may result in loss of adhesion or film cracking during thermal cycling. A good thermal-expansion match is necessary, whether or not one is dealing with an epitaxial system. In the case of HTS materials, this requirement is particularly important because of the brittleness of the superconductor.

**Surface quality:** The quality of the surface is one of the most important properties of a substrate since it is the place where the film-substrate interaction occurs. A uniform surface is necessary to insure a uniform, homogeneous film. If the surface is reactive with the film to be deposited, it must be passivated in a reproducible and uniform manner. Various types of irregularities make up the overall surface texture. The following categories of surface defects may be encountered:

**(i) on the atomic scale:** point defects, dislocation lines, monatomic ledges on cleavage planes, and twin boundaries.

**(ii) submicron features:** polishing scratches, pores due to less than theoretical density of the substrate, and impurity phases;

**(iii) micron scale:** grinding scratches, crystalline boundaries in polycrystalline materials, and pores;

(iv) **macrodefects:** surface warp, and cracks.

An ideal substrate would have a flat, dense surface and free of twins and other structural inhomogeneities. It would be desirable, at the very least, to grow films on a substrate that has no phase transitions within the temperature regime required for film processing.

**Substrate cleanliness:** The cleanliness of the substrate surface exerts a decisive influence on film growth and adhesion. A thoroughly cleaned substrate is a prerequisite for the preparation of films with reproducible properties. The choice of cleaning techniques depends on the nature of substrate, the type of contaminants, and degree of cleanliness required. Residues from manufacturing and packaging, lint, fingerprints, oil, and airborne particulate matter are examples of frequently encountered contaminants.

**Substrate homogeneity:** The quality of the bulk of substrate must also be reasonable. For example, if a substrate is predominantly a single phase but contains an appreciable amount of one or more additional phases, the surface quality is likely to suffer, and film may not grow equally well on all of the phases present. Grain boundaries in the substrate that appear on the surface may affect the microstructure and morphology of the film. The substrate should have the theoretical density of its constituent. Precipitates, dislocations and etc., throughout the bulk of the substrate



may also affect the quality of the surface, especially if the density is high.

**Substrate thermodynamic stability:** It is also highly desirable that the substrate be thermodynamically stable within the temperature range required to grow and process the thin film. The typical temperature range for PLD and sputtering techniques is  $\sim 800$  °C. A phase transition within this region can have dramatic effects on the surface quality of the substrate and on the stresses the film must undergo, even if the chemistry is not a problem. If a phase transition is inevitable, it must be as minor as possible, i.e., second order with no discontinuous volume change and minimal structural change.

**Buffer layer:** These are films layers that are grown directly on the substrate in order to alleviate some of shortcomings that a substrate may have. The most common reason to use a buffer layer is to avoid unwanted reaction between film and substrate. Obviously, the buffer layer must be chemically compatible with both materials. Some reaction between the buffer layer and substrate may be permissible if it is confined to a region near the interface. If the thermal-expansion mismatch between the HTS layer and substrate is large, a buffer layer with intermediate thermal properties may alleviate cracking of the film.

**Issues for growth of epitaxial films:**

The best HTS films grown to date, as determined by a multitude of metrics including critical current density, morphology, and stability over time, are epitaxial. Epitaxial growth requires the controlled crystallographic orientation of the film with respect to the substrate, lattice parameters, atomic positions, crystallographic orientation, etc. The better the match of all of these parameters, the more likely high-quality epitaxial growth is to occur. [17]

EFFECT	ISSUE			
	Lattice Match	Coincidence sites	Surface quality	Subs. Struct. quality
Presence of epitaxy	*	*	*	*
Epitaxial orientation	*	*	*	*
No. of epitaxial orientation	*	*	*	
Phase of film	*	*		
Interface quality	*	*	*	
Superconducting properties	*	*	*	*

Table 5.2: Issues in substrate selection for epitaxial films.

**Lattice match:** The possibility of epitaxial growth on a lattice requires at greatest 15% mismatch. As the field of epitaxial growth concentrated on semiconductor systems, in which the chemistry of the film and substrate are very similar, it became apparent that vanishingly small lattice mismatches were desirable to minimize the effects of dislocations and other

defects brought about by lattice dissimilarities. In the case of HTS materials, the issue is more open. In general, it seems desirable to minimize the lattice mismatch as much as possible. This seems to improve the ability to obtain singly oriented films.

**Coincidence sites:** There must also be a reasonably number of coincidence sites between the two lattices. These are atomic positions that coincide on either side of the interface. Frequently, although not always, this means that the film and substrate should have similar crystal structures. The higher the number of coincidence sites, the better the chance of good epitaxy. Similarity in structure is as important a criterion in determining a suitable HTS epitaxial substrate as is lattice match, although they are not independent. The surface termination of the substrate is also a crucial parameter in determining the quality of oriented of epitaxial growth.

**Surface quality:** The importance of surface properties in determining the quality of a film grown on it was discussed in the previous section. Still the critical importance of this parameter in epitaxial growth needs to be reemphasized. Disoriented grains frequently nucleate on irregularities on a surface, be they dirt, surface defects, or atomic steps due to substrate miscut or other treatment. The quality of a substrate surface can be affected by a number of treatments including cleaving, polishing of various sorts, and annealing in a variety of ambient. Slight disorientations of the substrate can have a profound effect on the epitaxial quality.

**Structural quality:** The structural quality of the substrate is even more important when epitaxial films are required than when they are not. It goes without saying that a single crystal film is possible essentially only when the substrate itself is single crystal. Impurity phase inclusions in the substrate very likely will affect the surface quality and ultimately the epitaxial quality as well. Twins in the substrate in many cases will affect the degree of orientation possible in the film. In general the crystalline quality of the film will be no greater than that of the substrate.

**Issues for applications:**

Before we start considering the materials required for the development of HTS films, it is useful to enumerate some of the actual device applications of HTS layer which are as follows:

**All-superconductive devices:** Superconductors are applied in electronics for all superconducting devices as their first application. Most of all superconducting devices presented to date involve the Josephson junction or some sort of restricted current flow. The substrate must be able to support HTS films of adequate quality for reproducible junction fabrication. Grain boundaries must exist only where desired, as in the grain-boundary junction. The grain-boundary junction requires either processing of the substrate before HTS film growth or the production of a bicrystal substrate.

Substrate Requirement	All IITS Devices	Hybrid IITS Devices	Integ. HTS & Semic. Devices	Intercon.	$\mu$ -wave appl.	Current carrying appl.
Support high quality films	*	*	*	*	*	*
Control grain boundaries	*	*	*			
Low dielectric loss	Varies		*	*	*	
Devices quality semicon. layers		*	*	*		
Low $\epsilon$			*	*		
Large area			*	*	*	*
Isotropic					*	
Low surface resistivity					*	
High-Jc films				*		*

Table 5.3: Issues in substrate selection for applications.

**Hybrid superconductor-semiconductor application:** The work on Hybrid superconductor-semiconductor devices and systems has been heeded for many years. Typically, three levels of hybridization are worth discussing:

- (i) Combining superconductor and semiconductor in a single device. In this device, the substrate must either be a semiconductor or be a material that can support both device-quality semi-conducting and HTS layer.
- (ii) Combining individual superconductor devices with semiconductor devices in an integrated circuit. If one is to fabricate integrated circuits using active superconductor and semiconductors and semiconductors to be combined on a single substrate that is compatible with both.

(iii) Combining superconducting circuits and semi-conducting circuits or chips into a complete system. In this case substrates must be able to support not only interconnections but also at least some of the semiconductor circuits. There must be low loss and the chips should be compatible with both classes of electronics material. Because of the high speeds involved, the dielectric constant of the substrate must be as low as possible.

**Microwave application:** Operation at microwave frequencies imposes the need for low loss substrate. Since the dielectric properties of the substrate have an important effect on device performance, the existence of a twinning transition in the processing range is entirely unacceptable, since it precludes device modeling. Microwave applications are not generally very sensitive to the dielectric constant of the substrate (as long as it is uniform and, preferably, isotropic for modeling convenience), but they do depend on having a low value of the loss tangent.

**Current-carrying application:** A metal substrate is generally preferred for current carrying applications since it serves as an alternate-current path in the case of a rise in the temperature of the superconductor. In addition to being a metal, substrates for these applications need to be able to support superconducting films that have a high critical current density and that probably are quite thick.

## 5.3 Characterisation

### 5.3.1 Magnetic Levitation

As we have discussed before, one of the basic properties of superconductor in the superconducting state is Meissner effect, which states that " a superconductor in the superconducting state never allows a magnetic flux density to exist in its interior". This is a basic phenomenon, which is responsible for magnetic levitation. In a sense it is the most easy and a quick way to test either our sample shows superconductivity or not.

In order to check the annealing profile for each sample preparation we have made superconducting pellets together with the samples. To check the magnetic levitation we have used a simple set up as shown in the figure below,

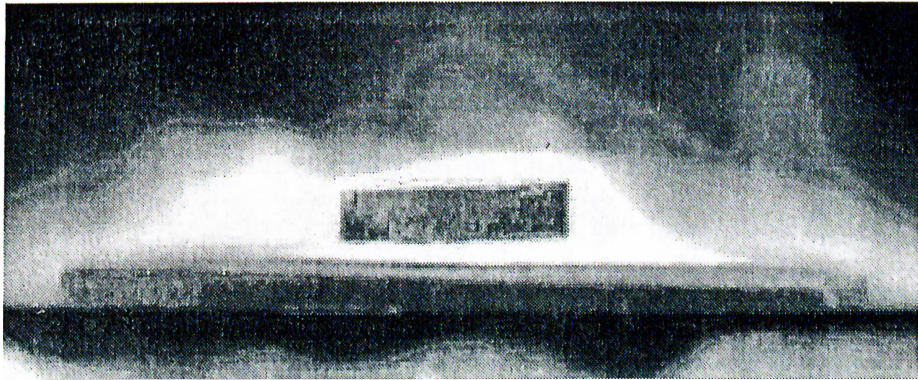


Figure 5.2: A high temperature superconductor in magnetic suspension..

As far as the  $T_c$  of the pellet is higher then the  $T_{c\_onset}$  the magnet stays on the surface of the pellet but after  $T_{c\_zero}$ , due to screening currents the magnet no longer stays on the surface. The suspension of the magnet in the air shows

how better the superconductor is. For all of our pellets, the magnetic levitation has been observed, but the one which is annealed in atmosphere environment shows better than all of the others, but in this case the room temperature resistance is higher than the others.

### 5.3.2 Resistance vs. Temperature

In most of the applications we are not just looking for the superconducting state but instead, are more interested in other properties like critical current,  $T_{c\_zero}$ ,  $T_{c\_onset}$ ,  $dR/dT$  (the slope of the transition region) etc., which are not possible to measure by the use of the above described methods. So the next step in the measurement is to measure the Resistivity vs. Temperature behaviour of the superconductors, as we have discussed in the section 4.5, where two different way for measuring the Resistance vs. Temperature is discussed.

The results of resistivity vs. temperature measurements for a thin film gradiometer (SQUID) superconductor on  $\text{LaAlO}_3$  are shown in Figure 5.3. In order to have a noise free curve we have used the four-probe method, using which we can eliminate the thermocouple effect, as discussed in section 4.4.1. As shown in the figure above for the temperature value above  $T_{c\_onset}$  the resistance decreases proportionally with decrease in the temperature. But below  $T_{c\_onset}$  the resistance makes a high slope of  $dR/dT$  and goes to zero value in magnitude at  $T_{c\_zero}$ . The critical temperature ( $T_c$ ) is obtained by performing the resistance vs. temperature measurement and the higher slope ( $dR/dT$  slope) determines the good quality of the superconductor. For this particular



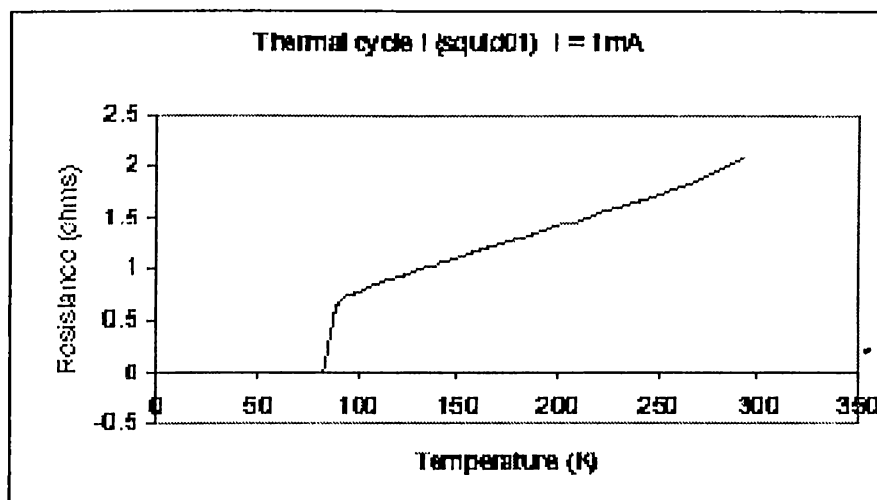


Figure 5.3: Temperature dependence of resistance for Y-Ba-Cu-O SQUID on MgO substrate. Measuring current is 1mA and critical temperature is about 90K.

measurement the critical temperature is about 90K.

Next important matter in resistance vs. temperature measurement is the effect of the bias current as shown in Figure 5.4. As shown in the figure, by increasing the bias current the  $T_c$  shifts to the high temperature and the  $dR/dT$  slope increases. The increase in the  $dR/dT$  is not only due to the bias current but also depends on many other factors which will be discussed in detail in the next chapter.

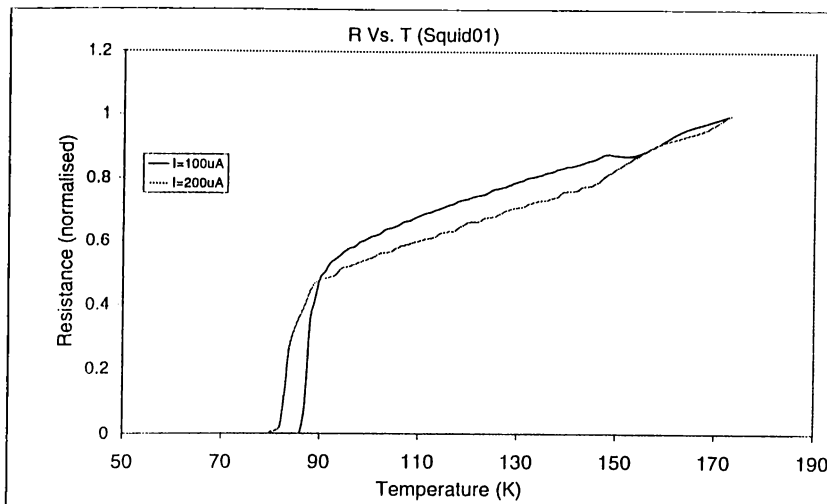


Figure 5.4: Effect of the bias current on the resistance vs. temperature measurement.

### 5.3.3 Mutual Induction

An apparatus providing a non-contact method to probe the current-induced destruction of superconductivity in thick film samples has been studied in section 5.4.2.

A thick film sample is positioned between a primary coil, which induces a supercurrent in the film, and a secondary coil that monitors flux penetration. A sine wave current is applied to the primary coil, generating an ac magnetic field and inducing a shielding supercurrent in the film. These supercurrents have the effect of reducing flux linking to the secondary coil to a value less than it would have been in the normal state. Therefore by monitoring the changes in the secondary coil signals we can detect the transition temperature ( $T_c$ ), the

critical current density ( $J_c$ ), and the critical field ( $H_c$ ).

Figure 5.5 shows the results of the measurement of secondary coil signal vs. external field for a film on  $LaAlO_3$  substrate. Although it doesn't provide as much information as the Resistance vs. temperature graph.

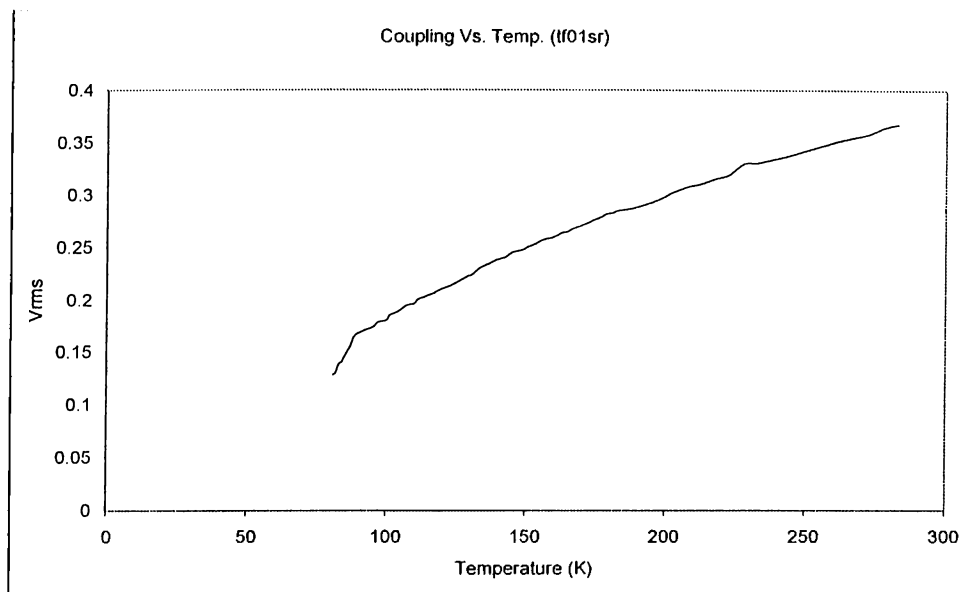


Figure 5.5: Temperature dependence of coupling voltage for thin film at  $LaAlO_3$  substrate.

For this particular graph the  $T_c$  is below 90K and the  $dR/dT$  ratio is also high. This could be due to many reasons, to be considered in the following.

As it is seen from the graph there is some kind of offset at the lowest temperature due to the external electromagnetic coupling. This can not be avoided

for the samples, which has the small area than the diameter of the primary coil.

Figure 5.6 shows a coupling voltage vs. bias current. This graphs provides the information about the critical current density for the particular sample. In order to do the  $J_c$  measurement, the temperature of the sample is fixed at 80K and by increasing the input current to the primary coil,  $J_c$  is derived from the data read by the lock-in amplifier. The delay in the change of the current causes the steps in the graph.

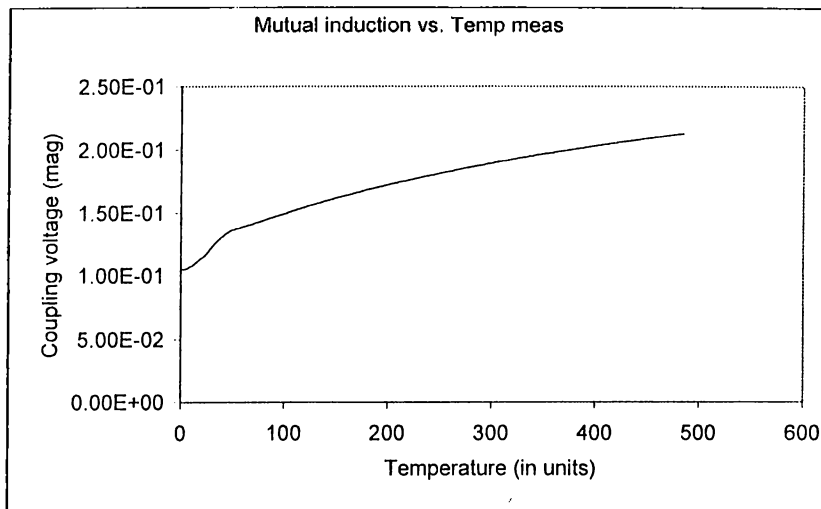


Figure 5.6: coupling voltage vs. input current applied to the primary coil at 80K for superconducting thin film.

### 5.3.4 Comparison between R vs. T and mutual induction measurement

As we have seen in the last two sections, we can perform resistance vs. temperature measurement and the mutual induction measurement in order to find the important parameters or the characteristics of the superconductor. Each method has its some draw backs as well as advantages which are discussed in the following.

Resistance vs. temperature gives us an accurate information about the behaviour of the resistance variations with respect to the change in the temperature. But in order to have the resistance vs. temperature measurement the electrical contacts with the samples are needed, which is the most important factor for characterization. Metallic contacts not only deteriorates the samples due to base chemical in the silver paint, but also relatively high contact resistance is developed at the interfaces when external lead wires are attached to the superconductor surface. A flow of moderate currents often results in heating of the contacts and leading to the deterioration of superconductor at the contacts giving rise to inaccurate measurement. Heating due to contacts also changes the temperature of the superconductor which shifts not only the  $T_c$  but also decreases the  $dR/dT$  slope, as observed in Figure ?? . On the other hand for mutual induction measurement, we don't need to have any kind of contact which in turn eliminates all the above-described drawbacks due to the contacts.

In order to do critical current measurement we need to apply a range of input currents. As we have seen by changing the bias current to high values, high probability of destroying the sample exists due to heating effect. This again goes back to the contact resistance and as discussed before, this heating can destroy the sample causing inaccurate  $J_c$  measurements. Hence direct application of high current densities can be avoided by using the mutual induction method.

A third important point according to resistance vs. temperature measurement is the thermocouple effect, which gives rise to an inaccurate reading of the resistance. According to the four-probe method we are providing the current and reading the voltage and hence there is an additional voltage component due to thermo-coupling at the contacts. Though this effect can be eliminated by use of quasi-dc measurement as discussed in sections 4.4.

The main problem with mutual induction measurement method is the residual coupling, which is mainly due to fringing effects. That is why we have not been able to find the  $T_{c\_zero}$  value in Figure 5.5. As far as the widening of the transition line is concerned, it is speculated to be due to the properties of the high temperature superconductors where we can observe the two critical fields,  $H_{c1}$  and  $H_{c2}$ . Fields between  $H_{c1}$  and  $H_{c2}$  do penetrate into the superconductor, and hence can be possible reason for not having a sharp  $T_{c\_onset}$  value. Secondly as discussed earlier, a leakage field occurs due to the size of the samples. This effect can be reduced by decreasing the size of the primary and secondary coils.

In general we can use both methods in order get the best results. Mutual induction method can be used as a quick check to determine the basic properties of the superconductor with out any impurity added to the samples. This in a sense, is good approach if we want to use the sample for the purposes such as further annealing. If initial tests are satisfying then for further details, the resistance vs. temperature measurements can be used.

### 5.3.5 Responsivity vs. frequency

In order to check the responsivity vs. frequency measurement thermal model discussed in section 3.4 has been used to calculate the frequency response. This model has been used for different substrates, and the predicted results are shown in Figure 5.7.

The measurement results for the thin films are discussed in section 6.4.

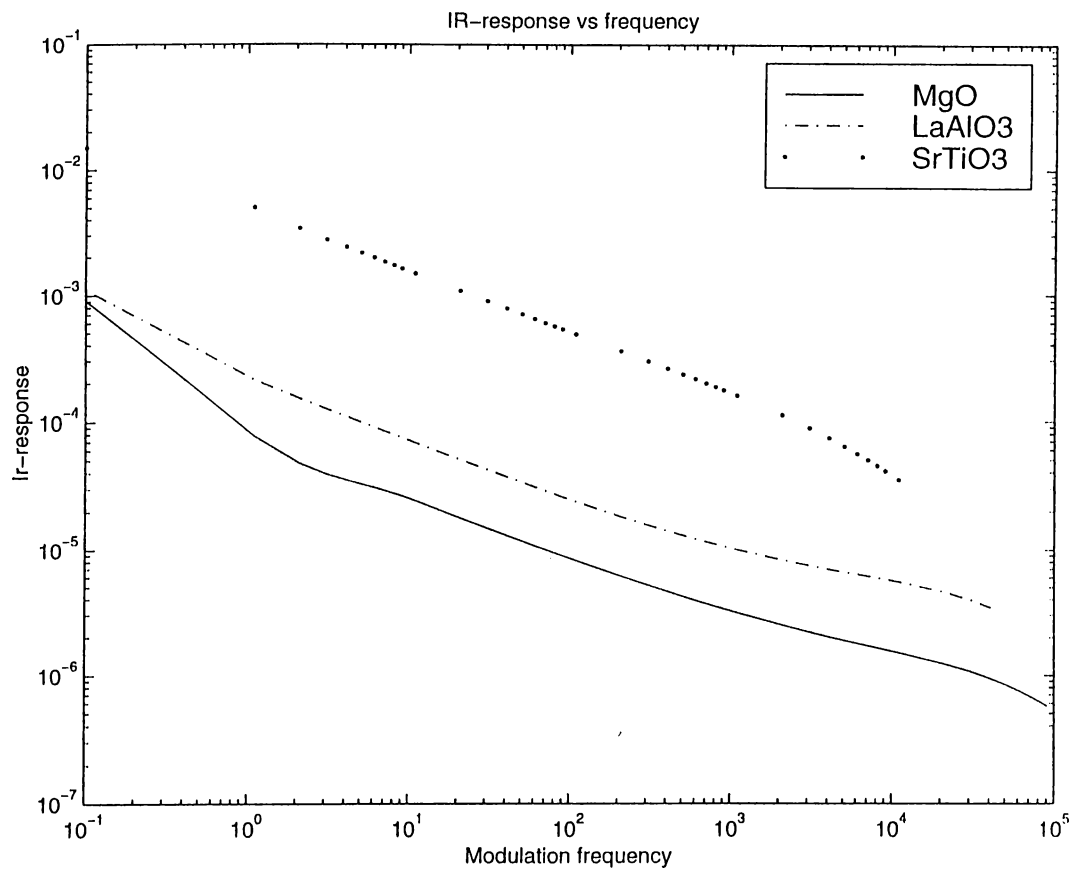


Figure 5.7: Response measurements by using the thermal model discussed in section 3.4, for different substrate materials.



## Chapter 6

# EXPERIMENTAL RESULTS AND THE ANALYSIS

### 6.1 Resistance vs. temperature measurement

The theoretical expectation of the behaviour of variation of the resistance of the SC with respect to the temperature is shown in Figure 6.1. In general the transition temperature is not very sensitive to small amounts of impurity, though magnetic impurities tend to lower the transition temperature considerably.

In the following section we will try to investigate in details the artifacts in the resistance vs. temperature measurements performed on the tape SC, the bulk SC, and the thin and thick film samples.

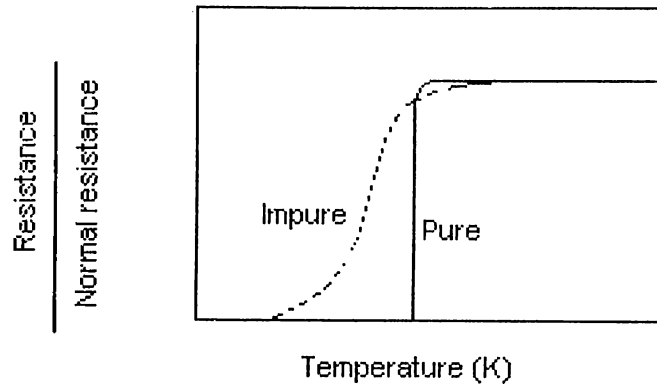


Figure 6.1: Typical Resistance vs. temperature curve for superconductors.

### 6.1.1 Superconducting Tape

In order to understand the basic properties of the superconductors and as a base test for the system a superconducting tape (BICC) has been investigated. The characteristic critical current density is about  $\sim 25 \text{ A}$ , critical current density of  $13 \pm 3 \text{ kAcm}^2$ , typical dimensions of  $3 \times 0.3 \text{ mm}$  and number of filaments up to 85. The superconducting tape used in this work was product of BICC Cables. We have used four-probe method to see the resistance vs. temperature behaviour, the corresponding graph of which is given in Fig. 6.2.

Figure 6.2 shows the effect of temperature on the resistance. As seen clearly that there are many fluctuations in voltage reading, which are due to the thermocouple effect of the contacts. So in order to reduce this fluctuations we need to do quasi-dc measurement. Figure 6.3 shows the average resistance due to the forward and reverse bias current through the tape.

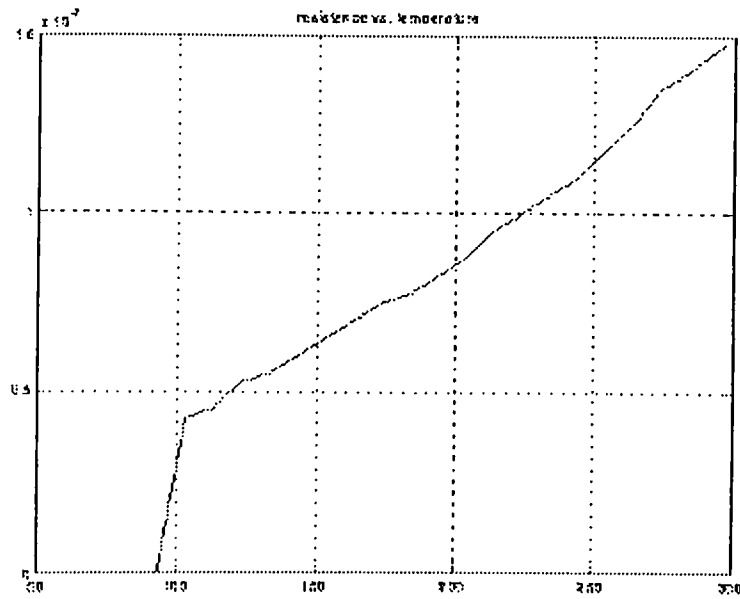


Figure 6.2: Resistance vs. temperature of the Bi-based Superconducting tape by using non quasi dc measurement.

According to the Figure 6.3 the  $T_c$  is found to be about the above 100K which is not expected for the used superconducting tape. The speculated reason for this shift of  $T_c$  is the effect of the electrical contacts and secondly the temperature gradient across the length of tape and the thermocouple effect at the electrical contacts.

According to the measurement done on the superconducting tape we have observed the following properties.

1. Contacts are the most important factor in resistance vs. temperature measurement.
2. Temperature gradient across the superconductor causes a shift in the curvewidening the transition.

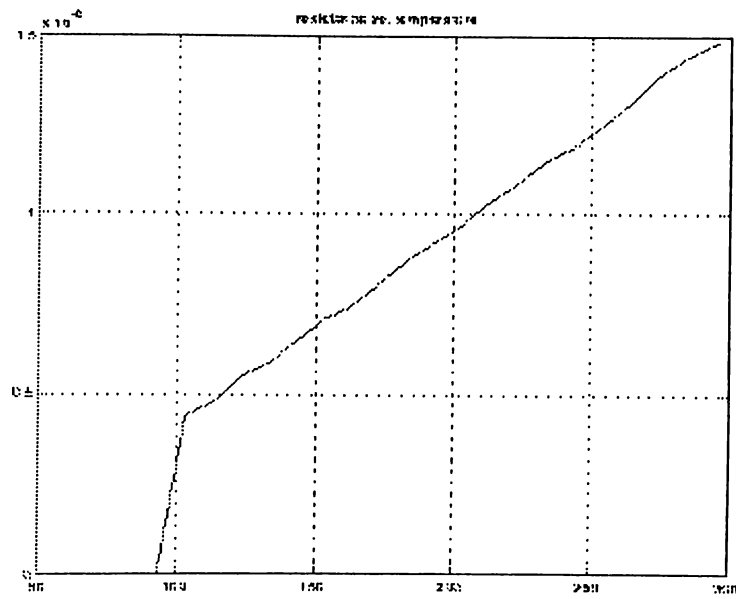


Figure 6.3: Resistance vs. temperature measurement for Bi-Based Superconducting tape .

3. Due to thermocouple effect at the contacts quasi-dc measurement is necessary for resistance vs. temperature measurement.

### 6.1.2 Superconducting Disk

In order to check the annealing profile and the effect of Argon atmosphere on the characteristics of superconductors, we have made bulk of superconducting disks. To improve the metal contacts, gold contact metallisation was done. By using the silver epoxy on the Gold pads the contacts to normal copper wire were made. We have prepared a characterization set up with which we can perform four-probe resistance vs. temperature measurement. The following

graphs show some of our observations about the disk and the effecting parameters.

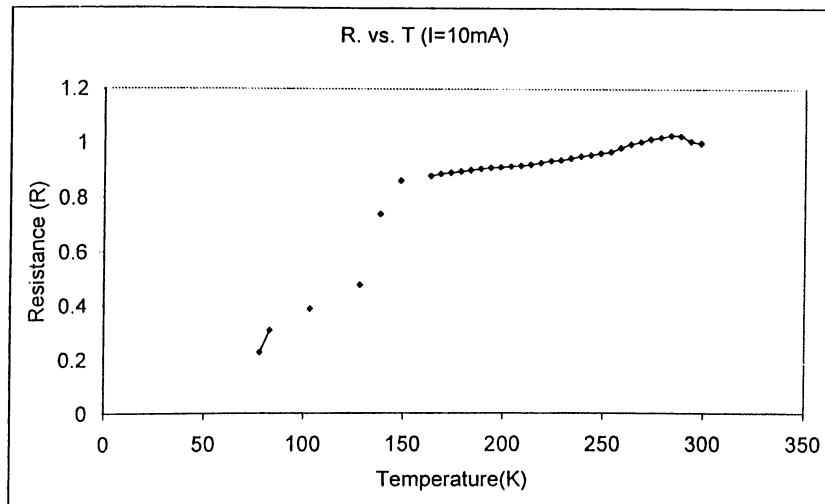


Figure 6.4: Resistance vs. temperature measurement effected due to unstable heating caused by the cooling process.

**Effect of unstable heating of disk** Figure 6.4 shows a resistance vs. temperature curve for a disk. The disc was annealed in Argon atmosphere for 8 minutes at  $950^{\circ}\text{C}$ , with oxidation temperature of  $470^{\circ}\text{C}$ . The maximum temperature was  $950^{\circ}\text{C}$  for one hour and eight minutes. In order to take the resistance vs. temperature measurement, disk was cooled down to 77 K and then was allowed to heat up to room temperature gradually.

According to the R vs. T curve we see that  $T_{c\_onset}$  is above 150 K. The measured high  $T_c$  transition for this material is speculated to be due to the high temperature gradient with in the sample or it may be due to the

thermal gradient between temperature sensor. According Fig. 6.5 is also a presence of second order phase near 77K. Which reaching the  $T_{min}$  77K but still there is some residual resistance, which shows the  $T_{c\_zero}$  is less than 77K. In this readings we have two things to be considered, first the presence of a second phase, which is not expected for  $YBa_2Cu_3O_7$  superconductor and secondly the  $T_c$  about 150K while it should be about 90K. In order to check the results we have applied different bias currents and the results are shown in the figure below,

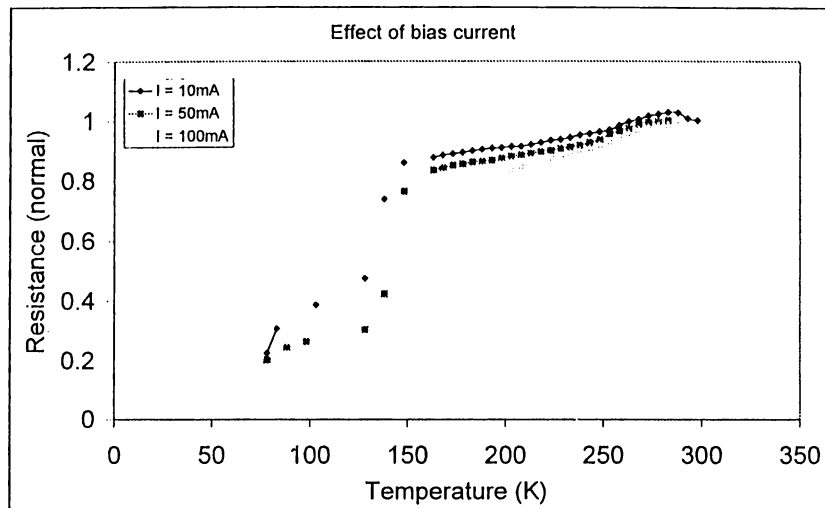


Figure 6.5: Effect of bias current under unstable heating of the disk due to non-equilibrium freezing process.

According to the observation of the result shown by some other group, by increasing the bias current the  $T_c$  is supposed to shift to lower temperatures and heating effect of the superconductor must have been increased but according to Figure 6.5. The increasing of bias current not only decreases the magnitude of the resistance but also the  $T_c$  shifts towards

high T. And most important thing is the presence of second order phase for all applied currents.

Analysing of these results leads to the fact that the measured R vs. T behaviour is due to unstable heating and the presence of temperature gradient not only across the superconductor but also in the vertical direction of the setup. In order to improve this we cooled the disk from room temperature to 77K, by taking the temperature steps into the consideration, minimizing the temperature gradient in the system.

**After eliminating the contact and unstable heating effect:** The results of a resistance vs. temperature measurement for the same disk after improving the contacts and removing the unstable heating effect is shown in Figure 6.6.

According to Figure 6.4 we see that  $T_{c\_onset}$  is about 90 K, while yet the was not reached. This could be caused by of the heating effect due to the bias current and it was speculated that the temperature of the upper surface of the disk was not at 77K.

Figure 6.7 shows the effect of bias current on the resistance vs. temperature curve as predicted [18]. This behaviour is the same as for the thick films where there is joule heating associated with the resistance of the patterns at high-bias currents. This power dissipation causes a temperature gradient across the thermal-conducting path. This gradient is

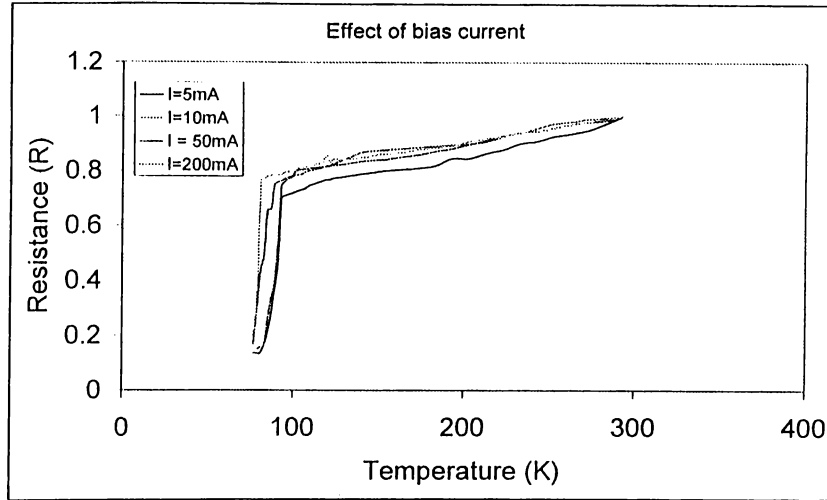


Figure 6.6: Resistance vs. temperature for SC. Disk (ds950ArO).

the basic cause of an error in the dc characterization. As seen from the figure, by increasing the bias current the  $T_{c\_onset}$  is shifted towards left and the slope of  $dR/dT$  has also been increased indicating the possible thermal runaway as well.

One other effect observed was that, by increasing the bias current, while keeping the temperature constant, the resistance of the sample increases. This effect is speculated to be due to the loss of the oxygen caused by the joule heating at relatively high bias currents.

**Effect of thermal cycle:** Thermal cycling effects the quality of the superconductor, and it not only effects the surface of the SC but also the contacts. The Figure 6.9 shows the effect of thermal cycle on the room temperature resistance. According to the study in this field, it has been



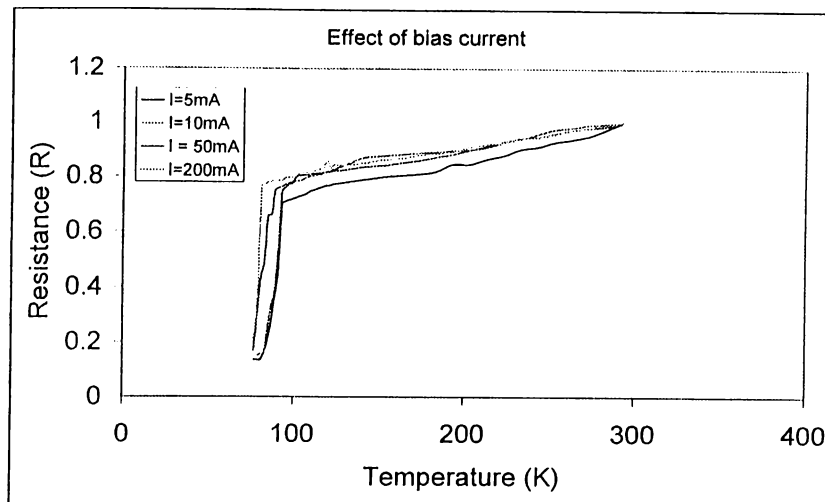


Figure 6.7: Effect of bias current on the resistance vs. temperature characterization for bulk of superconducting materials.

reported that shift of  $T_c$  due to bias current can be recovered but the shift of  $T_c$  due to thermal cycle can not be recovered. [18] The only way is to do the oxidation process once again but in most of the cases it is not possible due to the contact substances and the attached chemicals to the film which also degrade the superconductivity.

### 6.1.3 Resistance vs. temperature for thin and thick films

Resistance vs. temperature measurement is not only important to find out the basic properties but also defines the parameter for the responsivity of the bolometric detectors. In bolometric response, as discussed before, the flux of photons can directly or indirectly heat the superconductor and changes the

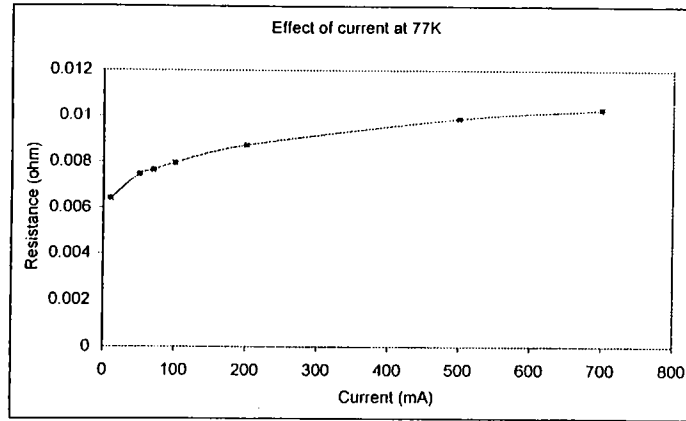


Figure 6.8: Effect of bias current on the resistance at fixed temperature (77K).

temperature of the material. This change in the temperature, which can be local, will be reflected in the resistance vs. temperature characteristic of the superconductor. For this type of detection the SC detector is biased where the temperature derivative of the resistance with respect to the temperature,  $dR/dT$ , is large. For bolometric response, the induced voltage change,  $\Delta V$ , will be equal to  $I (dR/dT) \Delta T$ , where  $I$  is the dc bias current across the detector. Important parameters of a bolometer are the temperature derivative of the resistance ( $dR/dT$ ), heat capacity and the effective thermal conductivity and/or the material used. In order to find all these properties it is required to perform the basic resistance vs. temperature measurement. The results for the thin film detectors are discussed in this section.

Figure 6.10 shows the resistance vs. temperature measurement for the SQUID (thin film superconductor). According to this figure the  $T_{c\_onset}$  of the sample is about the expected value of 90K, while  $T_{c\_zero}$  is at 85K, resulting in

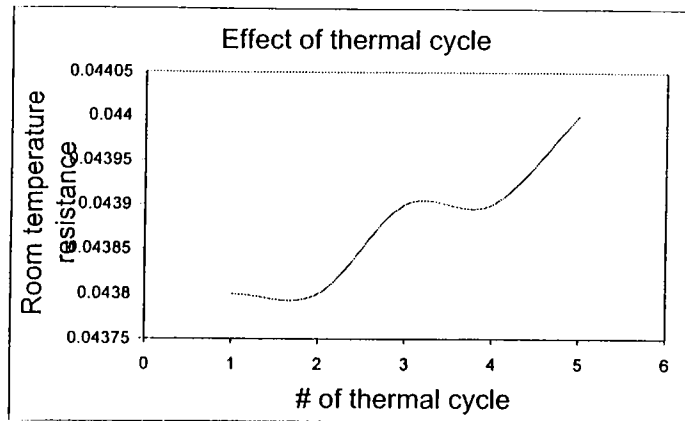


Figure 6.9: Effect of thermal cycle on the room temperature resistance for superconducting bulk resistance.

a transition width of about 5K.

Joule heating is associated with the resistance of the patterns at high bias current. Power dissipation due to joule heating causes a temperature gradient across the thermal conducting path.

At high bias current, Joule heating can cause a shift of  $T_{c\_onset}$  towards the lower temperatures. This shift is related to the temperature gradient across the film-substrate or the substrate-cold finger interface, depending on the film and substrate dimensions. Effect of the Joule heating depends on the type of the film, small area patterns like micobridges (SQUID) or large area patterns i.e. meander lines. According to the Figure 6.10 , we can see the following effects,

i) Increase in the bias current causes an increase in the normal state resistance

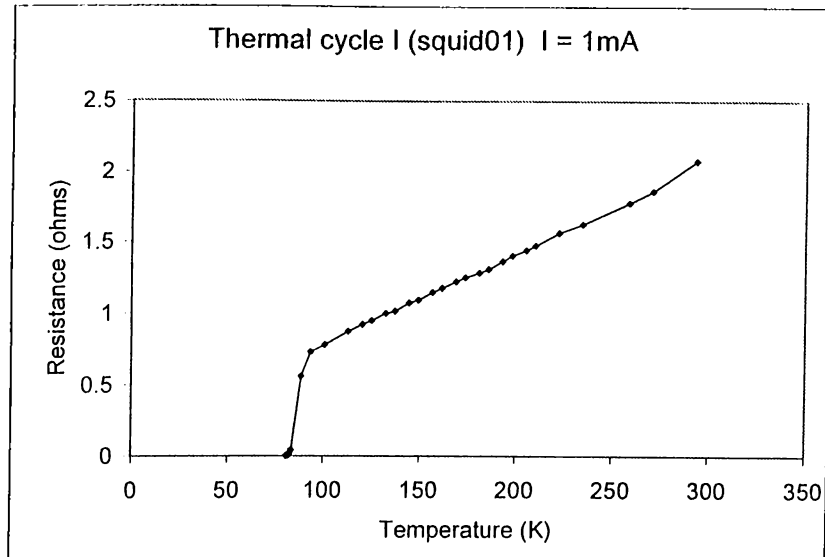


Figure 6.10: Resistance vs. Temperature measurement for SQUID at bias current of 1 mA, with  $T_c$  of about 90 K.

- ii)  $T_{c\_onset}$  shifts towards lower temperatures.
- iii) Transition width increases by increasing the bias current before reaching the thermal runaway.

For small area patterns the temperature gradient generated by Joule heating is mostly expected to be at the film substrate interface or across a thin layer of the substrate in the vicinity of SC path. For small area patterns the heat capacity of the substrate is the determining factor in the temperature gradient. For R vs.T measurement of such samples the temperature rise in the film can cause as thermal runaway, overheating the whole film, if a constant current source is used. If the controlled source is used, then a local thermal runaway creating a hot spot in the bridge would limit the overall heating. The

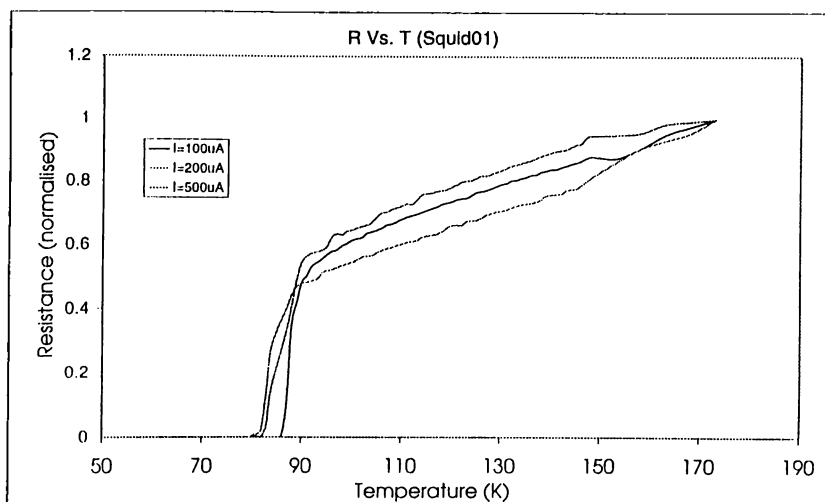


Figure 6.11: Effect of the bias current on the resistance vs. temperature measurement for SQUID01.

position of the hot spot is determined by the bias temperature relative to zero resistance temperature  $T_{c\_zero}$  and the variation of  $G$  with position.

For the samples with large area film pattern dimensions comparable to that of the substrate the temperature gradient is found to be mainly across substrate cold finger interface. In this case thermal boundary resistance at substrate-cold finger interface is found to be the determining factor in overall thermal conductance of the sample. There will not be a hot spot in such samples, and the whole SC film is considered to be at the same temperature.  $R$  vs.  $T$  characteristic by using constant current source, can cause a false sharper transition at high currents.  $T_{c\_onset}$  shifts due to higher bias current where has been interpreted to be an intrinsic shift by some groups. [18]

Together with the effect of the bias current, thermal cycling and the ambient atmosphere also effect the resistance vs. temperature characteristics. The effect of the thermal cycle is shown in the Figure 6.12 .

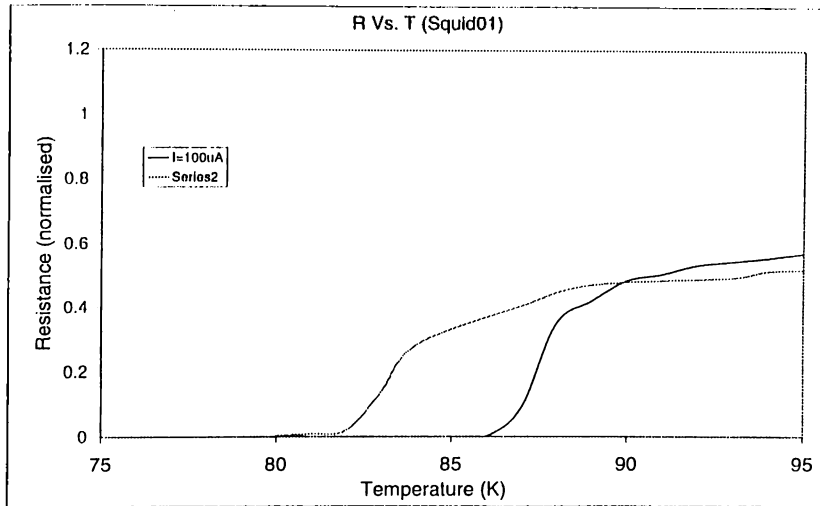


Figure 6.12: Effect of thermal cycle on the resistance vs. temperature measurement.

According to Figure 6.12 by increasing the number of cycles the transition width increases and the  $T_{c\_onset}$  also shifts towards lower T. But it has been shown [18] that the shift of the  $T_c$  is up to certain point after which the thermal cycle does not shift it further. It is found that the samples are sensitive to the ultimate vacuum and the thermal cycle to which the sample is exposed. It is already known that the lowering of  $T_c$  at low bias currents, which is interpreted to be due to the thermal cycles under vacuum, is not recoverable by exposing the sample to room temperature and atmosphere. The decrease of  $T_c$  caused by high-bias currents under vacuum was found to be recoverable.

## 6.2 Mutual induction vs. bias temperature

In the previous section we saw how we can use the four-probe method to determine some of the basic properties of the superconductors this is while we also have encountered the drawbacks in that method. In order to reduce some of these effects, As we have discussed in section 4.5 and 5.4, there exists one other methods which can be used to determine the critical current, critical current density, and critical magnetic field without effecting the sample it self.

The basic circuit for mutual induction measurement is given in Figure 4.14. In this section we will try to summarise the results for thin and thick films obtained using this method.

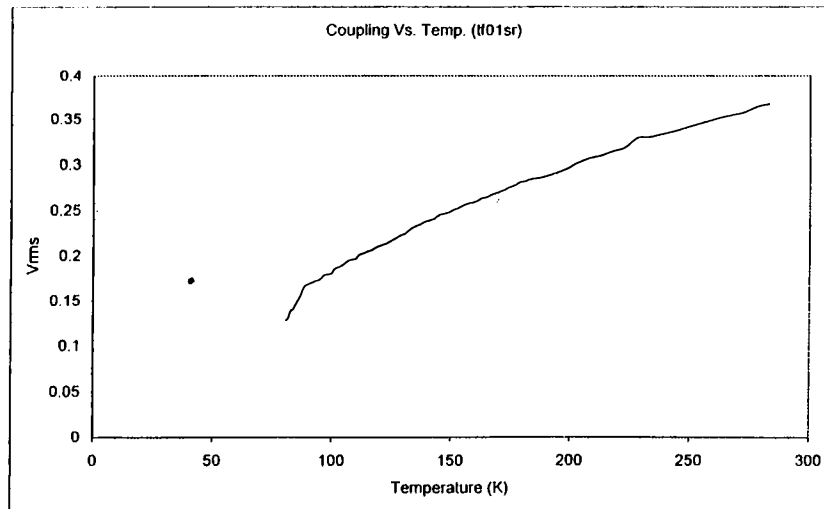


Figure 6.13: Mutual induction vs. temperature for thin film Superconductors.

Figure 6.13 shows the  $V_{coupling}$  (rms) of the secondary coil vs. Temperature of thin film superconductor bolometer detector on SiTrO3 substrate. According to this graph transition temperature is about 90K, as expected for YBCO material. Although  $T_{c\_onset}$  is almost clear but we are not to see the  $T_{c\_zero}$  for this graph. This might be due to the fringing effect because the sample area was a bit small compared that of the coils.

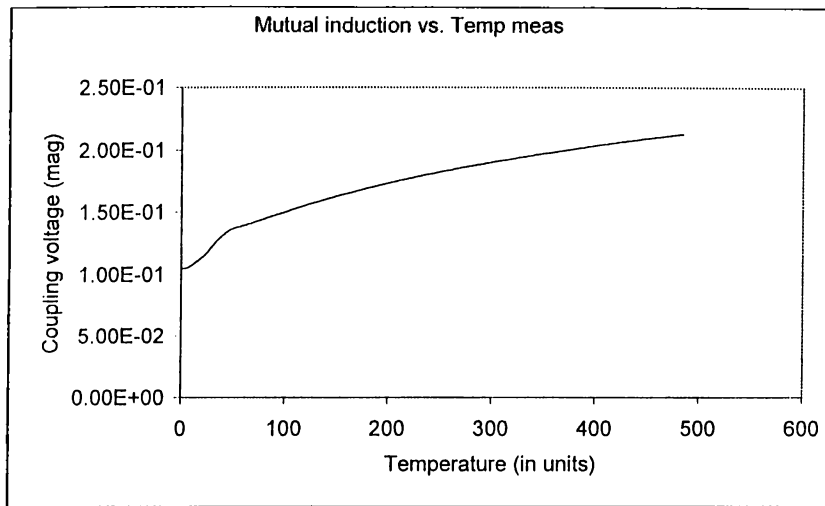


Figure 6.14: The effect on the mutual induction by reducing the temperature of the superconducting thin film on SrTiO3 substrate.

To compare this result we have repeated the experiment by using the computerized method in which we have used the lock-in-amplifier to read and store the data. The following graph show the above results.



Figure 6.14 shows the coupling voltage (in magnitude) vs. time. This graph which is not scaled with respect to the actual temperature shows a sharp transition and the  $T_{c\_onset}$  and  $T_{c\_zero}$  clearly. When compared to the R vs. T measurement, it is found that both show the same  $T_{c\_onset}$  of 90K. So this method can be developed further to reduce the fringing effect and by improving the characterization system we can also get more detailed information which can be achieved from direct resistance vs. temperature measurement.

### 6.3 Mutual induction vs. bias current

As we have seen there is an effect of bias current on the R. vs. T measurement and it causes shifts in the  $T_{c\_onset}$  and depending on the film it can widen spread the transition width. The same effect can be observed by using mutual induction method as well. The results shown in this section shows that by increasing the magnitude of applied voltage the output coupling voltage increases and the  $T_{c\_onset}$  voltage shifts toward lower T.

Figure 6.15 shows  $V_{coupling}$  (rms.) vs. the temperature curve for different bias currents. Here the bias current is the applied current to the primary coil. As it is obvious for the  $V_{primary}$  of 0.04 mV (can also be expressed in mA) we can see the  $T_{c\_onset}$  at about 80K. While for the  $V_{primary}$  greater than 0.04mV, although there is no obvious  $T_{c\_onset}$ , the trend shows a  $T_{c\_onset}$  at about 75K. For  $V_{primary}$  less 0.004 mV the  $T_{c\_onset}$  is about 85K. The reason for this shifting of the  $T_{c\_onset}$  might be the same as discussed for resistance vs. temperature

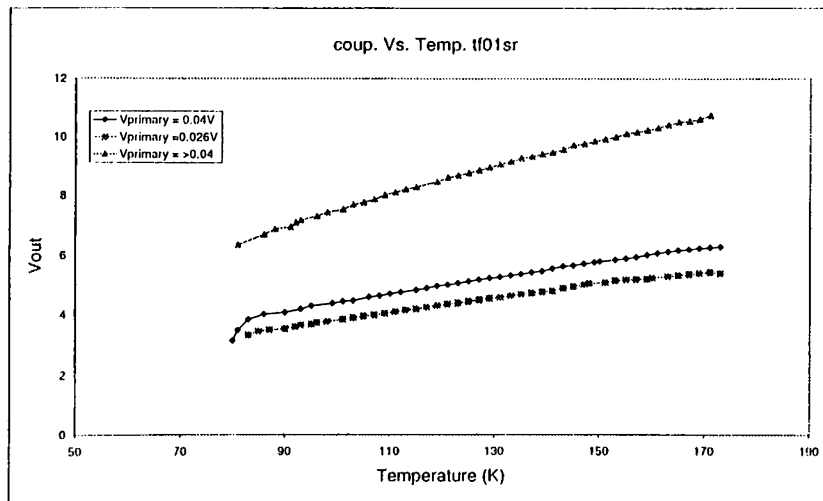


Figure 6.15: Effect of the bias current at the primary coil on the coupling vs. temperature curve.

measurement case in previous section. In using this method the only consideration is not to reach the critical magnetic field by applying high currents to the primary coil.

In order to find the critical current density, it is found to be efficient to use the mutual induction method. By fixing the temperature to be at 80K and increasing the bias current through the primary coil, the effect of the bias current can be observed.

Figure 6.16 shows input current to the primary coil vs. output current through the secondary coil. According to the graph, with increase of the applied bias current to primary coil, initially there is an increase in the output coupling current in secondary coil but there is a dip in this at about 0.5mA and

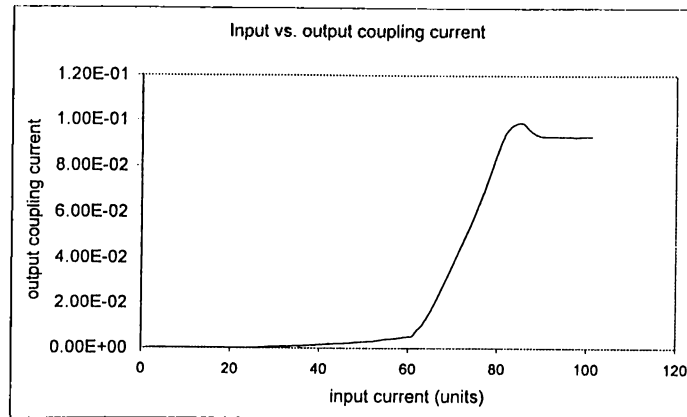


Figure 6.16: Measurement for the critical current density at 81K for the thin film SC on  $SrTiO_3$  substrate.

after that its increase is almost proportional to the increase in the bias current.

In the next graph we investigated the effect of the direction of bias current. According to this graph we see that the general behaviour is the same as was shown in the figure above. But by changing the direction of the current we have observed a shift in the curve toward the higher T.

## 6.4 Responsivity vs. frequency

Frequency response measurement has been done for SQUID. In the initial data the effect of contact resistance and undesired coupling of radiant light with the wires has been observed. In the figure below although the graph look like the

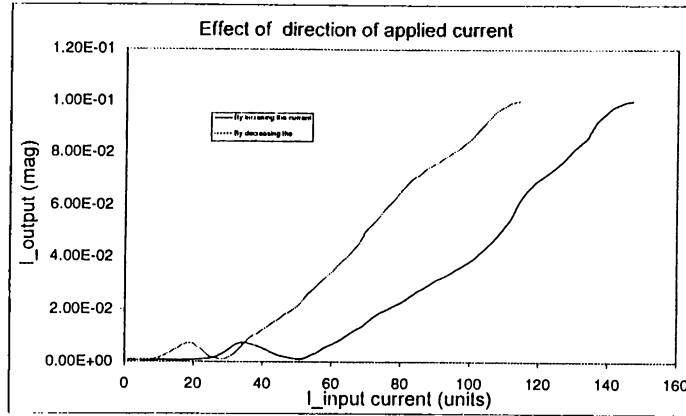


Figure 6.17: Effect of applied current to primary coil for thin film SC on  $SrTiO_3$  substrate.

one predicted by thermal model but it is not exact the same.

As clear from the Fig. 6.18, this plot is on linear scale and secondly the there are lots of fluctuations although the data has been averaged over 256 samples. By detail analysis of this graph it has been found that the major part of this graph is due to modulation with the contact resistance not with the sample it self. In order to improve the response contact resistance should be reduced by improving the contact metallisation.

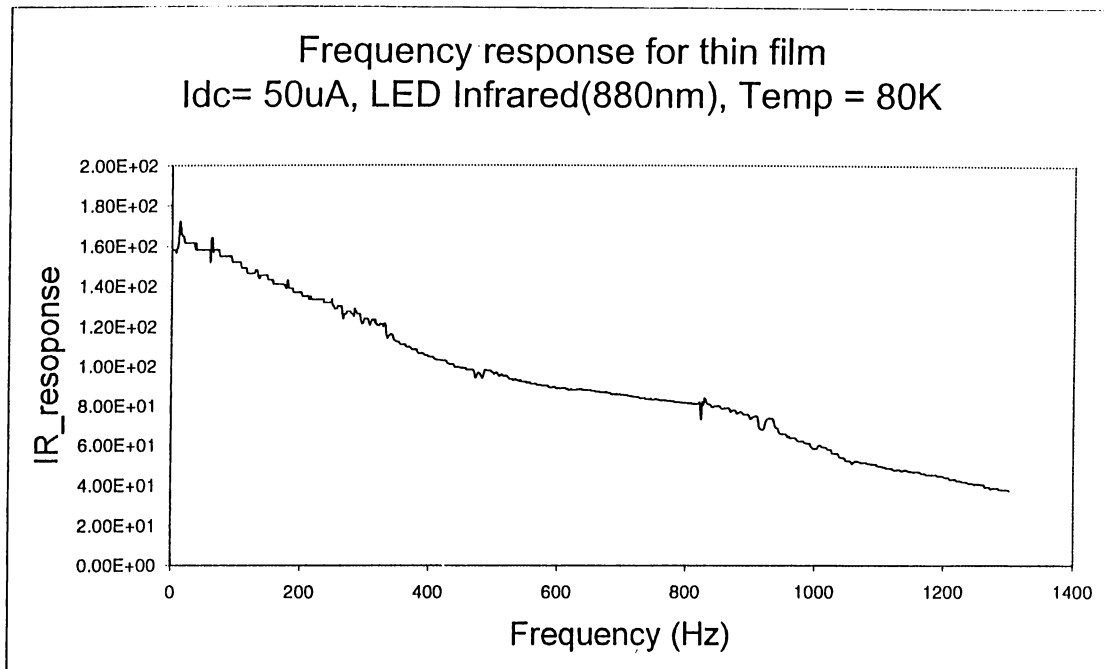


Figure 6.18: Frequency response for the SQUID on linear scale.

## Chapter 7

# SUMMARY AND CONCLUSIONS

A characterisation system has been developed for high- $T_c$  superconductive infrared detectors. Manufacturing of characterization setup consists of two parts; establishment of mechanical system to provide the working condition and electrical system for characterisation of the electrical parameters of the detectors.

The mechanical part of the system was manufactured in the direction to fulfil the following requirements; cool down the sample (detector) to the liquid nitrogen temperature and insulate it from the outer environment. A thermal model for the developed cryogenic system was purposed to understand the parameters which could hinder achieving the above mentioned characteristics for the system. The developed system is capable of maintaining the temperature of the sample at about and above 77K at room temperatures. It provides good

electrical insulation and insulation from the outer environment. It also has the capability to do simultaneous mutual induction measurement and frequency response measurement.

Electrical system was developed to characterize the detectors for the resistance vs. temperature measurement and frequency response analysis. A computerized system was established to perform resistance vs. temperature measurement. In order to perform the basic tests like measurement of the critical temperature, a mutual induction setup was established to do the measurements with out electrical contacts.

By using the home made setup for compressing the superconductor powder superconducting discs were fabricated. This was in order to check the effects of the annealing profiles and the environmental gases on the properties of the superconductors. Successful development of fabrication process made it possible to produce SC disc at Bilkent, being presently used in experiments for undergraduate level experiments.

Present thermal model for the superconducting edge-transition infrared detectors has been investigated to control and improve the physical parameters, which can effect the responsivity and detectivity of the detectors. Base on the above observations, a new method of fabrication has been purposed. In order to implement this method a mechanical setup has been developed. Initial test on the thick film produced by this method although did not provide sufcing

results but revealed some promising properties like electrical conductivity, adhesion of the film to the substrate. The thickness of these films is about 30 to 40  $\mu m$  while controllable by the duration of the deposition time.

Using the developed cryogenic set up the thick films produced by new method and thin films produced by laser ablation technology were characterized. The results of resistance vs. temperature measurement for the thick film show that the film quality in terms of critical temperature is yet not sufficing for the application. After investigating the basic reasons for the poor quality, efforts have been done to improve the similar of thick films. In order to find out the effect of contacts on these films, experiments have been done on very high quality laser ablated thin films (SQUIDS). The resistance vs. temperature and frequency response measurements has shown that the contacts should be further improved. Different methods have been investigated to improve the electrical normal-superconductor contacts and the contact resistance for the thick and thin films.



# APPENDIX A

## Computer program for Quasi-dc analysis of thick and thin film superconductors

In order to measure resistance vs. temperature measurement computer software has been developed. By using this software we can do quasi-dc analysis.

The following algorithm is applied for the automation.

1. Ask user to enter.

- temperature range.

- temperature interval.
- current on the sample.
- overall gains of amplifiers.
- channel numbers for temperature and resistance.

## 2. Initializations

- initialize the current temperature to  $T_{start}$ .
- open the data files for ready to write in.

## 3. view the temperature

- if temperature is within the range to be examined then
  - view the temperature increase regarding current temperature
  - a. if it is temperature interval then
    - read  $V+$  on the sample
    - switch the current

read V- on the sample

update the current temperature value

- else if it is smaller than  $T_s$  goto step # 3.

- else it is grater then  $T_{final}$  goto finish.

4. Calculate the Resistance and Temperature

5. Store the data into a data file as two columus of Temperature and Resistance

6. Check temperature if we are at the upper side of the range

- if we are out of range then goto finish

- else goto step # 3.1.1

7. finish

- close the data file

- end

# APPENDIX B

## Tables

	Therm. Cond. [W/(cm.K)]			Integ. Values (W/cm)		
	4.2K	77K	300K	0-4.2K	4.2-77K	77-300K
Sapphire	2.7	10	0.46			
Copper						
OFHC	2.5	5.2	4.0	7.5	700	900
ETP				6.5	715	914
Aluminum	0.03	0.57	1.21		223	505
Constantan	0.008	0.18	0.23	0.012	10.2	44.6
Manganin	0.005	0.13	0.22	0.009	6.3	37.7
Stainless	0.0025	0.08	0.15	0.006	3.3	27.4
Pyrex	0.001	0.0045	0.01	0.002	0.18	1.83
Teflon	0.005	0.024	0.027		0.132	0.57
Nylon	0.00013	0.002	0.0003			

Table B.1: Thermal Conductivity and Integrated Thermal Conductivity for common Cryogenic Building Materials.

Mat.	T <sub>c</sub> (K)	Θ <sub>D</sub> (K)	H <sub>c</sub> (mT)	N(E <sub>F</sub> )	$\frac{2\Delta(0)}{k_b T_c}$	λ <sub>ep</sub>
Nb	9.25	276	206	0.91	3.6	0.85
Tc	7.80	411	141	0.62	3.6	0.65
Pb	7.20	96	80.3	0.28	4.5	1.55
V	5.40	383	141	1.31	3.4	1.0
Ta	4.47	258	83	0.77	3.5	0.75
Hg	4.19	87	41.1	0.15	4.6	1.6
			H <sub>c2</sub>			
NbN	17.3	309	47	0.45	4.3	1.06
ZrN	10.7	349	0.3	0.34	-	0.67
MoC	14.3	620	9.8	0.53	-	0.67
NbC	11.6	355	2.0	0.33	-	0.72
Nb <sub>3</sub> Ge	23.2	302	38	0.95	4.2	1.80
Nb <sub>3</sub> Ga	20.3	-	34	1.18	4.1	1.74
V <sub>3</sub> Ga	16.5	310	27	2.7	4.0	1.17
V <sub>3</sub> Si	17.1	330	25	2.5	3.6	1.10
HfV <sub>2</sub>	9.4	187	20	2.05	-	1.00
PbMo <sub>6</sub> S <sub>8</sub>	15.3	411	60	0.67	3.84	1.20
PbMo <sub>6</sub> Sc <sub>8</sub>	6.7	294	7	0.24	-	0.66

Table B.2: Properties of selected superconductors.  $H_c$  at 0K is given for the elemental materials and  $H_{c2}$  at 0K for the compounds, which are all type II superconductors. While the units of  $H_c$  are mT, those of  $H_{c2}$  are  $10^4$ Oe=1T.  $N(E_F)$  is the density of states at the Fermi energy and its units are states/(atom-eV); it is obtained from the linear term in the normal-state specific heat.

		Spec. Heat [J/(g.K)]			Integ. Values (J/g)	
	4.2K	77K	300K	0-4.2K	4.2-77K	77-300K
Sapphire		0.062	0.80			
Copper	0.0001	0.19	0.39	0.0002	5.4	79.6
Aluminum	0.0003	0.34	0.83	0.0005	8.4	170.4
Stainless		0.16	0.48			
Pyrex	0.0002	0.20	0.76	0.0003	6.2	

Table B.3: Specific Heat Capacity and Integrated Values for common Cryogenic Building Materials.

Cryogen	Temp. (K)	Cooling Capacity (J/cm <sup>3</sup> )	Liquid NBP	Density (g/L) Gas NBP	Gas STP	Cost (\$/liquid liter)
Helium	4.2	2.6	125	16.7	0.656	7
Hydrogen	20.4	31	70	1.33	0.061	
Neon	27.1	103	1210	9.5	0.810	225
Nitrogen	77.3	161	808	4.41	1.12	0.55
Argon	87.4	229	1400	5.76	1.78	3
Oxygen	90.2	243	1140	4.75	1.29	0.75
Freon-14	145.1	218	1960	7.2		
Freon-13	191.8	220	1505	7.9		
Water	373.1	2443	1000			

Table B.4: Common Cryogenics and Their Characteristics.

Thermocouple Type	Names of Materials	Useful Appl. Range
B	Platinum 30% Rhodium (+) Platinum 6% Rhodium (+)	2500 3100F 1370 170C
C	W5Re Tungsten 5% Rhenium (+) W5Re Tungsten 26% Rhenium (+)	3000 -3100F 1650 2315C
E	Chromel (+) Constantan (-)	200 1650F 95 900C
J	Iron (+) Constantan (-)	200 1400F 95 760C
K	Chromel (+) Alumel (-)	200 2300F 95 1260C
N	Nicrosil (+) Nisil (-)	1200 2300F 650 1260C
R	Platinum 13 % Rhodium (+) Platinum(-)	1600 2640F 870 1450C
S	Platinum 10 % Rhodium (+) Platinum(-)	1800 2640F 980 1450C
T	Copper (+) Constantan (-)	330 660F 200 350C

Table B.5: Thermocouple types, structure and application temperature rangess.

<b>EVAPORATIVE METHODS</b>	
<b>Vacuum Evaporation</b> Conventional vacuum evaporation Electron-beam evaporation	Molecular-beam epitaxy (MBE) Reactive evaporation
<b>GLOW-DISCHARGE PROCESSES</b>	
<b>Sputtering</b> Diode sputtering Reactive sputtering Bias sputtering Magnetron sputtering Ion beam deposition Ion beam sputter deposition Reactive Ion plating Cluster beam deposition(CBD)	<b>Plasma Process</b> Plasma enhanced CVD Plasma oxidation Plasma anodization Plasma polymerization Plasma nitridation Plasma reduction Microwave ECT plasma CVD Cathodic arc deposition
<b>GAS-PHASE CHEMICAL PROCESSES</b>	
<b>Chemical vapor deposition (CVD)</b> CVD epitaxy Atmospheric-pressure CVD Low-pressure CVD Metallorganic CVD Laser-induced CVD Electron-enhanced CVD	<b>Thermal forming Processes</b> Thermal oxidation Thermal nitridation Thermal polymerisation  Ion implantation
<b>LIQUID-PHASE CHEMICAL TECHNIQUES</b>	
<b>Electro process</b> Electroplating Electroless plating Electrolytic anodization Chemical reduction plating Chemical displacement plating Electrophoretic	<b>Mechanical techniques</b> Spray pyrolysis Spray-on techniques Spin-on techniques  Liquid phase epitaxy

Table B.6: Survey and Classification of Thin-film deposition Technologies.



EFFET	ISSUE						
	Chem. Comp.	Ther. match	Surf. quality	Subs. cleanliness	Subs. homogeneity	Subs. ther. Stab.	Buff. layers
Max. process. temperature	*	*				*	*
Reacted layer at interface	*			*			*
Impurity in film	*			*			*
Impurity in substrate	*						*
Film adhesion	*	*			*		*
Film cracking		*					*
Film microstructure			*	*	*	*	*
Film composition	*						*
Film morphology			*	*	*	*	*
Film uniformity			*	*	*	*	*
Supercond. properties	*	*	*	*	*	*	*

Table B.7: Global issues in substrate selection.

# Bibliography

- [1] J. W. Lynn, *High Temperature Superconductivity*, ch. Crystallography. Springer Verlag, 1990.
- [2] J.D.Jorgensen, B.W.Veal, W.K.Kwok, G.W.Crabtree, A.Umezawa, L.J.Nowicki, and A.P.Paulikas. *Phys.*, 1987.
- [3] R.J.Cava, B.Batlogg, C.H.Chen, E.A.Rietman, S.M.Zahurak, and D.Werder, "Nature," 1987.
- [4] S.Massidda, A.J.Freeman, and D.D.Koelling. *Phys.*, 1987.
- [5] Vanderah, *Chemistry of Superconductor Materials*. Noyes, 1992.
- [6] C. Kittel, *Introduction to Solid State Physics*, ch. Phonons II Thermal Properties. John Wiley & Sons, 7th ed., 1996.
- [7] M.Fardmanesh, M.Ihsan, A. R. K.Scoles, and K.Pourrezae, "Thick and thin film y-ba-cu-o infrared detector,"
- [8] M.Fardmanesh and A.Rothwarf, "Analytic modeling of patterned high  $T_c$  superconductive bolometers: film and substrate interface effects," *SPIE*, pp. 469-479, 1998.

- [9] C. Kittel, *Introduction to Solid State Physics*, ch. Free Electron Fermi Gas, pp. 164-168. John Wiley & Sons, 1996.
- [10] C. Kittel, *Introduction to Solid State Physics*, ch. Superconductivity. John Wiley & Sons, 1996.
- [11] F. P. Incropera and D. P. Witt, *Fundamentals of Heat and Mass Transfer*. John Wiley & Sons, 1990.
- [12] A. E. Ureyen and B. Ozel, "Automation of measurement of high temperature superconductor films," tech. rep., Bilkent University Ankara Turkey, 1999.
- [13] M. Fardmanesh, A. Rothwart, M. H. Jang, K. J. Scoies, and Somtyag, "Multilayer  $\text{YBa}_2\text{Cu}_3\text{O}_7$  thick film superconductors on metal and ceramic substrate,"
- [14] B. Gülbahar, "Characterization of high- $t_c$  superconducting films by induction technique," tech. rep., Bilkent University Ankara Turkey, 1999.
- [15] M. Fardmanesh, K. Scoies, A. Rothwarf, Esanchez, E. Brsha, and P. Davie, "Annealing study of  $\text{YBa}_2\text{Cu}_3\text{O}_x$  and  $\text{YBa}_2\text{Cu}_4\text{O}_x$  screen printed thick film,"
- [16] C. Jia, "Investigation of thin films heterostructures and devices of ceramic superconductors by means of high-resolution electron microscopy." Institut für Festkörperforschung.
- [17] J. M. Phillips, "Substrate selecton for high temperature superconducting thin films," *Appl. Phys.*, vol. 79, no. 4, pp. 1829-1848, 1996.

- [18] M.Fardmanesh, A.Rothwarf, and K.J.Scole, "YBa<sub>2</sub>Cu<sub>3</sub>O<sub>7-x</sub> infrared bolometers: Temperature-dependent responsivity and deviations from the  $dr/dt$  curve," *Appl.Phys*, vol. 77, no. 9, pp. 4568 – 4575, 1995.
- [19] M.Fardmanesh, A. Rothwarf, and K.J.Scle, "Noise characteristics and detectivity of YBa<sub>2</sub>Cu<sub>3</sub>O<sub>7</sub> superconducting bolometers: Bias current and frequency and and temperature dependence," *Appl. Phys*, vol. 79, no. 4, pp. 2006–201, 1996.
- [20] M.Fardmanesh, K.Scoles, and A.Rothwarf, "Characteristics of patterned YBa<sub>2</sub>Cu<sub>3</sub>O<sub>7-x</sub> superconducting thin film bolometer: Artifacts related to joule heating and ambient pressure and microstructure," *IEEE Transaction*, pp. 69–78, 1998.
- [21] R.Feenstra, T.B.Lindemer, J.D.Budai, , and M.D.Galloway, "Effect of oxygen pressure on the synthesis of YBa<sub>2</sub>Cu<sub>3</sub>O<sub>7x</sub> thin film by post-deposition annealing," *Appl. Phys*, vol. 69, no. 9, pp. 6569–6585, 1991.
- [22] S. Sanchez, M. Elwenspoek, C. Gui, M. J. E. de Nivelte, R. de Vries.Piet A.J.de Korte, M. P.Bruijn, J. Wijubergen, W. Michalke, E. Steinbeiss, T. Heidenblut, and B. Schwierzi, "A high  $t_c$  superconductor bolometer on a silicon nitride membrane," *IEEE Transaction*, vol. 7, no. 1, pp. 62–68, 1998.
- [23] F.S.Galasso, D.B.Fenner, L.Lynds, C.E.Rossman, D.Potrepka, J.I.Budnick, and L.G.Carreiro, "An assessment of synthesis effects on the high  $t_c$  superconducting transition: with application to thin film bolometer devices," *Applied Superconductivity*, vol. 4, no. 3, pp. 119–133, 1996.

- [24] M.P.Siegal, J. M.Phillips, A. Hebard, R. Dover, R.C.Farrow, T.H.Tiefel, and J. Marshall, "Correlation of structural quality with superconducting behavior in epitaxial thin films of  $\text{Ba}_2\text{YCu}_3\text{O}_{7-x}$  on  $\text{LaAlO}_3(100)$ ,"
- [25] Y. Matsuoka, E. Ban, and H. Igawa, "Properties of high  $T_c$  screen printed ybaco films prepared under flowing helium," *Supercond. Sci. technol.*, vol. 2, pp. 300-303, 1998.
- [26] Y. Matsuoka, E. Ban, and H. Ogawa, "High  $T_c$  screen printed ybaco films prepared by liquid phase processin method," *Physics D*, vol. 22, pp. 1935-1937, 1989.
- [27] J. Tabuchi and K. Utsuni, "Preparation of superconducting ybaco thick films with preferred c axis orientation by a screen printing method," *Appl.Phys.*, vol. 53, no. 7, pp. 606-608, 1988.
- [28] N. P.Bansal and R. N.simons, "High  $T_c$  screen printed  $\text{YBa}_2\text{Cu}_3\text{O}_{7-x}$  films: Effect of the substrate material," *Appl. Phys.*, vol. 53, no. 7, pp. 603-605, 1988.
- [29] K. Kasprak, R. Walters, S. Onishi, and A. Elshabini-Riad, "Optimization of superconductive properties on ceramic substrates," *ISHM proceeding*, pp. 588-592, 1990.
- [30] A.Kapitulnik and K. Char, "Measurements on thin film high  $T_c$  superconductors," *IBM j. Res. Develop.*, vol. 33, no. 3, pp. 252-261, 1989.
- [31] S. Xu, C. Ong, Y. Zhou, B.L.Low, L.F.Chen, and X.Zhang, "The effects of heating and annealing processes on the surface morphology and quality of double-sided  $\text{YBa}_2\text{Cu}_3\text{O}_{7-x}$  thin films," *Physics C*, vol. 297, pp. 43-51, 1998.

- [32] P. S. Takebayashi, , and M. Murakami, "Origin of subgrain formation in melt grown ybco bulks," *Physica C*, vol. 297, pp. 216-222, 1998.
- [33] R. Roy, R. guo, A.S. Bhalla, and L.E. Cross, "Thin film growth not epitaxy in htsc film growth," *American vacuum Society*, vol. 12, no. 2, pp. 269-27, 1994.
- [34] J. R. Sheats, N. Newman, R. C. Taber, and P. Merchant, "Effects of processing on electrical properties of ybco films . ii. in situ deposition processes," *American vacuum Society*, vol. 12, no. 2, pp. 388-392, 1994.
- [35] W. Song, D. Liu, S. Juao, D. Lu, C. An, L. Lu, H. Yang, and Z. Li, "In situ deposition of  $YBa_2Cu_3O_{7-x}$  superconducting thin film without high pressure oxygen during film cooling," *American vacuum Society*, vol. 12, no. 2, pp. 533-536, 1994.
- [36] A. Kulpa, A.C.D. Chaklader, and G. Roemer, "Sintering time effect on electrical properties of ybco," *Physica C*, vol. 190, pp. 219-224, 1992.
- [37] J.-M. Heintz, M. Sanx, E. Marquestaut, J. Etourneau, and J. pierre Bonnet, "Influence of bco on th sintering and the properties of ybco based ceramics," *Am. Ceram. Soc.*, vol. 74, no. 5, pp. 998-1002, 1991.
- [38] E.Z. Meilikhov, "Critical currents and current-voltage characteristics of high temperature superconducting ceramics," *Appl. Superconductivity*, vol. 4, pp. 61-78, 1996.
- [39] J.W. Ekin, S.E. Russek, C.C. Clickner, and B. Jeanneret, "In situ nobel metal/ybco thin film contacts," *Appl. phys.*
- [40] S. Jin, M.E. Davis, T.H. Tiefel, R.B. Vandover, R.C. Sherwood, H.M. Obryan, G.Q. Kammlott, and R.A. Fastnacht, "Low resistivity

- contacts to bulk high  $t_c$  superconductors," *Appl. Phys.*, vol. 54, no. 25, pp. 2605-2607, 1989.
- [41] M. Maus, "Hts rf-squid-planar gradiometer mit langer Basislänge für die Inspektion von Flugzeugfelgen," Master's thesis, Department of Mathematisch-Naturwissenschaftlichen Fakultät Rheinischen Friedrich-Wilhelms-Universität Bonn, 1999.
- [42] B. Seeber, *Handbook of Applied Superconductivity*, vol. 1. Institute of Physics Publishing Bristol and Philadelphia, 1998.
- [43] J. D. Vincent, *Fundamentals of Infrared Detector Operation and Testing*. John Wiley & Sons, 1990.
- [44] J. W. Lynn, *High Temperature Superconductivity*. Springer-Verlag, 1990.
- [45] G. Burns, *High Temperature Superconductivity: An Introduction*. Academic Press Inc., 1992.
- [46] A. J. Chapman, *Heat Transfer*. Macmillan Publishing Company New York, 1984.
- [47] A. Rose-Innes and E. Rhoderick, *Introduction to Superconductivity*. Pergamon, 1988.
- [48] Schuegraf, *Handbook of Thin-Film Deposition Processes and Techniques*. Noyes, 1988.